TOWARD MOLECULAR IMAGING PROBES TO DETECT CRYPTIC BACTERIAL INFECTIONS

TOWARD MOLECULAR IMAGING PROBES TO DETECT CRYPTIC BACTERIAL INFECTION

By

Lisset Barbara Llano Piedra, B. Sc.

A Thesis

Submitted to the School of Graduate Studies

in Partial Fulfillment of the Requirements

for the Degree

Master of Science

McMaster University

MASTER OF SCIENCE
(Chemical Biology Graduate Program)

McMaster University
Hamilton, Ontario

TITLE: TOWARD MOLECULAR IMAGING PROBES TO DETECT CRYPTIC BACTERIAL INFECTION

AUTHOR: Lisset Barbara Llano Piedra, B. Sc.

SUPERVISOR: Dr. Paul Berti

NUMBER OF PAGES: xiv, 97

Abstract

Infectious diseases represent one of the leading causes of death globally. Prompt diagnosis is essential for the onset of clinical treatment but certain cases of underlying bacterial infection deep in the body can remain undiagnosed for weeks. Hidden bacterial infection is the leading cause of fever of unknown origin (FUO), which is observed in 2 % of all hospital admissions around the world. Molecular imaging of bacterial infections is the ideal non-invasive diagnostic tool, but all available probes also detect inflammation. Two targets were selected for development of bacteria-specific molecular imaging probes, namely iron-uptake pathways and peptidoglycans involved in the synthesis of the cell wall. Both, Gram-positive and Gram-negative bacteria use iron-binding molecules called siderophores to scavenge iron from their surroundings. The structural similarities between Fe^{3+} and Ga^{3+} allow siderophores to be radiolabelled with $^{67/68}Ga$ and visualized by nuclear medicine techniques. The clinically proven siderophore Deferoxamine (Dfo) has a plasma half-life of only 5.5 min that does not favor its direct use as a probe. Dfo derivatives with improved pharmacokinetics properties were designed and tested on *Staphylococcus aureus* cultures. The ciprofloxacin and the ethyloxycarbonyl derivatives of DFO at the primary amino position were among the most successful conjugates targeting the siderophore active-transport mechanism and reaching high relative uptake rates. Furthermore, the peptidoglycan pathway of Gram-positive bacteria was *in vitro* targeted with vancomycin conjugated to ^{67}Ga-Dfo which showed even higher labelling capacity

than ^{67}Ga-Dfo within a few minutes of exposure. *In vitro* siderophore studies remain challenging due to the lack of methods for the preparation of rigorously iron-depleted media. We developed an iron chelating method with the goal of creating iron-free growth media.

Acknowledgements

I would like to take this opportunity to thank my supervisor, Dr. Paul Berti, for his kind support and valuable guidance along the way. I feel lucky for having found not only a great supervisor but also a great professor. You will always have my deepest gratitude and my most sincere admiration.

Special thanks to my supervisory committee, Dr. John Valliant and Dr. Alex Adronov. I appreciated every single thought or comment of yours and the way you have shaped my critical thinking with many of your interesting questions.

None of my work could have been possible without the close collaboration of Dr. Joseph Ioppolo and Omid Beiraghi who were in charge of the synthesis of the molecular imaging probes.

Likewise, I owe my first days of hands on experience in the lab to Deanna Caldwell, to whom I am especially grateful.

Additional thanks to Megan Blacker, for her contribution to this project and her helpful guidance through my lab work in the Nuclear Reactor Building.

Thanks to Christina (Cheng) Li for her initial contributions to the development of a novel iron-chelating resin.

I am also thankful for the opportunity I had to be part of the multidisciplinary group of students working in the NSERC CREATE Training Program in Molecular Imaging Probes. What is more, every meeting dedicated to

the communication and critical understanding of our scientific research was always a remarkable experience.

Now I would like to thank all current Berti lab members, Vincent Azhikannickal, Naresh Balachandran, Simanga Gama, Maren Heimhalt plus other dear members who have already left the lab, Rasa Bakhtiari, Elizabeth Curiel, Jennifer Wild, Kelvin Tsao, Jennifer Li and Krishna Patel. To all of you, thanks for your kind friendship and cheerful support.

My final words are dedicated to my husband and our little son. I thank you both for your great understanding, constant patience and unconditional love.

Table of Contents

List of Figures

List of Tables

List of Abbreviations

5-SSA	5−sulfosalicylic acid
^{67}Ga-Dfo-Tz	^{67}Ga-Dfo-succinyl-tetrazine
^{68}Ga-FOXE	^{68}Ga-ferrioxamine E
^{68}Ga-TAFC	^{68}Ga-triacetylfusarinine C
ABC	ATP-binding cassette
BAIs	biomaterial-associated bacterial infections
BLI	bioluminescence imaging
CAS	chrome azurol S
CT	computed tomography
D-Ala-D-Ala	D-alanyl-D-alanine
Dfo	Deferoxamine, also known as Desferrioxamine B
DPTA	diethylene triamine penta-acetic acid
EDTA	ethylenediaminetetraacetic acid
FDG	^{18}F-2-fluoro-2-deoxyglucose
FLI	fluorescence imaging
FMI	fluorescence molecular imaging
FUO	fever of unknown origin
HDTMA	hexadecyltrimethylammonium bromide
HMPAO	hexamethylproplyleneamine oxime
MRI	magnetic resonance imaging
MRSA	methicillin resistant *S. aureus*
NAG	N-acetylglucosamine
NAM	N-acetylmuramic acid
NHS	trans-cyclooctene *N*-hydroxy-succinimidyl
NIR	near-infrared
PBS	phosphate buffered saline
PET	positron emission tomography
SBPs	siderophore binding proteins
SDS	sodium dodecyl sulfate
SPECT	single-photon emission computed tomography
SSTI	skin and soft tissue infections
TMS or TMS_0	Tris-Minimal Succinate growth medium made without added $FeCl_3$
TMS_{0CR}	TMS that was first treated with the non-specific chelator Chelex® 100 before addition of the Mg and Ca salts, followed by Dfo-Sepharose resin treatment of the complete medium

TMS_{0R}	TMS that was treated with Dfo-Sepharose resin
TMS_{0R+R}	TMS that was treated with Dfo-Sepharose resin and includes fresh resin added to the medium
TMS_{10}	TMS including 10 μM added $FeCl_3$
Tz	Tetrazine
vanc-TCO	vancomycin-*trans*-cyclooctene

Chapter 1 - **INTRODUCTION**

1.1. Overview

Being able to detect bacterial cells directly using molecular imaging probes would be a major step forward in diagnosing fever of unknown origin. The use of siderophores for the design of molecular imaging probes is attractive because the vast majority of bacteria can use these high affinity iron-binding molecules to survive in iron-depleted environments, including human hosts. Simulating the physiological iron scarcity during *in vitro* assays provides a more realistic approach for the testing of molecular imaging probes prior *in vivo* assays. Restricting environmental iron contamination of the growth medium during *in vitro* assays requires a novel iron chelating strategy and improved monitoring of iron concentrations.

Thanks to well documented structural and functional similarities shared by Ga^{3+} and Fe^{3+}, siderophores can be labelled with $^{67/68}Ga^{3+}$. Both have similar ionic radii (0.62 Å vs 0.65 Å), charges, coordination preferences[1] and Ga has even been used as a structural analogue of Fe in iron-binding proteins such as transferrin[2], lactoferrin[3], ovotransferrin[4] and bovine spleen purple acid phosphatase.[5]

The siderophore uptake pathway can mediate the internalization of antibiotic-siderophore complexes.[6] Linking antibiotics, or alternatively aryl or alkyl groups, to siderophores could potentially improve the pharmacokinetic

properties of the resulting labelled-siderophore-based complexes. On the other hand, $^{67/68}$Ga-labelled siderophores can serve as tracers of siderophore-antibiotic complexes following the same pathway of their respective unmodified-antibiotic molecule. Either way, the ultimate goal is to develop a new drug capable of imaging infection with high affinity and specificity. Deferoxamine (Dfo) and Dfo derivatives were the siderophore-based complexes studied throughout this thesis.

1.2. Fever of unknown origin

Fever of unknown origin (FUO) affects roughly 2 % of hospitalized patients around the world. It is defined as persistent fever higher than 38.3°C for at least three weeks, the source of which remains uncertain after one week of comprehensive investigation.[7, 8, 9] Infections, malignancies, collagen vascular diseases, and autoimmune disorders like Celiac disease, account for the majority of cases of FUO. Infections are the most common cause of FUO in cases that are eventually diagnosed, followed by malignancy and non-infectious inflammatory diseases. Quick, accurate localization and diagnosis of the cause of FUO would markedly improve patients' treatment.[10, 11] Imaging infections with high specificity has remained challenging for more than 40 years. Most probes for detecting hidden infection also detect inflammation, which can have many other causes.

1.3. Molecular imaging probes

Radiographs, ultrasonography, computed tomography (CT), and magnetic resonance imaging (MRI) are currently used to monitor morphological changes due to generalized infection. CT and MRI provide particularly useful data in detecting organ and musculoskeletal late stages of infection. It is also important to note that morphological distortion induced by post-surgical changes, scarring, and presence of foreign materials may interfere with the outcome of these imaging modalities.[12]

As a complement to these techniques for morphological imaging, there are several radiolabelled markers (i.e., proteins and cells) that have been developed for imaging infectious processes by either single-photon emission computed tomography (SPECT) or positron emission tomography (PET). Examples of isotopes that are used chemicaly include ^{99m}Tc, ^{111}In, ^{68}Ga, and ^{18}F, which have been applied to labelling leukocytes and their cellular products, in addition to labelling therapeutic molecules such as antibiotics, monoclonal antibodies, and experimental therapeutics by use of chelator to link the metal ion to the targeting vector.[13]

Exogenously radiolabelled patient-derived leukocytes later re-injected into the donor patient, is a common practice for the clinical detection of an underlying infection. But at the same time, this clinical method is also used for the detection of a range of inflammatory disorders.[14, 15] The detection of infection-associated inflammation frequently leads to additional confirmation of the underlying

infection by positive blood tests or biopsies and non-specific symptoms of the patients, such as fever and general malaise.[16]

The use of SPECT imaging agent ^{67}Ga-citrate and its PET counterpart ^{68}Ga-citrate also belong to the current standard protocol for clinical imaging of infection, mainly for the study of osteomyelitis, lung infection, and FUO. ^{67}Ga-citrate was used in 1971 for imaging infection and inflammation. ^{67}Ga-citrate binds in ionic form to circulating transferrin as an analogue of iron. It is still the most commonly used radiopharmaceutical for imaging infections in the world despite its very low specificity. During acute inflammation, ^{67} Ga-citrate accumulates at the site of inflammation due to the locally enhanced vascular permeability, where it binds with high affinity to lactoferrin excreted by leukocytes, or to siderophores produced by microorganisms in low iron environments. Around 25 % of the total injected dose is excreted through the urinary system, while the rest is retained in bone, bone marrow, liver, and soft tissues.[17]

[^{18}F]-2-Fluoro-2-deoxyglucose (FDG), is another common PET agent for diagnosis of localized infectious, inflammatory, or neoplastic causes of FUO. FDG is transported across the cell membrane by the GLUT glucose transporter proteins. Intracellular FDG is phosphorylated to FDG-6 phosphate by hexokinase, and the phosphorylated molecule remains trapped inside the cell. ^{18}F-FDG accumulates in activated lymphocytes, monocytes, and granulocytes because these cells use glucose as an energy source only after activation during a

metabolic burst. Unfortunately, ^{18}F-FDG can show uptake in any kind of cell with high glycolytic activity and may provide a false-positive result.[18]

In addition to current nuclear medicine imaging methods some attempts has been made to enhance optical imaging techniques towards the development of new probes targeting infections, although they remained of limited chemical utility due to limited depth of penetration.[19] Other important limitations for the development of new probes is that there are few fluorescent dyes that are FDA approved.[20] Fluorescence molecular imaging (FMI) technology is a promising imaging method where small depth of penetration is needed such as the intraoperative detection of tumours for guided surgery and the targeting of biomaterial-associated bacterial infections (BAIs). Van Oosten *et al*. published a promising optical imaging probe following this second approach. A near-infrared (NIR) fluorophore IRDye 800CW was conjugated to the antibiotic vancomycin, which is used to treat Gram-positive bacteria, the most common causative agents of soft tissue infections and BAIs. NIR optical imaging with this bacteria-specific vancomycin-based probe was able to detect both invasive infections *in vivo* and BAIs post mortem (Figure 1.1, Figure 1.2).[21]

One experiment consisted of inducing myositis (muscle inflammation and soreness) in mice limbs using bioluminescent mutant strains of *S. aureus* (Xen36) and *E. coli* (Xen16). After systemic administration of the probe, the site of infection successfully traced the *S. aureus* site of infection by co-localization of

probe fluorescence and bacterial luminescence (Figure 1.1). As expected, *E. coli* cells were not detected, as vancomycin does not bind Gram-negative bacteria.

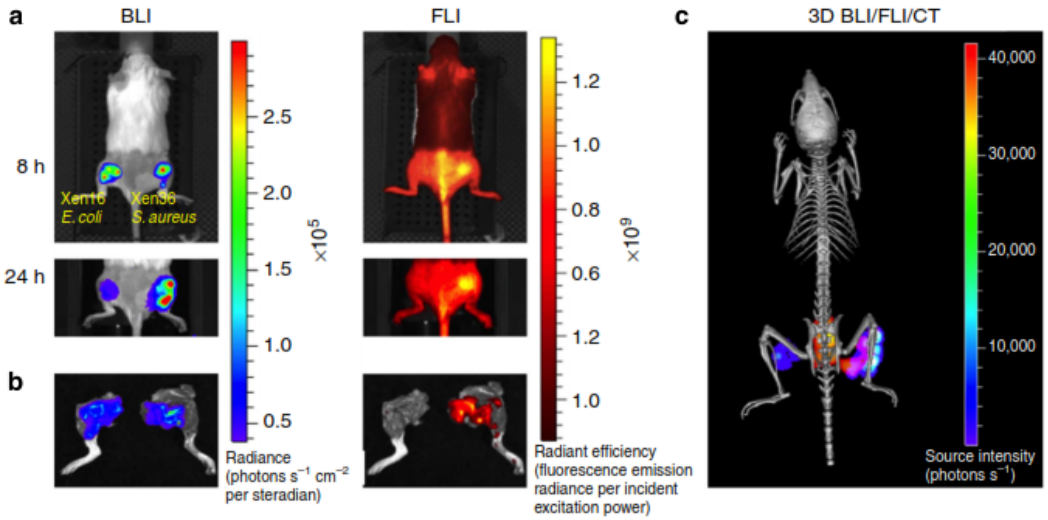

Figure 1.1 *In-vivo* imaging of bacterial induced thigh infection using fluorescent probe vanco-800CW.

(a) Imaging of a mouse with induced left-thigh-infection using bioluminescent *E. coli* and induced right-thigh-infection using bioluminescent *S. aureus* at 8 and 24 h after intravenous administration of vanco-800CW. Left column: bioluminescence imaging (BLI); Right column: fluorescence imaging (FLI). (b) Removed muscle tissue infected with *E. coli* (left) and the *S. aureus* (right) from the mouse shown in (a). (c) Micro-computed tomography (CT) imaging of the mouse from (a) showing co-localization of bioluminescence of right thigh corresponding to *S. aureus* infection and fluorescence of vanco-800CW. No visible fluorescent signal on the left leg infected with *E. coli*. Vanco-800CW fluorescent signal also visible in the bladder.
Reprinted by permission from Macmillan Publishers Ltd: Nature Communications (Ref. 21), copyright (2013).

In a human post-mortem implant model, Van Oosten *et al*. explored the specificity and sensitivity of the probe recognition at the depth of a surgical implant in a human ankle (Figure 1.2). The probe specificity was demonstrated through the use of implant devices coated with Gram-positive *Staphylococcus epidermidis* and inserted into a post-mortem ankle (Figure 1.2(a)). Only implants pre-incubated with both vanco-800CW and the bacterial culture were detectable. The sensitivity was assessed by implanting paper strips that had been spotted with

labelled *S. aureus* (Figure 1.2(b)). Cells were detectable at 2.5×10^8 CFU•mm^{-2} and 1.25×10^8 CFU•mm^{-2}, but not 6.3×10^7 CFU•mm^{-2}.

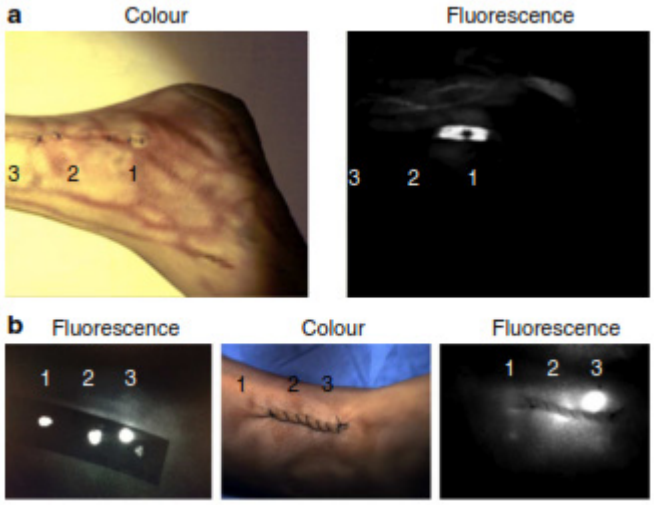

Figure 1.2 Human post-mortem imaging of implant associated infection model using fluorescent probe vanco-800CW.

(a) *S. epidermidis* biofilm was either applied (1 & 3) or not (2) to implant devices. Implant devices 1 and 2 were incubated with vanco-800CW before surgically placing the three devices in a post-mortem ankle. Non-invasive imaging of the ankle was performed with a clinical multispectral fluorescence camera. (b) *S. aureus* cells labelled with vanco-800CW were spotted onto a Whatman paper strip at the following concentrations: (1) 6.3×10^7 CFU mm^{-2}; (2) 1.25×10^8 CFU mm^{-2}; (3) 2.5×10^8 CFU mm^{-2} and they were later imaged either before (left) or after surgical application onto a post-mortem ankle (right).

Reprinted by permission from Macmillan Publishers Ltd: Nature Communications (Ref. 21), copyright (2013).

These were promising results for the detection of bacterial infection with high specificity. However, the limited depth of penetration of optical imaging remained an obstacle for the detection of hidden infections.

The development of infection-specific probes with high depth of penetration, as opposed to infection-associated inflammation, continues to be a critical step towards enhanced accuracy of clinical imaging of infection. Targeting bacterial specific growth factors like siderophores or the bacterial cell wall can

potentially lead to the discovery and development of new probes with greater specificity and sensitivity.

1.4. Bacterial iron uptake and siderophores

A fundamental principle of microbial pathogenesis is that bacterial pathogens must overcome host iron limitation to establish a successful infection. The sole exceptions are the iron-independent pathogens *Borrelia burgdorferi*, which causes Lyme disease,[22] and the syphilis pathogen, *Treponema pallidum*.[23] For the majority of the pathogenic bacteria though, the most generalized way of overcoming host iron limitation has been through the synthesis of iron-binding growth factors known as siderophores.[24] Some siderophores may be secreted in order to deprive competing organisms of iron.[25, 26]

Siderophores, coordinated to iron, are accumulated by microorganisms' specific translocation mechanisms.[27, 28] Gram-negative bacteria have specific outer membrane receptors for Fe-siderophore complex uptake. Once recognized, Fe-siderophore complexes traverse the cytosolic membrane in a process driven by the cytosolic membrane potential and mediated by the energy-transducing TonB-ExbB-ExbD system. Complete translocation occurs after periplasmic binding proteins shuttle Fe-siderophores from the outer membrane receptors to cytosolic membrane ATP-binding cassette (ABC) transporters which sequentially release Fe-siderophores into the cytosol, where the complexes are probably dissociated by reduction due to the relatively low affinity of siderophores for ferrous iron (Figure 1.3A).[28]

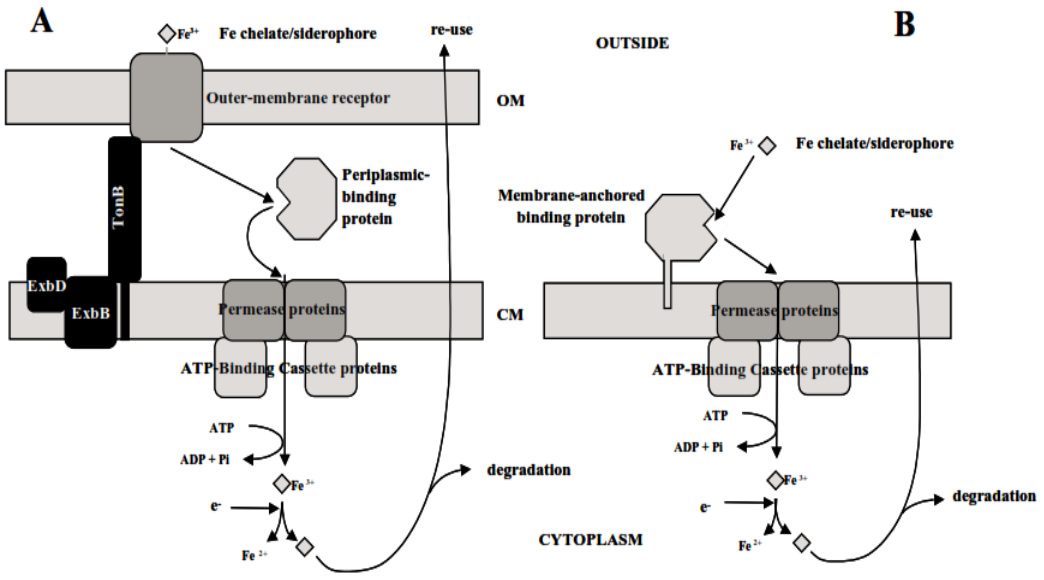

Figure 1.3 Schematic representation of siderophore mediated iron uptake.
(A) Gram-negative and (B) Gram-positive bacteria.
Figure taken from Ref. 22: Andrews, S. C., Robinson, A. K., and Rodriguez-Quiñones, F. Bacterial iron homeostasis. FEMS Microbiol. (2013) Rev. 27, 2-3, 215–237, by permission of Oxford University Press.

Since Gram-positive bacteria do not have an outer membrane, Fe-siderophore complex uptake happens in a single step mediated by binding-protein-dependent ABC permeases that are analogous to those employed by Gram-negative bacteria. However, the binding protein is generally a lipoprotein tethered to the external surface of the cytosolic membrane in Gram-positive organisms, as opposed to a soluble protein in the Gram-negative periplasmic space (Figure 1.3B).[28] Siderophore binding lipoproteins can bind not only to Fe-siderophores (iron-chelated) but also to apo-siderophores (iron-free). This permits two distinct Fe-siderophore uptake pathways in Gram-positive bacteria. The first is the siderophore-shuttle mechanism, in which the siderophore binding proteins (SBPs) exchange Fe(III) from a Fe-siderophore to a protein-bound apo-siderophore,

followed by uptake with no intermediate iron-reduction involved (Figure 1.3, Figure 1.4, step 2 to 4). The second pathway is the displacement mechanism, in which the initially bound apo-siderophore is released from the siderophore-binding protein (SBP), followed by Fe-siderophore binding to the SBP and subsequent uptake (Figure 1.4, step 5 to 7).[29, 30]

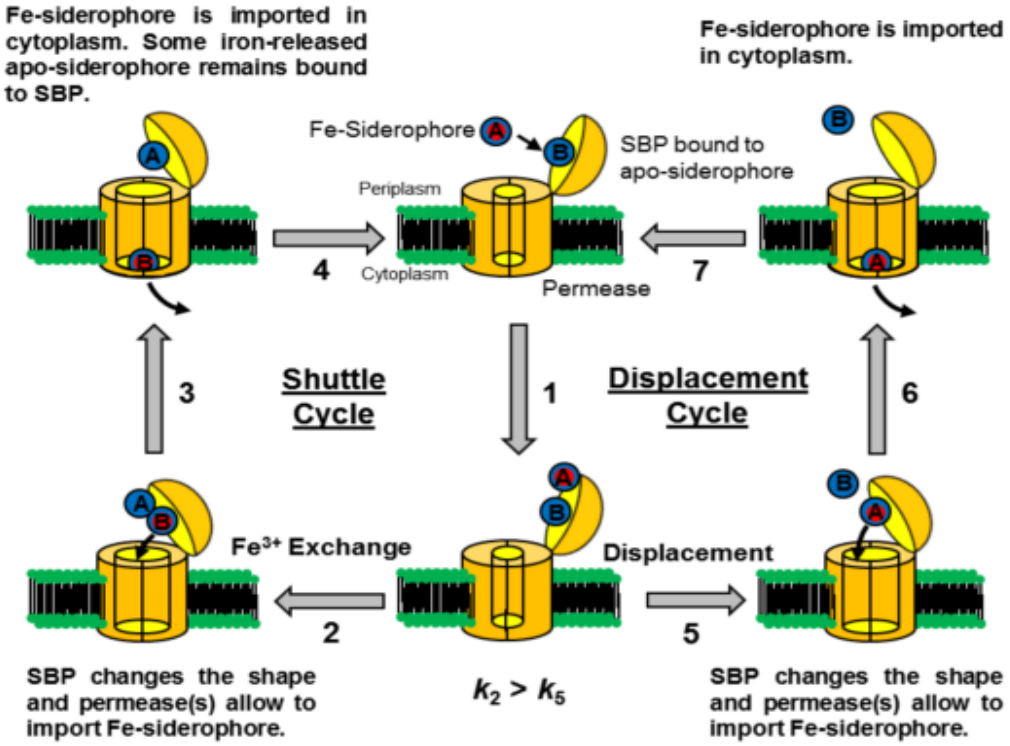

Figure 1.4 Models of the Gram-positive siderophore-shuttle mechanism and displacement mechanism.

(Step 1) A Fe-siderophore approaches SBP occupied by an apo-siderophore. At this step two alternatives are possible: the shuttle pathway (steps 2−4) or the displacement pathway (steps 5−7). Shuttle pathway: (Step 2) Iron gets transferred from the Fe-siderophore to the apo-siderophore in the binding pocket of the SBP. (Step 3) The new Fe-siderophore (B) enters the cell and the resulting apo-siderophore (A) may remain to be bound to the SBP. (Step 4) The receptor gets occupied by an apo-siderophore. Displacement pathway: (Step 5) The Fe-siderophore displaces the apo-siderophore and occupies the binding pocket. (Step 6) The original Fe-siderophore (A) is transported into the cell. (Step 7) The SBP gets bound to the nearby apo-siderophore. Gram-positive bacteria use both mechanisms with the siderophore-shuttle pathway as the preferred one.
Reprinted with permission from {Ref. 30}. Copyright {2014} American Chemical Society.

The fact that the shuttle mechanism is preferred over the displacement mechanism results particularly advantageous to bacteria growing under iron restricted conditions where the bacterial production of siderophores is especially high and consequently leads to increased apo-siderophore concentration in the vicinity of the cell surface. If metal exchange did not take place, iron-uptake would be inhibited by the accumulation of apo-siderophores around SBPs, with higher probabilities of being bound to them. Furthermore, SBPs are able to mediate iron exchange with other siderophores that they do not produce. This enhances the possibility of iron scavenging from other organisms' siderophores without the need for internalizing them. The versatile iron-uptake mechanisms of SBPs allow bacteria to obtain iron from free iron or weak iron-chelators in addition to their own siderophores.[30] The siderophore-shuttle mechanism has also been described in Gram-negative bacteria.[31, 32]

Siderophores usually form hexadentate octahedral complexes with ferric iron and normally employ hydroxamates, catechols and/or α-hydroxycarboxylates as extremely effective Fe^{3+} ligands. [33, 34] Approximately 500 siderophores have been characterized; they can be classified according to the functional groups they

use as iron ligands (Figure 1.5).

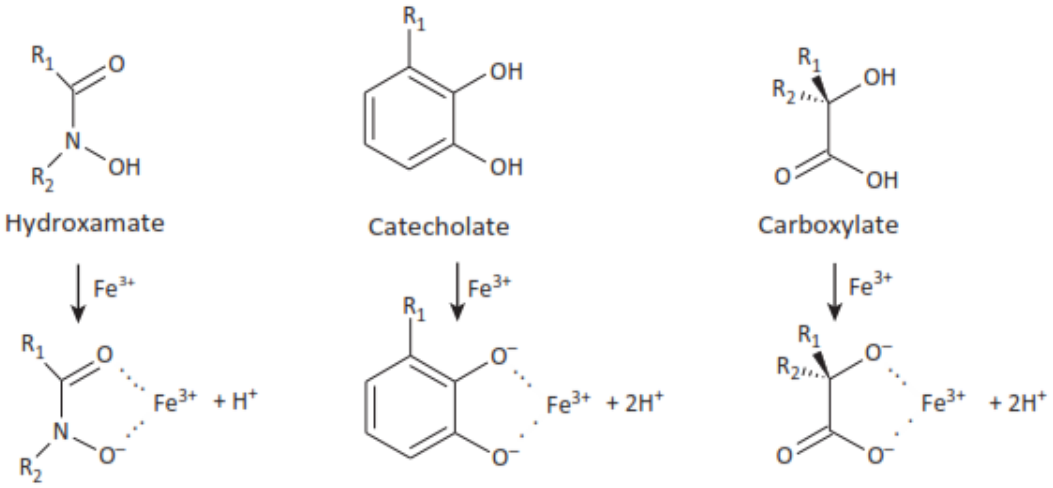

Figure 1.5 Siderophores iron coordination.
(up) The main structural component of siderophores that is responsible for iron coordination. (down) Complexes of the main functional groups of siderophores with iron (Fe3+).
Reprinted from: Trends in Pharmacological Sciences, 35, Agnieszka Górska, Anna Sloderbach, and Michał Piotr Marszałł, Siderophore-drug complexes: Potential medicinal applications of the 'Trojan horse' strategy, 442- 449, Copyright (2014), with permission from Elsevier.

Siderophores are produced by bacteria, fungi and plants to scavenge iron. Surprisingly, enteric bacteria possess a transport system for ferrichrome, a siderophore produced by a soil fungus.[24] Presumably, due to environmental pressure and the need for metabolic economy, thievery mechanisms like this have evolved, allowing to pick up iron-complexed compounds synthesized by other microorganisms. This could be particularly advantageous for the design of a molecular imaging probes sensitive to a majority of pathogenic bacteria.

In fact, promising results following this approach have been recently published on PET imaging of a fungus, *Aspergillus fumigatus,* in a rat infection

model using labelled hydroxamates-based siderophores ^{68}Ga-triacetylfusarinine C (^{68}Ga-TAFC) and ^{68}Ga-ferrioxamine E (^{68}Ga-FOXE) (Figure 1.6, Figure 1.7).[35]

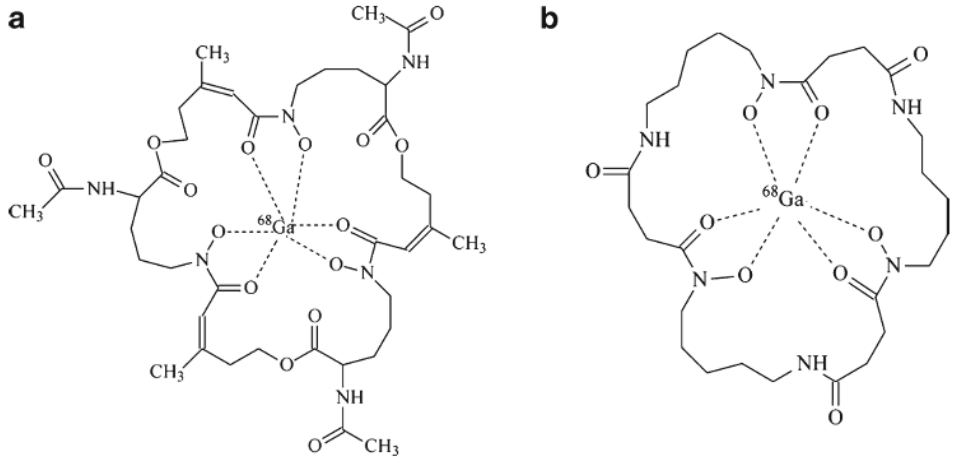

Figure 1.6 Chemical structures of (a) ^{68}Ga-TAFC and (b) ^{68}Ga-FOXE.
68Ga-TAFC: 68Ga-triacetylfusarinine C; 68Ga-FOXE: 68Ga-ferrioxamine E. *Reprinted from ref. [35]: Springer and World Molecular Imaging Society/ Molecular Imaging and Biology, 16, 2014, 102-108, ^{68}Ga-triacetylfusarinine C and ^{68}Ga-ferrioxamine E for Aspergillus infection imaging: Uptake specificity in various microorganisms, Milos Petrik, Hubertus Haas, Peter Laverman, Markus Schrettl, Gerben M. Franssen, Michael Blatzer, Clemens Decristoforo, Fig. 1; with kind permission from Springer Science and Business Media.*

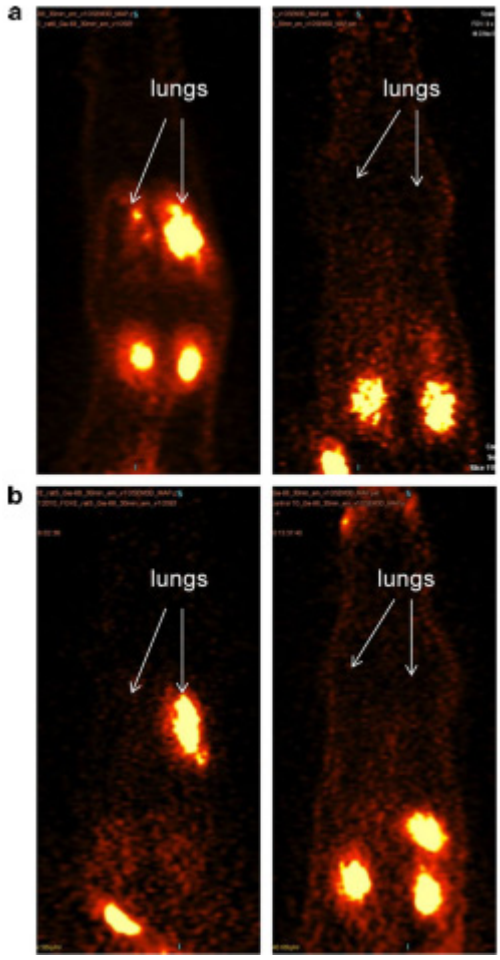

Figure 1.7 *In vivo* PET imaging of the *A. fumiga*tus rat infection model using ^{68}Ga-TAFC and ^{68}Ga-FOXE

(a) PET imaging of rat 1 h after intravenous administration of ^{68}Ga-TAFC. (b) PET imaging of rat 1 h after intravenous administration of ^{68}Ga-FOXE. (left side images) rats with *A. fumiga*tus lung infection; (right side images) non-infected rats. *Reprinted from Ref.* [35]*: Springer and World Molecular Imaging Society/ Molecular Imaging and Biology, 16, 2014, 102-108, ^{68}Ga-triacetylfusarinine C and ^{68}Ga-ferrioxamine E for Aspergillus infection imaging: Uptake specificity in various microorganisms, Milos Petrik, Hubertus Haas, Peter Laverman, Markus Schrettl, Gerben M. Franssen, Michael Blatzer, Clemens Decristoforo, Fig. 3; with kind permission from Springer Science and Business Media.*

In vivo PET imaging in the *A. fumigatus* rat infection model showed rapid accumulation of ^{68}Ga-siderophores in the lungs of infected animals, while there

was no lung uptake in non-infected animals (Figure 1.7). The only visible organs were kidneys and bladder; the main clearance route of these compounds.

1.5. Novel molecular imaging probes targeting microbial siderophore-uptake pathways

Deferoxamine, also known as Desferrioxamine B (Dfo), (Figure 1.8), is a hydroxamic acid-based siderophore produced by the actinobacteria *Streptomyces pilosus.*[36] It has been used clinically as a chelator agent since 1962 to increase elimination of iron via urine in patients experiencing iron poisoning as a result of prolonged blood transfusion therapies for the treatment of β-thalassemia or sickle cell disease.

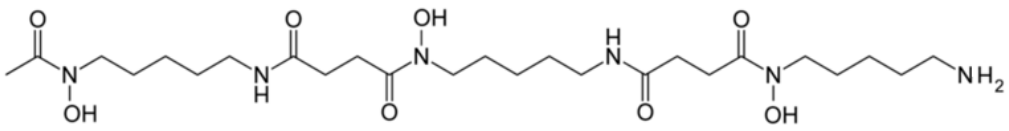

Figure 1.8 Dfo structure.

The free iron concentration in equilibrium in the extracellular fluids of the human host is in the order of 10^{-24} M.[37] Dfo has a high Fe(III) affinity ($K_a \approx 10^{31}$),[24] and it can remove Fe(III) from transferrin.[38, 39] Transferrin is a human high-affinity Fe(III)-binding glycoprotein that scavenges extracellular iron to deprive pathogenic bacteria.[40] Thus, a good strategy to visualize cryptic

bacterial infections is to exploit their ferri-siderophore active uptake pathways to internalize radiolabelled ferri-siderophores or their analogues.

Since Ga(III) and Fe(III) share a similar ionic radii, coordination chemistry and ligand preferences, radioactive isotopes of Ga (^{67}Ga and ^{68}Ga) can be employed as Fe(III) analogues to label siderophores.[5] A siderophore coordinated to $^{67/68}$ Ga will deliver the radioactive isotopes of Ga to bacterial cells, making sites of infection traceable by SPECT and PET imaging techniques respectively.

The fact that Dfo is commercially available in the deferoxamine mesylate salt form and its primary amine can be functionalized without significantly affecting its Fe(III) binding properties, makes Dfo an ideal siderophore for this approach to trace hidden infections. The ultimate goal is to create Dfo derivatives with improved pharmacokinetic properties. ^{67}Ga-Dfo uptake occurs over 6 hours in bacterial culture, while Ga-Dfo clearance from mice happens in less than 6 min (Figure 1.9),[41] consistent with Dfo's half-life in human circulation of 10 to 30 min.[42]

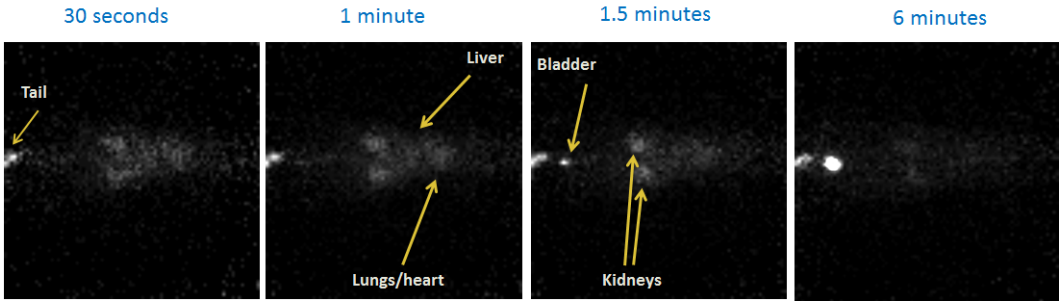

Figure 1.9 ^{67}Ga-Dfo is excreted from a healthy mouse in less than 6 min.
From left to right: (1) Imagine of a mouse after been intravenously injected in the tail vein with ^{67}Ga-Dfo. Noticeable signal at the site of injection. (2) Same mouse 1 min

after injection. Signal started to develop around liver and lungs. (3) After 1.5 min enhanced signal of kidneys and bladder. (4) The tracer has been clear out from the body and there is mostly accumulation at the bladder 6 min after injection. (Figure courtesy of Megan Blacker).

1.5.1. Probe design

One approach to increasing a compound's circulation time is to increase its lipophilicity.[43] In hopes of improving its serum half-life, Dfo was derivatized with alkyl and aryl groups at its primary amine group (Figure 1.10). Several alkyl groups had been previously synthesized and tested, resulting in modest *in vitro* bacterial uptake except for the (6-aminohexyl)oxycarbonyl amine derivative of Dfo (Dr. Joseph Ioppolo and Deanna Caldwell, personal communication). In order to complement the library of tested carbamates derivatives compounds, the ethyloxycarbonyl derivative of DFO at the primary amino position was included for *in vitro* assessment as well. In addition, the n-hexyl derivative was synthesized and *in vitro* tested.

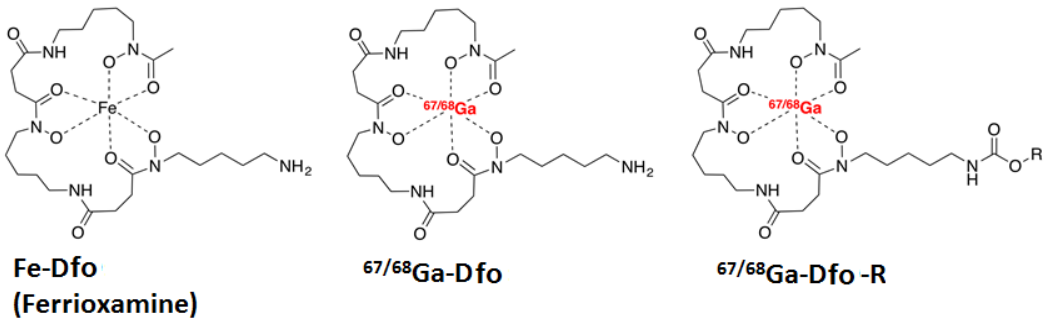

Figure 1.10 Dfo and Dfo-carbamate derivative iron and gallium coordination.
R = alkyl, aryl (Figure courtesy of Dr. Joseph Ioppolo).

Quinoline derivatives have previously shown some potential as antimicrobial agents.[44, 45] Quinoline derivatives of Dfo might be expected to enhance cell binding, since quinoline derivatives of Dfo have shown to cross biological barriers, most frequently through passive transport, which strongly depends on their lipophilicity.

Ciprofloxacin is a well-known broad-spectrum antibiotic that targets both Gram-negative and Gram-positive bacteria by rapidly inhibiting DNA synthesis, with serum elimination half-lives of 3 to 5 hours.[46, 47] Making a Dfo-ciprofloxacin conjugate could not only bring about the potential for enhanced pharmacokinetic properties for the labelled siderophore, but also it could open the door to new strategies for the development of new antibiotic-Dfo complexes where Dfo can serve as an adjuvant for the delivery of the former antibiotic molecule.

1.6. Novel molecular imaging probes targeting the cell wall of Gram-positive bacteria

Gram-positive bacterial cells are surrounded by layers of peptidoglycan, a crosslinked carbohydrate polymer that functions as a protective exoskeleton. These peptidoglycan layers enable bacteria to resist high internal osmotic pressures and play an important role in maintaining cell shape.[48, 49] Targeting peptidoglycan, a defining bacterial feature essential for survival, presents a highly specific route for targeting bacteria; thus, the use of drugs targeting these

polymers on the cell surface remains as an attractive option for the design of imaging agents.

Vancomycin is an antibiotic that inhibits the growth of Gram-positive bacteria by blocking cell wall synthesis through specific recognition of emerging peptidoglycan ending in D-Ala-D-Ala, and subsequent blocking of peptidoglycan cross-linking ability. The reason why vancomycin most likely exhibits poor activity against Gram-negative bacteria is because it is too large to cross the outer membrane.[50, 51]

Van Oosten *et al*. published a promising *in vivo* and post mortem assessment results using vancomycin conjugated to infrared fluorophore IRDye 800CW (Figure 1.11, Figure 1.1, Figure 1.2).

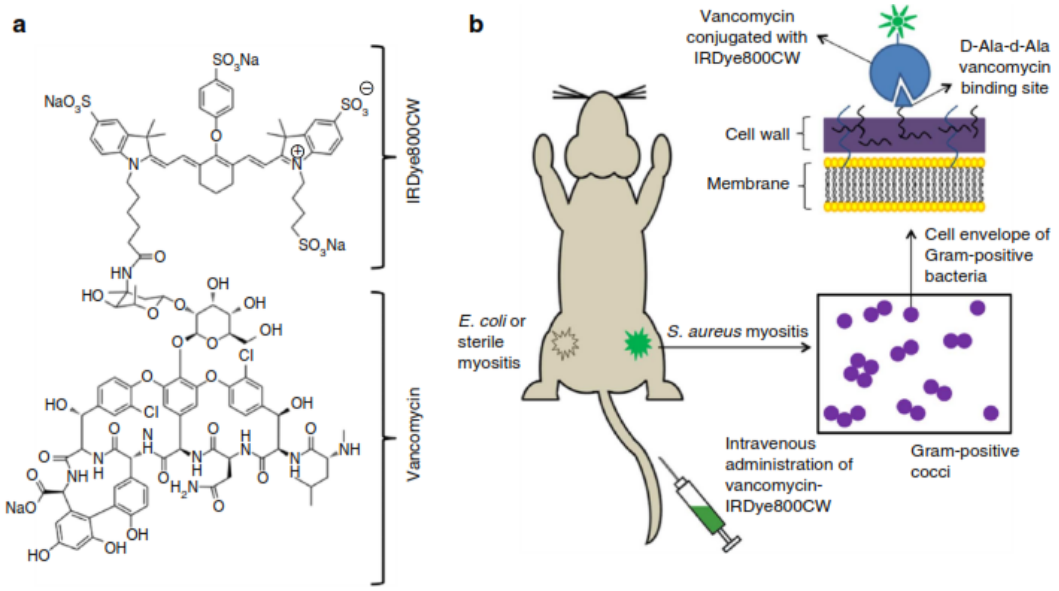

Figure 1.11 Van Oosten, M. *et al.* experimental approach for *in-vivo* imaging of thigh infection using optical imaging probe vancomycin-IRDye 800CW.

(a) Structure of vanco-800CW complex resulting from vancomycin conjugated to near infrared fluorophore IRDye 800CW. (b) Schematic representation of the experimental approach for imaging mice injected with either *S. aureus* (*S. aureus* myositis), *E. coli* (*E. coli* myositis) or Cytodex beads (sterile myositis), and later detection of *S. aureus* with vanco-800CW.

Reprinted by permission from Macmillan Publishers Ltd: Nature Communications (Ref. 21), copyright (2013).

The success of this optical imaging probe drew our attention to the possibility of targeting Gram-positive bacterial cell wall with a radiolabelled probe instead, which would not have any penetration depth issue. Since functionalizing Dfo at its primary amine has been proved to be successful without perturbing the chelating properties of Dfo, Omid Beiraghi used a similar approach for the design of a new probe vancomycin conjugated to radiolabelled Dfo, shown on Figure 1.12

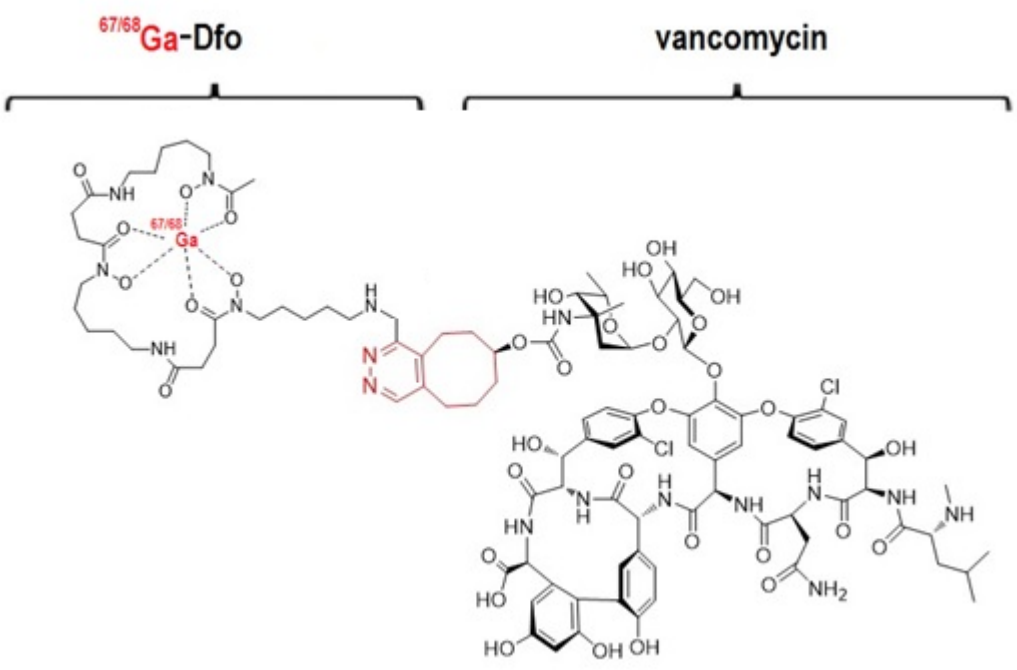

Figure 1.12 Main structure of $^{67/68}$Ga-Dfo-vanc conjugate.
(Figure courtesy of Omid Beiraghi).

Furthermore, targeting Gram-positive bacteria using vancomycin is clinically relevant as more than 99 % of clinical *S. aureus* isolates remain susceptible to vancomycin. Vancomycin has been the cornerstone of treatment for patients with methicillin resistant *S. aureus* (MRSA) infections.[52, 53]

1.7. Bacterial Models for *in vitro* studies

The Infectious Diseases Society of America named ESKAPE pathogens, a group of antibiotic-resistant bacteria that account for two-thirds of observed clinical infections. The ESKAPE organisms are *Enterococcus faecium*, *Staphylococcus aureus*, Enterobateriaceae species *Klebsiella*

pneumoniae and more recently included *Escherichia coli*, *Acinetobacter baumannii*, *Pseudomonas aeruginosa* and *Enterobacter* species.[54, 55, 56]

S. aureus, which causes skin, respiratory and wound infections is particularly relevant, as it is the leading cause of skin and soft tissue infections (SSTI) responsible for substantial morbidity and mortality around the world.[52, 57, 58, 59] More people die of MRSA infection in US hospitals than of HIV/AIDS and tuberculosis combined.[60] On the other hand, pathogenic *E. coli,* mainly related to urinary tract infections, and blood stream infections has separately emerged as the Gram-negative bacteria with the most clinical relevance.[61, 62]

SENTRY, one of the most comprehensive antimicrobial surveillance programs worldwide, reported in the period from 1998 to 2004 that *S. aureus* ranked first as a causative agent of SSTI, with an overall prevalence of 44.6 % in North America, 37.5 % in Europe and 33.5 % in Latin America. *E. coli* ranked second in Latin America (14.0 % prevalence), third in Europe (10.8 %) and fourth in North America (7.2 %).

More recently, the World Health Organization (WHO) Global Report on Antimicrobial Resistance Surveillance in 2014 presented *S. aureus, E. coli* and *K. pneumoniae* as the leading causes of hospital-associated infections, with more than 50% of them resistant to commonly used specified antibacterial drugs in many locations.[62]

In the light of the clinical relevance of Gram-positive *S. aureus* and Gram-negative *E. coli,* both were chosen as bacterial models for the *in vitro* assessment

of molecular imaging probes targeting the siderophores-uptake pathway and peptidoglycan synthesis in the cell wall.

1.8. **Chrome azurol S assay for Fe(III)**

The ternary complex of Fe(III) / chrome azurol S(CAS) / hexadecyltrimethylammonium bromide (HDTMA) has an extinction coefficient of ~ 100 000 $M^{-1}cm^{-1}$ at 630 nm in a solution buffered at pH 5.6, and is used to detect Fe(III) colorimetrically. The dye is orange in the absence of Fe(III), changing to blue in the presence of Fe(III). HDTMA is a cationic detergent that is added to CAS agar or CAS buffer to stabilize the Fe-CAS indicator complex. 5−Sulfosalicylic acid (5-SSA) is used as a shuttle to speed up iron exchange between the CAS/ HDTMA complex and aquairon(III) complexes or other weak chelators, Similarly, 5-SSA's ability to quickly chelate iron to form a low stability complex speeds the transfer of Fe(III) to siderophores in the solution.[63, 64, 65] The CAS assay only detects free Fe(III); it has negligible affinity for Fe(II), and it cannot effectively compete with siderophores for Fe(III) binding. In addition, as discussed in Chapter 2, it appears to be unable to displace hydrating water and hydroxide ions from aquairon(III) complexes. Piperazine is used as a buffer because its pK_{a2} = 5.55 is close to the desired pH 5.6, it is highly water soluble, has good stability in storage, and does not react with proteins.[66, 67]

Figure 1.13 shows the general structure of CAS and 5-SSA.

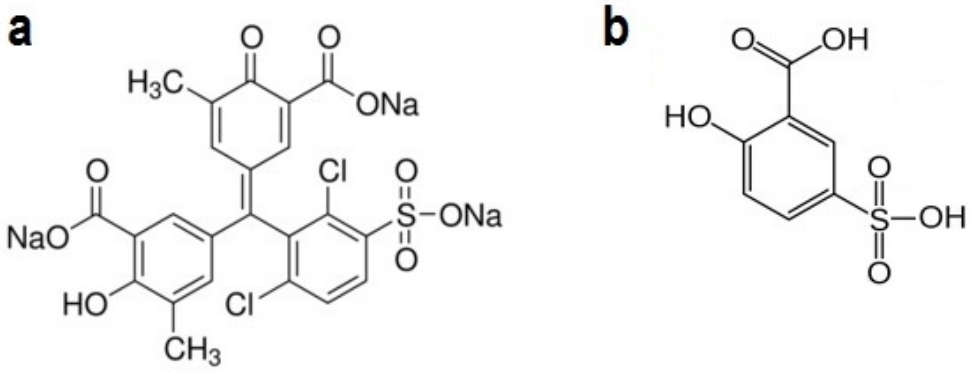

Figure 1.13 CAS buffer active ingredients that coordinate to Fe(III).
(a) Chrome azurol S (CAS); (b) 5-sulfosalycilic acid (5-SSA).

Chapter 2 - **IRON SCAVENGING RESINS**

2.1. Introduction

Growing bacterial cultures in rigorously iron-free media is a challenge because even media with no added iron contain enough for bacterial growth. This is a general problem for any research involving iron uptake and siderophores. In our work, specifically, it was a problem because we wanted to create media that were sufficiently iron-deficient that bacteria would be forced to take up iron-siderophore complexes in order to survive. At present, there is no protocol or commercially available product to accomplish this.

In order to create highly iron-deficient solutions, our goal was to create an easy to use solid-phase iron scavenger. We accomplished this by coupling Dfo to a commercially available resin, cyanogen bromide-activated Sepharose® 4B. We determined the iron binding capacity of the resulting new Dfo-Sepharose resin required to remove trace amounts of Fe(III) from the medium. This new chelating method made possible to reduce Fe(III) to undetectable concentrations; however, *E. coli* cells were still able to grow in this media.

2.2. Materials and Methods

2.2.1. Colorimetric assay to determine Fe(III) concentration

Chrome azurol S (CAS) assay

The CAS assay was used to measure free Fe(III) concentrations in solution, and to monitor the Fe(III)-binding capacity of Dfo-resin preparations. The assay was performed essentially as described previously.[65]

CAS buffer (50 mL) was prepared by mixing 15 mL of 28.73 % (w/v) piperazine, 6 mL of 10 mM hexadecyltrimethylammonium bromide (HDTMA), 10 mL of 40 mM of 5-sulfosalicylic acid and 3.75 mL of 4 mM CAS dye (Chromeazurol S, the indicator for metal titration). The pH was adjusted to 5.6 and the volume adjusted to 50 mL with ddH_2O.

A standard curve of 0 to 20 µM Fe(III) was prepared by making serial dilutions of 100 µM $FeCl_3$ in 10 mM HCl into ddH_2O, as described below (Table 2.1), followed by addition of 500 µL CAS buffer.

Table 2.1 Standard curve preparation for CAS assay

$[Fe^{3+}]$ (μM)	Volume of 100 μM $FeCl_3$ in10 mM HCl (μL)	ddH_2O(μL)	CAS (μL)
0	0	500	500
1	10	490	500
2	20	480	500
4	40	460	500
6	60	440	500
8	80	420	500
10	100	400	500
20	200	300	500

Samples were prepared by taking 500 μL aliquots (diluted with ddH_2O, if necessary, to a final volume of 500 μL) and adding them to 500 μL of CAS buffer. Standards and samples were vortexed, then transferred into 1.5 mL disposable plastic cuvettes, and A_{630} values were read using Cary 100 UV-Vis spectrophotometer.

Because the standard curve was not linear, a second order equation was used to fit [Fe(III)] vs A_{630} :

$$A_{630} = a[\text{Fe(III)}]^2 + b[\text{Fe(III)}] + c$$

[Fe(III)] in samples was calculated using fitted values of *a*, *b*, and *c*:

$$[\text{Fe(III)}] = \frac{-b + \sqrt{b^2 - 4a(c - A_{630})}}{2a}$$

Pre-cleaning procedure for CAS buffer

CAS dye was treated with a number of reagents in an attempt to remove potential contaminants. Ethylenediaminetetraacetic acid (EDTA) (BioShop

Canada Inc.), charcoal (Sigma-Aldrich) and the chelating resins Chelex® 100 (Sigma-Aldrich), Dowex® 50XW8 (Alfa Aesar), Chelating Sepharose™ and SP Sepharose™ (GE Healthcare Bio-Sciences AB) (Figure 2.1) were tested.

The routine pre-treatment of CAS buffer with resins was the following: 50 mL of CAS buffer was treated with 1.5 to 2.5 g of each resin by gentle shaking incubation at room temperature for 16 to 24 h. EDTA was used to treat CAS buffer at a concentration of 10 mM by adding 7.4 mg of EDTA, disodium dehydrate to 2 mL of CAS buffer and leaving it with gentle shaking incubation at room temperature for 16 to 24 h. Charcoal was briefly tested by using 0.1 g to treat 2 mL of CAS buffer, then it was vortexed and spun down. Immediate disappearance of CAS buffer color was observed after charcoal treatment indicating the removal of CAS from the solution; therefore, charcoal treatment was quickly discontinued. As Chelex® 100 performed best, the final purification method selected was to treat 50 mL CAS buffer with 2.5 g of Chelex® 100 resin sodium form (Sigma-Aldrich, ≥ 0.3 meq/mL wet binding capacity, 0.6 meq/g binding capacity - heavy metal ions) by gentle shaking incubation at room temperature for 16 to 24 h.[68]

2.2.2. Iron-deficient Tris-minimal succinate (TMS) growth medium.

Tris-minimal succinate (TMS) growth medium was made essentially as described previously, except that whereas the normal recipe called for 10 μM $FeCl_3$, called TMS_{10}, it was sometimes made without added $FeCl_3$, called TMS_0.[69]

Concentrated (25×) Tris minimal salts stock was prepared by dissolving 145 g of NaCl, 92.5 g of KCl, 27.5 g of NH_4Cl, 3.55 g of Na_2SO_4, and 6.8 g of KH_2PO_4 in 1 L ddH_2O with vigorous stirring. TMS was prepared by mixing 40 mL from 25× Tris minimal salts stock with 12.1 g of Tris base, 16.6 g of succinate, 50 mL of 20 % casamino acids (w/v) and ddH_2O up to ~ 800 mL. The pH was adjusted to 7.4, followed by autoclaving (121 ºC for 20 min). To the autoclaved preparation, the following filtered sterilized ingredients were added: 2 mL of tryptophan (10 mg/mL), 1 mL cysteine (22 mg/mL), 1 mL thiamine (16.9 mg/mL), 1 mL nicotinic acid (1.23 mg/mL), 1mL pantothenic acid (0.5 mg/mL), 1 mL biotin (0.01 mg/mL), 1 mL $MgCl_2$ (95.3 mg/mL), 1 mL $CaCl_2$ (11.1 mg/mL), and 1 mL $FeCl_3$ (100 mM) for TMS_{10}, or no added $FeCl_3$ for TMS_0. Autoclaved ddH_2O was used to adjust the final volume to 1 L of TMS medium.

2.2.3. Iron depleted TMS growth media (TMS_{0R}, TMS_{0RC}, TMS_{0R+R})

Dfo coupled to cyanogen bromide-activated Sepharose® 4B resin

The initial protocol for Dfo coupling to Sepharose was developed by Christina (Cheng) Li, (personal communication). Cyanogen bromide-activated Sepharose® 4B resin (0.4 g) was washed with 10 mL of 1 mM HCl in a 14 mL Falcon tube. The tube was gently shaken for 10 min at room temperature and later centrifuged at 5450 *g* at 4 °C for 6 min. Supernatant was discarded and the resin was washed with 10 mL of 1 mM HCl, gently shaken, and spun down twice under

the same conditions. The resin was then washed twice with 10 mL of ddH_2O by inverting the tube gently three to four times, centrifuging each time at 5450 *g* at 4 °C for 6 min, and decanting the supernatant. The resulting hydrated resin had a packed volume of ≈ 2 mL.

A Dfo solution (1.2 mM, 5 mL) in 0.1 M $NaHCO_3$, pH 8.4, was added to the resin and left on a rocker to gently shake at room temperature for 6 h or overnight. The following day, the tube was centrifuged at 5450 *g* at 4 °C for 6 min. The supernatant was discarded and the pellet was washed with 10 mL of 0.1 M $NaHCO_3$, pH 8.4, twice, using the same centrifugation conditions. Then, 10 mL of 0.2 M glycine, pH 8 was added to the pellet and left on the rocker to gently shake at room temperature for 2 h in order to react with any remaining CNBr-activated sites on the resin. The resin was washed with 10 mL of 0.1 M $NaHCO_3$, pH 8.4, followed by a wash with 10 mL 0.1 M NaOAc, pH 4, then twice with 10 mL of 0.1 M $NaHCO_3$, pH 8.4, under the same centrifugation conditions. The resulting Dfo-Sepharose resin contained 3 nmol Dfo / µL packed volume of wet resin. After the last washing step, 8 mL 0.1 M $NaHCO_3$, pH 8.4 were added to the resin which was finally stored at 4°C.

Dfo-Sepharose resin capacity assays

The Fe(III) binding capacity of Dfo-Sepharose was determined by measuring residual free Fe(III) in treated solutions. The procedure was modified over time, including adding 0.5 mM 5-sulfosalycilic acid (5-SSA) to help

maintain Fe(III) in solution during the assays (see Results). Two typical procedures were developed.

Procedure 1:

In a 2 mL centrifuge tube containing 500 µL of 100 µM $FeCl_3$ in 0.1 M NaOAc, pH 5.6, a 10 µL packed volume of Dfo-Sepharose resin was added. The tube was left to gently rock for 2 h at room temperature. The resin was then separated from the solution and triplicate 100 µL aliquots were taken for the CAS assay to determine the free Fe(III) concentration. At the same time, triplicate CAS assays were performed on the equivalent untreated solution. The number of moles of Fe(III) removed solution per µL of resin was calculated as follows:

Fe(III) binding capacity ($nmol/\mu L_{wet\ resin}$)

$$= ([Fe(III)]_i - [Fe(III)]_f) \times V_{buffer} / V_{wet\ resin},$$

where $[Fe(III)]_i$ is the initial Fe(III) concentration in buffer, $[Fe(III)]_f$ is the final concentration after resin treatment, V_{buffer} is the initial buffer volume, and $V_{wet\ resin}$ is the volume of wet resin added.

Procedure 2:

In a 14 mL Falcon tube, 10 mL of 10 µM $FeCl_3$ were prepared in 0.5 mM 5-SSA, 0.1 M NaOAc, pH 5.6. Aliquots of 1 mL, 2 mL and 4 mL were transferred to 14 mL Falcon tubes, and 10 µL of Dfo-Sepharose resin (wet packed volume) was added to each. The tubes were left gently rotating. Aliquots (100 µL) were collected at t = 2 h, 4 h and 24 h, and free [Fe(III)] determined. Then the resin iron-binding capacity was calculated as in Procedure 1.

TMS_{0R}: TMS_0 scavenged with Dfo-Sepharose resin

TMS_{0R} was iron-deficient TMS, TMS_0, treated with Dfo-Sepharose resin. For routine scavenging of TMS_0 with Dfo-Sepharose to make TMS_{0R}, 320 µL of wet packed volume of coupled Dfo-resin preparation, was used to treat 5 mL of TMS. In order to do this, a stock of 2 mL packed volume of resin siting in the bottom of a 14 mL Falcon tube containing 8 mL of 0.1 M $NaHCO_3$, pH 8.4, was gently vortexed to resuspend the resin. A 1.6 mL aliquot of resuspended resin in bicarbonate storage solution was transferred to a new 14 mL Falcon tube and centrifuged at 5450 *g* at 4 °C for 6 min. This 1.6 mL aliquot is the equivalent of 320 µL of wet packed volume of resin upon removal of bicarbonate storage solution. After the tube was centrifuged, the supernatant was carefully discarded. The resin was washed with 1.6 mL of ddH_2O, centrifuged at 5450 *g* at 4 °C for 6 min and ddH_2O was carefully discarded. Then, we added 5 mL of TMS to the 320 µL of wet packed volume of resin and we left the tube under gently rotating conditions at 4°C overnight (16 to 24 h). This treatment condition is equivalent to 64 µL of packed wet volume of Dfo-resin/ mL of TMS, or 13 mg of dry CNBr-activated Sepharose® 4B resin per mL of TMS, since 0.4 g of dry CNBr-activated Sepharose® 4B render 2 mL of packed volume resin. After overnight treatment, the treated media was filter sterilized and the resin was washed in ddH_2O and stored in 0.1 M $NaHCO_3$, pH 8.4, at 4°C for future regeneration.

TMS_{0RC}: TMS_0 scavenged with Chelex® 100 and Dfo-Sepharose resin

The TMS_0 recipe was followed, except that $MgCl_2$ and $CaCl_2$ were initially left out. Then, 2.5 g of dry Chelex® 100 resin was added to 50 mL of medium and it was rocked gently at 4°C for 16 to 24 h. The following day, the Chelex® 100 was decanted, and 50 µL each of filtered sterilized ultrapure $MgCl_2$ (95.3 mg/mL) and $CaCl_2$ (11.1 mg/mL) were added. Then, 320 µL of wet packed volume of coupled Dfo-resin was added to a 14 mL Falcon tube containing 5 mL aliquot of this preparation keeping treatment condition of 64 µL Dfo-Sepharose resin per mL of TMS. The tube was left under gently rotating conditions at 4°C for 16 to 24 h. After overnight treatment, the treated media was filter sterilized and the resin was washed in ddH_2O and stored in 0.1 M $NaHCO_3$, pH 8.4, at 4°C for future regeneration.

TMS_{0R+R}: TMS_{0R} with added fresh Dfo-Sepharose resin

After decanting the Dfo-Sepharose resin used to prepare TMS_{0R}, fresh Dfo-Sepharose resin was added to the treated media keeping treatment condition of 64 µL Dfo-Sepharose resin per mL of TMS, or 13 mg of dry CNBr-activated Sepharose® 4B resin per mL of TMS.

Regeneration of Dfo-Sepharose resin

The protocol was first developed by Christina (Cheng) Li (personal communication). Used Dfo-Sepharose resin was washed with 5 volumes of ddH_2O, and the water decanted. The resin was resuspended in 5 volumes of

10 mM Dfo in 0.1 M NaOAc buffer, pH 4. This was left rocking at 4ºC for 16 to 24 h. The following day the Dfo solution was decanted and the resin was washed twice with ddH_20 and stored in 0.1 M $NaHCO_3$, pH 8.4, at 4°C.

Monitoring Escherichia coli growth

A preservation culture of *E. coli* (ATCC 700926) in 20 % glycerol was scratched and grown into 5 mL TMS_0 (including or not 5-SSA) in a sterile 14 mL Falcon tube at 37 °C with shaking at 300 rpm for 16 to 24 h. The OD_{600} of the overnight culture was measured and the aliquot size was calculated to create 5 mL culture with OD_{600} = 0.1. Four aliquots were pelleted by centrifugation at 12 500 *g* for 1 min, washed with 5 mL of fresh medium (TMS_{10}, TMS_0, TMS_{0R}, TMS_{0RC}, or TMS_{0R+R}), then pelleted again and resuspended in 5 mL of fresh medium. Culture was incubated at 37 °C with shaking at 300 rpm shaking for 24 h. The OD_{600} was monitored every hour from 0 to 6 h and at 24 h.

2.3. Results

2.3.1. Pre-cleaning procedure of CAS buffer

The colour of freshly made CAS buffer changed over time, indicating possible dye degradation. Also, in titrations of siderophore-containing solutions the apparent Fe(III) concentrations became significantly negative (i.e., A_{630} was lower than for the iron-free standards) at high siderophore concentrations. The apparently negative Fe(III) concentration was an artifact of the CAS assay that was observed when the samples had a lower A_{630} value than the blank sample. The reason for this artifact is unclear; it could be due, for example, to CAS dye degradation or metal contamination.

In early experiments with untreated CAS dye, the apparent Fe(III) concentration became increasingly negative with Dfo-Sepharose treatment (see Section 2.3.4). Different treatments of CAS dye were attempted to remedy these problems. Although none of the treatments entirely eliminated the negative apparent Fe(III) concentrations, some reduced the magnitude of the negative values, and reached a clear minimum value even in the presence of excess Dfo-Sepharose. Treatments were evaluated through siderophore titrations to detect apparently negative Fe(III) concentrations, as well as visible spectra between 330 and 730 nm where Fe(III)-bound CAS buffer has a absorption maximum near 630 nm.[65] CAS dye was treated with cation exchange resins, namely Chelex®100,

Dowex® 50WX8, Chelating Sepharose™, and SP Sepharose™ (Figure 2.1), as well as EDTA and charcoal.

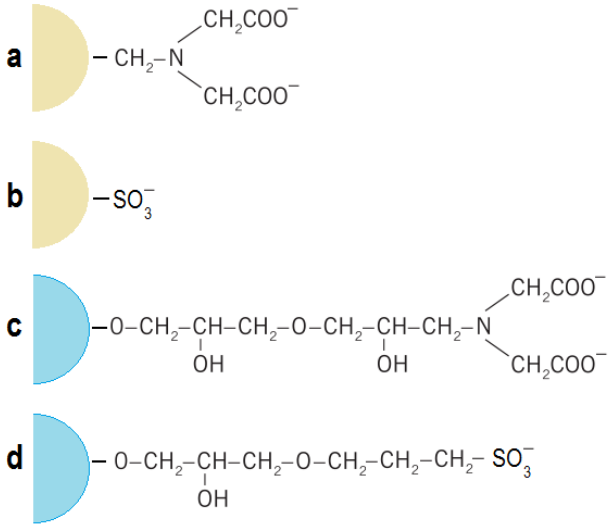

Figure 2.1 Chelating resins tested for the assessment of best pre-cleaning conditions of CAS buffer.
(a) Chelex®100; (b) Dowex® 50WX8; (c) Chelating Sepharose™; (d) SP Sepharose™. Beads: hydrophobic bead represented in color beige: Styrene-divinylbenzene; hydrophilic bead represented in color blue: Sepharose.

Changes in the spectra of treated CAS buffers were visible, though no treatment was unambiguously better than the others (Figure 2.2). Chelex® 100-treated CAS buffer still gave negative apparent Fe(III) concentrations in Dfo-Sepharose titrations, but less than untreated CAS buffer (Figure 2.3), and the apparent Fe(III) concentration plateaued at very high amounts of Dfo-Sepharose. In contrast, treatment with Dowex® 50WX8 led to lower negative apparent Fe(III) concentration values compared to the ones resulting from untreated CAS buffer (Figure 2.4). No treatment of the CAS buffer eliminated negative apparent Fe(III) concentrations. Chelex® 100 treatment was selected for routine use based

on its better ability of alleviating the tendency of increasing negative apparent Fe(III) concentrations as a results of an experiment artifact.

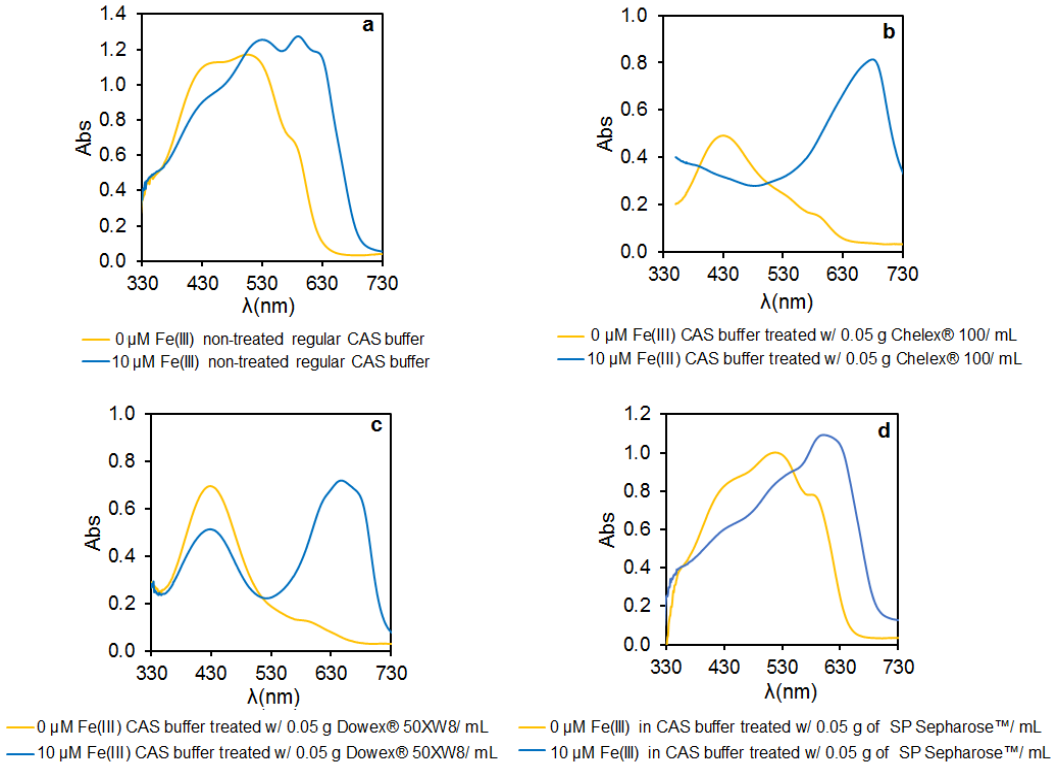

Figure 2.2 CAS buffer absorption spectra (330 to 730 nm) including 0 and 10 µM Fe(III).
(a) Non-treated CAS buffer; (b) CAS buffer treated with Chelex® 100 resin (0.05 g/ mL); (c) CAS buffer treated with Dowex® 50XW8 resin (0.05 g/ mL); (d) CAS buffer treated with SP Sepharose™ resin (0.05 g/ mL).

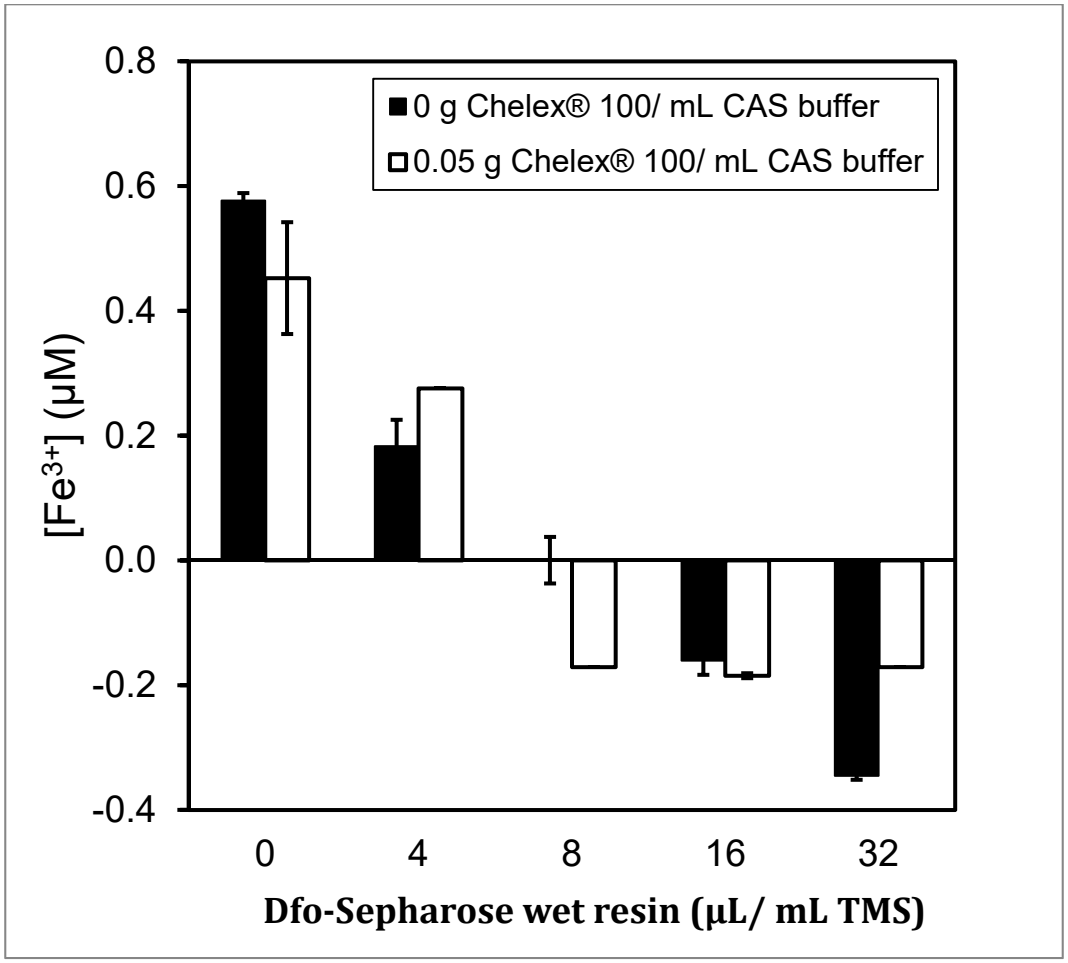

Figure 2.3 CAS assay (CAS buffer treated with Chelex® 100 or not) showing removal of Fe(III) from TMS using Dfo-Sepharose Resin.

Iron concentration determined by CAS assay using either CAS buffer treated with 0.05 g Chelex® 100/ mL or non-treated.

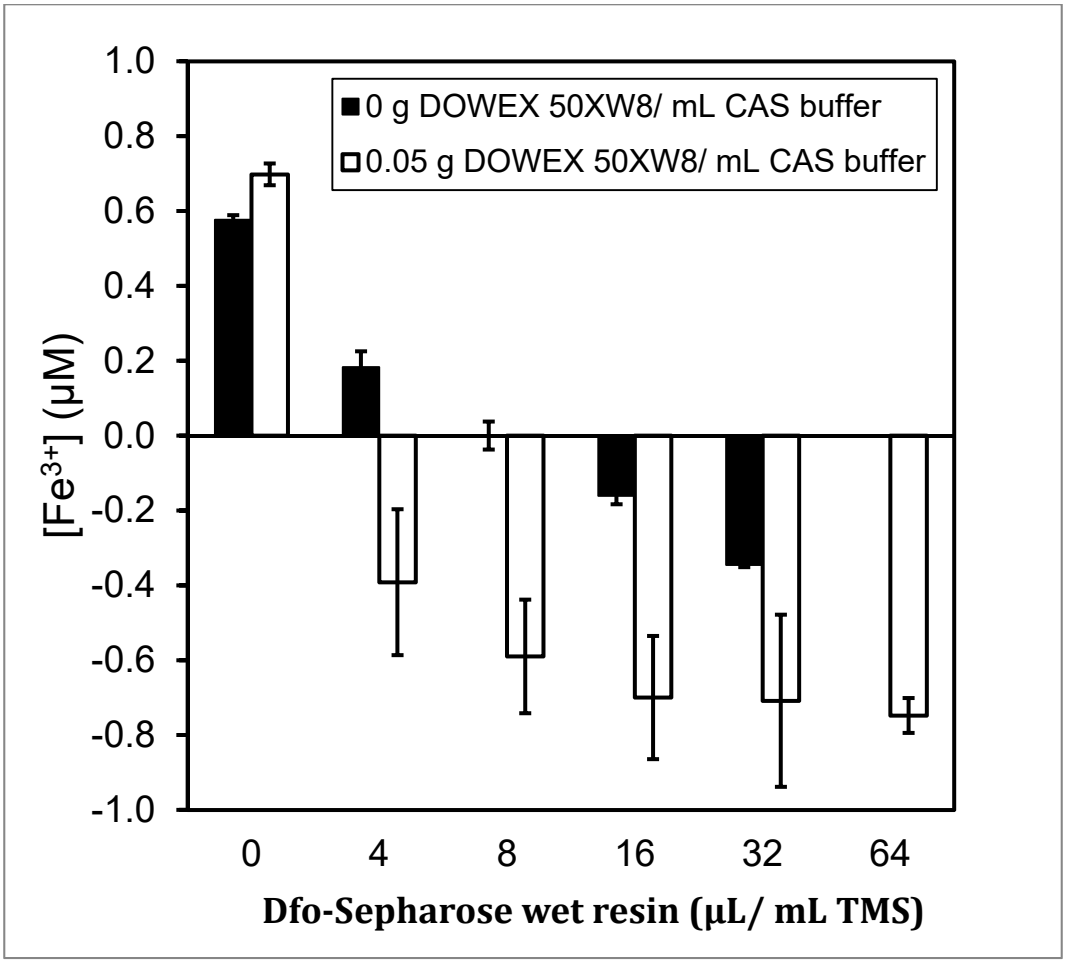

Figure 2.4 CAS assay (CAS buffer treated with Dowex® 50XW8 or not) showing removal of Fe(III) from TMS using Dfo-Sepharose Resin.
Iron concentration determined by CAS assay using either CAS buffer treated with 0.05 g Dowex® 50XW8/ mL or non-treated.

2.3.2. Using 5-sulfosalycilic acid (5-SSA) to stabilize Fe(III)-containing solutions

In the course of determining the Fe(III)-binding capacity of Dfo-Sepharose, it was found that Fe(III)-containing solutions prepared in 0.1 M NaOAc, pH 5.6 were not stable (Figure 2.5). Solutions freshly made from a stock 100 mM $FeCl_3$ solution in 0.1 M HCl contained the expected Fe(III) concentration

of 100 μM. However, the apparent Fe(III) concentrations started decreasing in hours, and decreased 10-fold over 48 h. There was no visible precipitate, and there were no known Fe(III) chelators in the solution, which suggests that the Fe(III) ions were forming tightly-bound aqua complexes.[70] Tight interactions between Fe(III) and water molecules rendered it unavailable to bind with the CAS dye, leading to its apparent disappearance from solution.

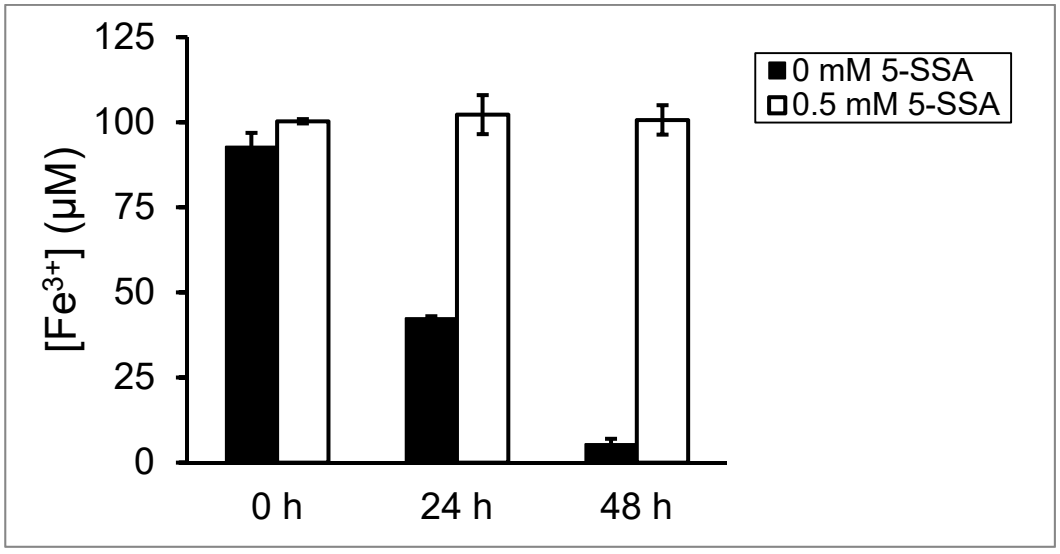

Figure 2.5 Stability of Fe(III) in 0.1 M NaOAc, pH 5.6 and 0.5 mM 5-SSA in 0.1 M NaOAc, pH 5.6 for up to 48 h.
Apparent Fe(III) concentrations were measured in solutions with or without 0.5 mM 5−SSA in 0.1 M NaOAc, pH 5.6 using the CAS assay.

On the assumption that Fe(III) aqua complexes were the problem, several conditions were tested for their ability to maintain Fe(III) concentrations in solution. These included the nitrogen-containing buffers to interact with Fe(III), namely 0.1 M piperazine, pH 5.6, or 0.2 M Tris-Cl, pH 7. 5-SSA (0.05 to 8 mM) in either 0.2 M Tris, pH 7, or 0.1 M NaOAc, pH 5.6 was also tested. The 5-SSA is a low affinity Fe(III) chelator that is used in the CAS assay to accelerate Fe(III)

binding to the CAS dye. Solutions of 0.5 mM to 2 mM 5-SSA in 0.1 M NaOAc, pH 5.6 were the most successful at maintaining Fe(III) in solution, and were used routinely thereafter.

In order to test the Fe(III)-binding capacity of Dfo-Sepharose resin, a solution containing 10 µM $FeCl_3$ and 0.5 mM 5-SSA was treated with 10 µL of packed wet volume of Dfo-Sepharose resin from 0 to 24 h (Figure 2.6). Non-treated solution remained stable, with close to 10 µM Fe(III) measured through the course of the experiment. The iron-binding capacity determined by this method was 1.4 ± 0.3 nmol/µL of resin. Preliminary results also showed that the capacity apparently declined after 2 h treatment.

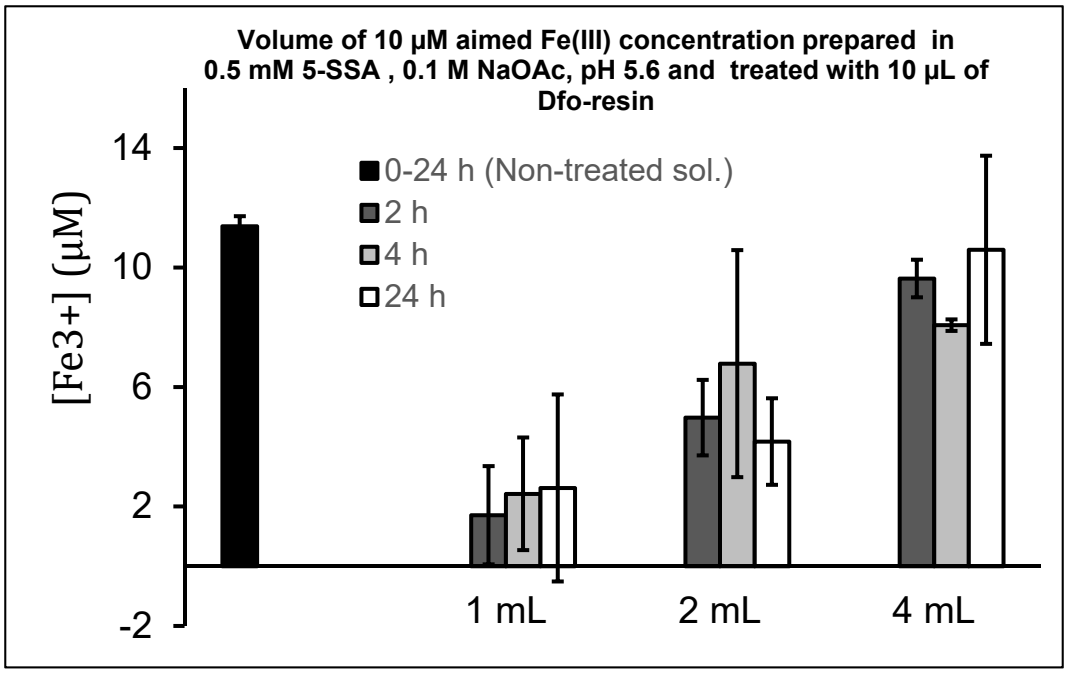

Figure 2.6 Fe(III) concentrations after Dfo-Sepharose resin treatment.
Three aliquots (1 mL, 2 mL and 4 mL) were taken from same stock solution prepared at aimed concentration of 10 µM $FeCl_3$ in 0.5 mM 5-SSA in 0.1 M NaOAc, pH 5.6 and were later treated with 10 µL of packed wet volume of Dfo-Sepharose resin to determine the iron-binding capacity of the resin from 0 to 24 h.

Fe(III) concentrations in TMS were also determined by CAS assay with or without the addition of 0.5 mM 5-SSA to the growth medium (Figure 2.7).

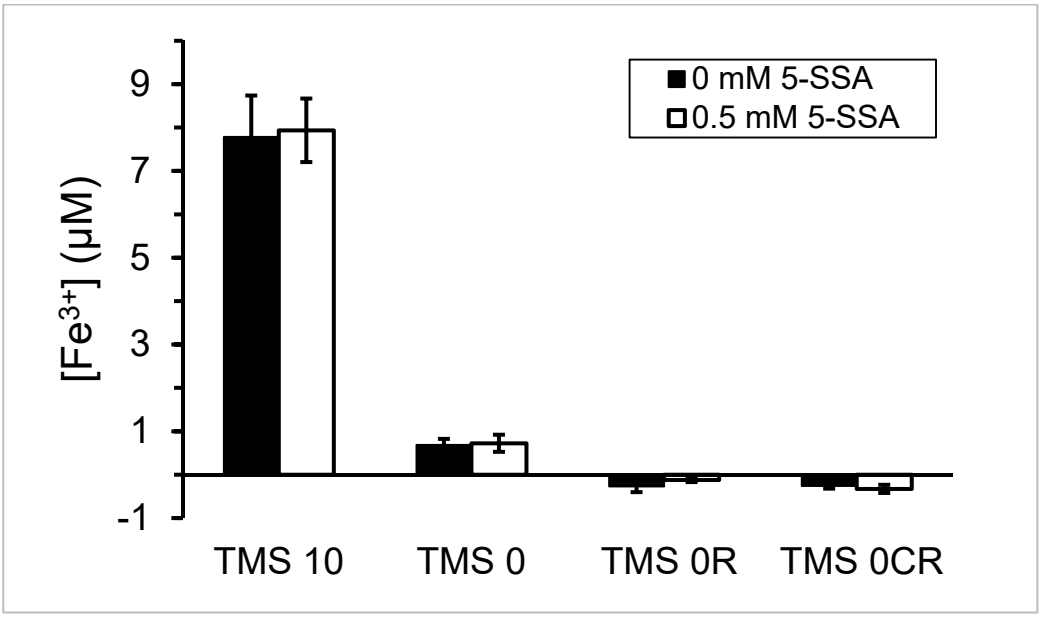

Figure 2.7 Fe(III) concentrations in treated TMS media preparations.
TMS_{10}: TMS including 10 µM $FeCl_3$, TMS_0: TMS without added Fe(III), TMS_{0R}: TMS_0 treated with Dfo-Sepharose resin, TMS_{0CR}: TMS treated with Chelex® 100 resin prior to the addition of Mg and Ca, then treated with Dfo-Sepharose resin after Ca and Mg were added.

2.3.3. Dfo-Sepharose resin capacity assays

CNBr-activated Sepharose was derivatized with Dfo (Figure 2.8).

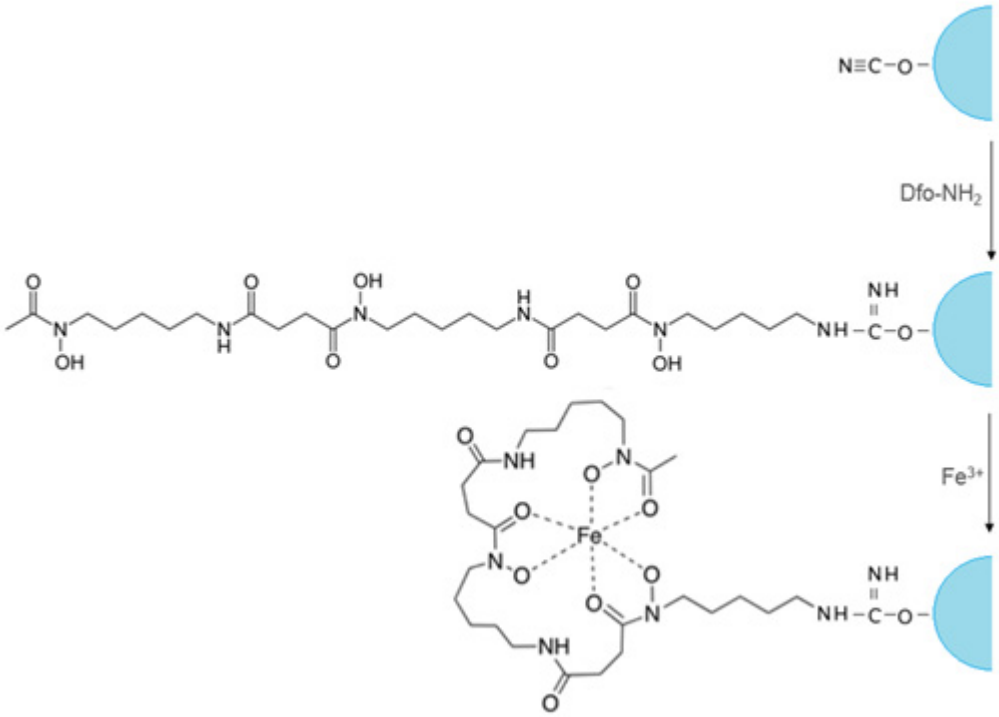

Figure 2.8 Dfo coupled to cyanogen bromide-activated-Sepharose® 4B resin. (up): Cyanogen bromide-activated-Sepharose®4B resin main active structure, (middle): Dfo coupled to Sepharose resin, (down): Dfo coupled to Sepharose resin chelating properties in the presence of Fe(III).

The Fe(III)-binding capacity of Dfo-Sepharose was found to be 3.8 ± 0.5 nmol/µL when 500µL of 100 µM $FeCl_3$ in 0.1 M NaOAc, pH 5.6, was treated with 10 µL of packed volume of Dfo-Sepharose resin for 2 h. This is consistent with the value of 3.1 ± 0.3 nmol/µL previously reported by Christina (Cheng) Li (ChemBio 4GG9 thesis).

2.3.4. Escherichia coli growth in normal and iron-depleted TMS medium

As the goal of this part of the project was to create media sufficiently depleted in Fe(III) that bacteria could not grow, various treatments of TMS

medium were tested. Early experiments did not contain 5-SSA in the growth medium, but later experiments did.

TMS medium normally contains 10 μM added $FeCl_3$.[69] This was called TMS_{10}. TMS medium made without added $FeCl_3$ was called TMS_0. TMS that was treated with Dfo-Sepharose resin was TMS_{0R}, and TMS that was first treated with the non-specific chelator Chelex® 100 before addition of the Mg and Ca salts, followed by Dfo-Sepharose resin treatment of the complete medium, was called TMS_{0CR}. Resin-treated medium TMS_{0R} that includes fresh added resin was referred as TMS_{0R+R}.

TMS_{0R} was used during the initial experiments followed by trials on TMS_{0CR} and TMS_{0R+R}. *E. coli* growth after 24 h (Figure 2.9) was very similar for cultures grown in resin-treated media, namely TMS_{0R}, TMS_{0CR} and TMS_{0R+R}. Although the level of bacterial growth was affected by reduced amount of Fe(III) in the growth medium, bacteria grew well in resin-treated media overall. Given the uncertainty in the Fe(III) concentrations in treated media we need an alternative method for the detection of [Fe(III)] to confirm that iron can be rigorously removed from growth media.

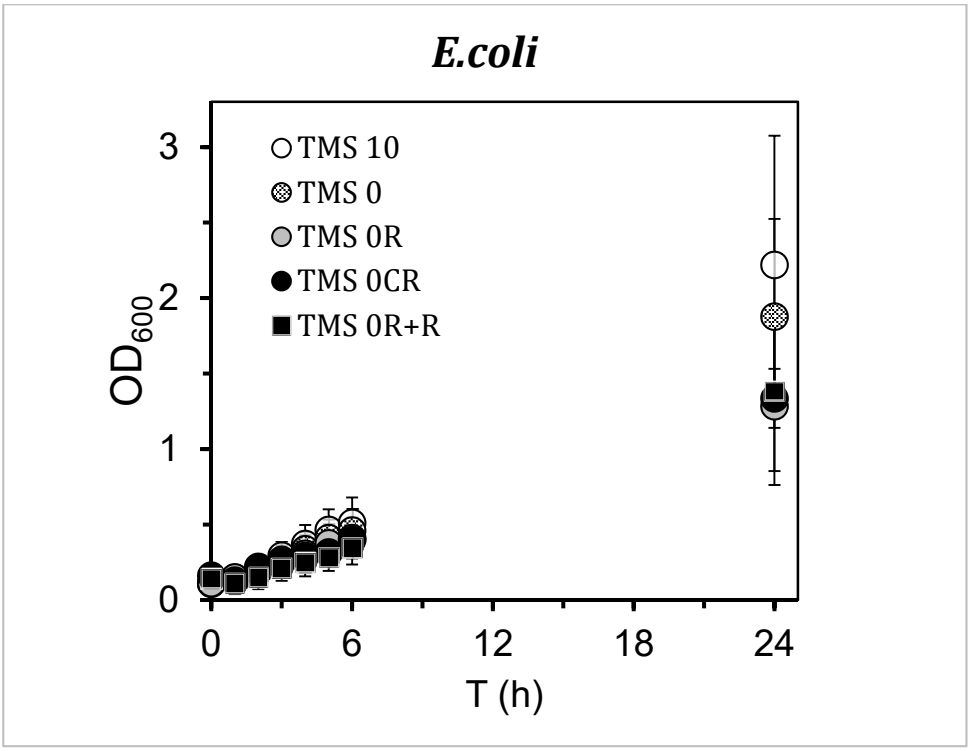

Figure 2.9 *Escherichia coli* growth in TMS media
TMS_{10}: normal TMS (includes 10 µM $FeCl_3$); TMS_0: TMS without $FeCl_3$; TMS_{0R}: TMS_0 treated with Dfo-Sepharose resin; TMS_{0CR}: TMS treated with Chelex® 100 resin prior to the addition of Mg and Ca, then treated with Dfo-Sepharose resin after Mg and Ca were added; TMS_{0R+R}: TMS_{0R} with fresh Dfo-Sepharose resin added.

E. coli growth in TMS_{10}, TMS_0, and TMS_{0R} was followed every hour from 0 to 6 and at 24 h by measuring the OD_{600} in the presence or not of 0.5 mM 5-SSA in each growth medium (Figure 2.10).

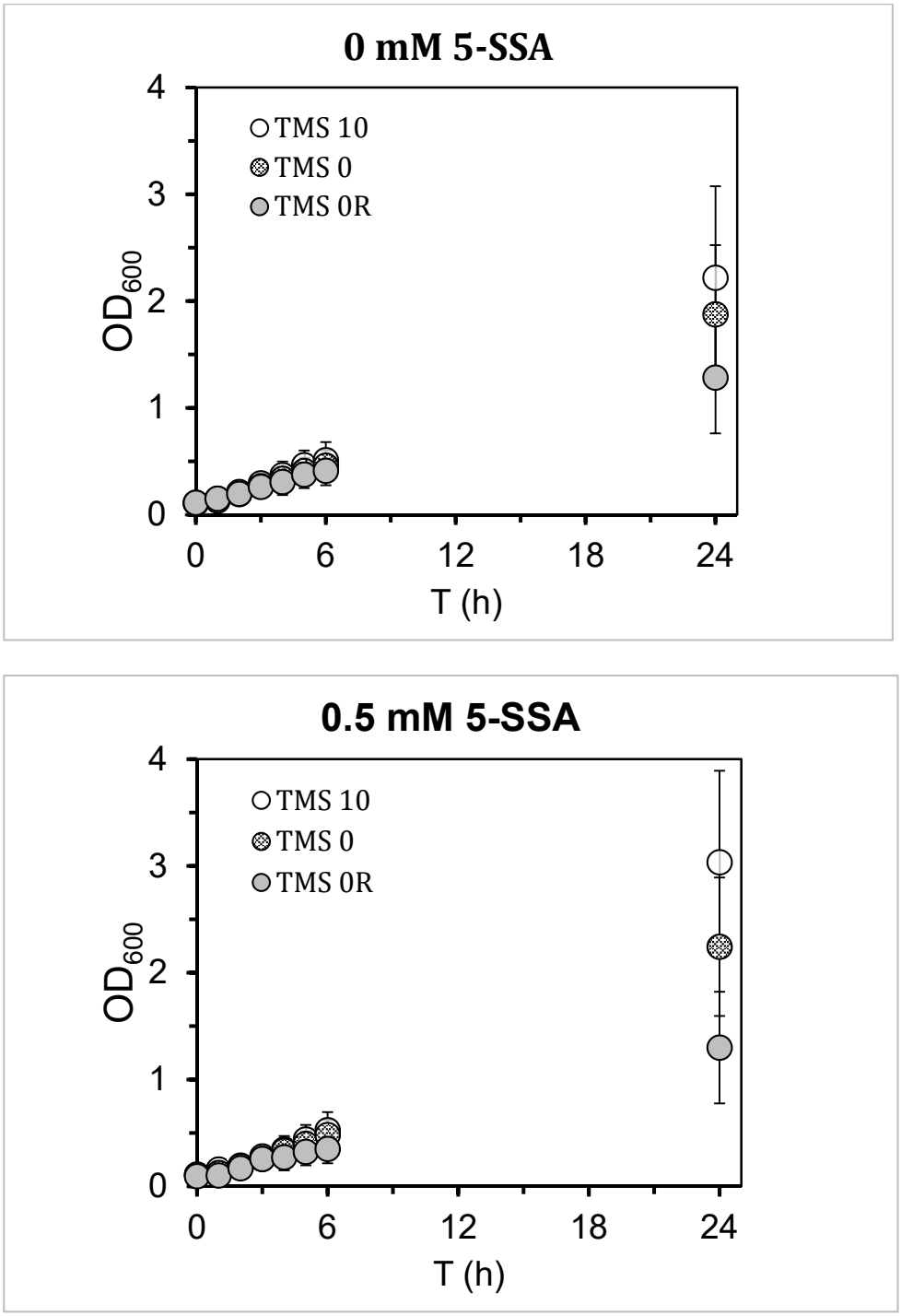

Figure 2.10 *Escherichia coli* growth TMS media with and without 0.5 mM 5-SSA. TMS_{10}: normal TMS (includes 10 µM $FeCl_3$), TMS_0: TMS without $FeCl_3$, TMS_{0R}: TMS_0 treated with Dfo-Sepharose resin.

2.4. Discussion

2.4.1. CAS buffer pre-cleaning procedure

Ideally, the CAS solution should have distinctive absorption spectra in the presence and absence of Fe(III). Non-treated CAS buffer showed signs of unknown contaminants (Figure 2.2a). The contaminants were most likely some combination of metal ions and/or hydrophobic molecules, since best treatments corresponded to non-specific cation exchange resins on a strongly hydrophobic beads, namely Chelex® 100 and Dowex® 50XW8 (Figure 2.2b, Figure 2.2c). CAS buffer treated with Chelex® 100 had a reduced A_{630} level compared with untreated and CAS buffer treated with either SP Sepharose™ or Chelating Sepharose™ resin but should contribute to higher level of sensitivity of CAS assay. Chelex® 100 treatment of CAS buffer alleviated very large negative apparent Fe(III) concentrations TMS_{0R}, but did not completely eliminate the apparent negative Fe(III) concentrations (Figure 2.3). Dowex® 50XW8 treatment also improved the CAS assay's performance, but to a much lower extent compared to Chelex® 100 (Figure 2.4).

2.4.2. Dfo-Sepharose resin capacity assays

The Dfo-Sepharose resin capacity determined in 0.1 M NaOAc, pH 5.6, was 3.8 ± 0.5 nmol/μL of resin; in the presence of 0.5 mM 5-SSA in 0.1 M NaOAc, pH 5.6, it was 3 times smaller than the originally estimated, i.e.,

1.4 ± 0.3 nmol/μL of resin. It is not clear why the apparent Fe(III) concentration increased after the first 2 h of treatment (Figure 2.6). It would have been expected to decrease until the resin was saturated with Fe(III). After that, the Fe(III) concentration should remain stable, near zero.

2.4.3. Escherichia coli growth in normal and iron-depleted TMS medium

Including 0.5 mM 5-SSA did not appear to affect the growth of *E. coli* cells in TMS_{0R} (Figure 2.10). Cells grown in non-treated media had increased growth levels and the difference in growth became more pronounced between them (TMS_0 and TMS_{10}). This difference, most likely relate to the ability of 5- SSA to enhance Fe(III) bioavailability in the media. The fact that cells grown in resin-treated media did not experience significant decreases in growth rate suggests that Fe(III) was still present in the medium in spite of efforts to rigorously remove it. Nonetheless, it appears that iron is a limiting nutrient under these conditions, as there was some decrease in growth rates.

Chapter 3 - ^{67}GA-DFO AND DERIVATIVES: BACTERIAL UPTAKE

3.1. Introduction

The commercially available and clinically proven Dfo is an attractive siderophore for the development of a molecular imaging probe; however, its short plasma half-life of around 5.5 min[41] does not allow sufficient time for uptake by bacterial cells. Bacterial uptake assays using ^{67}Ga−Dfo have shown that levels of uptake increased overtime with a peak value around 6 h of exposure. Hence, our goal was to find a Dfo-derivative with improved pharmacokinetic properties that either stays longer in circulation or is taken up more quickly.

Dfo derivatives were prepared by modifying Dfo at its primary amine with the addition of alkyl or aryl groups, polyethylene glycol, or broad-spectrum antibiotics to modify the molecule's size, polarity, lipophilicity and bacterial binding properties without affecting Dfo's chelating ability. Dfo-derivatives were tested *in vitro* in *S. aureus* using ^{67}Ga−Dfo as the control and excess Ga-Dfo as the competitive blocking control. The majority of derivatives reached uptake rates around 40 % of ^{67}Ga-Dfo. The highest level of uptake was particularly observed for the ciprofloxacin derivative of Dfo at 6 h which reached around 70 % of ^{67}Ga-Dfo's uptake.

3.2. Materials and Methods

^{67}Ga-Dfo-Eoc, ^{67}Ga-Dfo-cipro, ^{67}Ga-Dfo-*N*-(2-methylquinoline), ^{67}Ga-Dfo-*N*-hexyl and ^{67}Ga-Dfo-EG_3-NH_2 were synthesized by Dr. Joseph Ioppolo and Omid Beiraghi from the Valliant Research Group (Table 3.1 and Figure 3.1).

Table 3.1 Description of abbreviated names of Dfo-derivatives

Abbreviated name	Description
Dfo-*N*-hexyl	hexyl derivative of DFO at the primary amino position
Dfo-Eoc	ethyloxycarbonyl derivative of DFO at the primary amino position
Dfo-*N*-(2-methylquinoline)	quinoline derivative of DFO at the primary amino position
Dfo-EG_3-NH_2	triethylene glycol amine derivative of DFO at the primary amino position
Dfo-cipro	ciprofloxacin derivative of DFO at the primary amino position

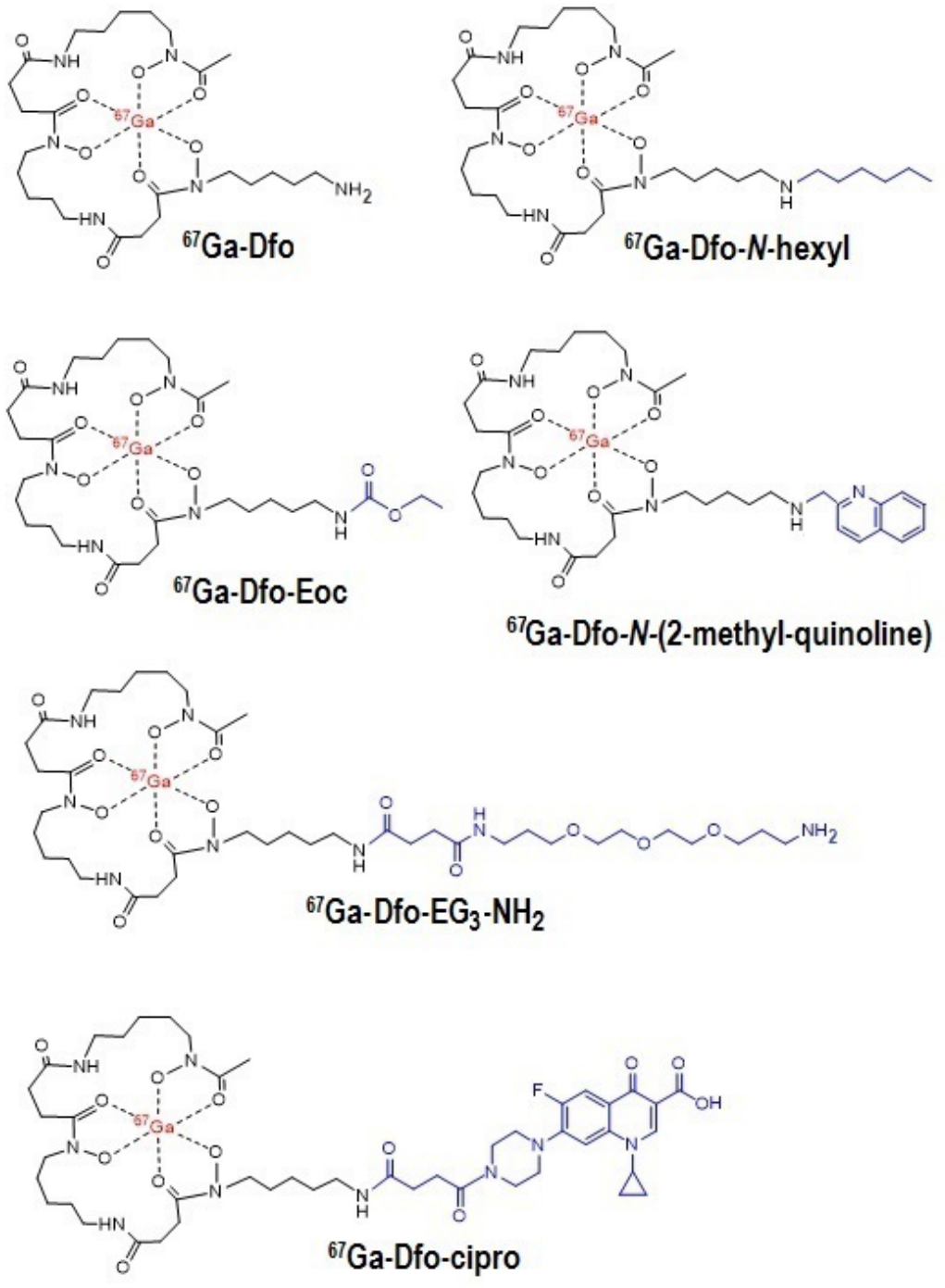

Figure 3.1 General structure of Dfo derivatives coordinated to ^{67}Ga.
(Figure courtesy of Dr. Joseph Ioppolo and Omid Beiraghi.)

Table 3.2 log$D_{7.4}$ of standard Dfo and derivatives

	log$D_{7.4}$	Std dev
^{67}Ga-Dfo	-2.92	± 0.04
^{67}Ga-Dfo-cipro	-1.40	± 0.01
^{67}Ga-Dfo-EG_3-NH_2	N.D.	
^{67}Ga-Dfo-*N*-quinoline	-1.11	± 0.04
^{67}Ga-Dfo-Eoc	-0.77	± 0.01
^{67}Ga-Dfo-*N*-hexyl	1.25	± 0.05

(Lipophilicity as a measured of the 1-octantol: PBS partition coefficient log*D* at physiological pH 7.4 of Dfo-derivatives were determined by Dr. Joseph Ioppolo and Omid Beiraghi). (N.D. = not determined).

3.2.1. In vitro uptake of ^{67}Ga-Dfo and ^{67}Ga-Dfo derivatives in Staphylococcus aureus

A 20 % glycerol preservation culture of *Staphylococcus aureus* (ATCC 25923) was scratched and grown into 45 mL of iron-deficient Tris-Minimal Succinate (TMS_0) growth medium[69] at 37 °C with 300 rpm shaking for 16 to 24 h. Then, OD_{600} of the culture was measured to determine the aliquot size needed to create a 4.5 mL culture with OD_{600} = 2. At OD_{600} = 2, *S. aureus* is in the exponential growth phase, a good starting point for Fe(III) uptake experiments. The aliquots were pelleted by centrifugation at 12 500 *g* for 1 min, washed in fresh TMS_0 medium, then pelleted again under the same centrifuging conditions, then resuspended in 4.5 mL of radioactive uptake medium.

Radioactive uptake medium consisted of 5 mL TMS_0 with added ^{67}Ga-Dfo (control) or the ^{67}Ga-Dfo derivative to a final specific radioactivity of 7.4 Bq/ µL. In subsequent experiments with each batch of ^{67}Ga-labelled complexes, the

chemical concentration of Dfo or Dfo-derivatives was held constant, with corresponding decreases in ^{67}Ga radioactivity as it decayed. ^{67}Ga has a half-life of 78 h.[71]

To ensure ^{67}Ga-Dfo-derivatives are taken up by the same uptake pathway as ^{67}Ga-Dfo, competitive blocking assays using excess unlabelled Dfo were performed. Media in the blocking experiments was prepared in TMS_0 as described above, but with the addition of 50 µM Ga-Dfo.

During uptake assays, the *S. aureus* cultures were incubated at 37 °C with shaking at 300 rpm for up to 24 h. A 500 µL aliquot was removed from each culture tube and centrifuged at 12 500 *g* for 1 min every hour from 0 to 6 h and at 24 h. To ensure that pellets were not disturbed, 480 µL of each supernatant was collected into a 12 × 55 mm Ria plastic test tube (PerkinElmer). Pellets were washed with 500 µL ice-cold phosphate buffered saline (PBS), pH 7.4, (Life Technologies) and centrifuged at 12 500 *g* for 1 min. Again, to ensure pellets were not disturbed, only 500 µL of each supernatant were collected into the same Ria test tube for counting. The remaining pellets then were washed in 400 µL of 5 % sodium dodecyl sulfate (SDS, w/v) and left to lyse for 30 to 45 min at room temperature. A 300 µL aliquot from each lysed pellet was transferred to a separate Ria test tube for counting. Remaining lysed pellets were frozen at -20 °C for protein assays. All Ria test tubes were counted for 1 min using Wizard 1470 Automatic Gamma Counter (PerkinElmer) at the end of each experiment. The

resulting count per minute (cpm) values were used to calculate uptake of the ^{67}Ga-Dfo and its derivatives.

Frozen lysed pellets were thawed at room temperature and protein concentrations were determined following manufacturer's instructions using Pierce™ BCA Protein Assay Kit, using bovine serum albumin as a standard. The total protein concentration of every pellet was determined in triplicate.

Uptake was finally expressed as the ratio of ^{67}Ga in the pellet as a fraction of the total radioactivity (% uptake = cpm_{pellet} / (cpm_{pellet} + $cpm_{supernatant}$) × 100%) and it was normalized to total protein concentration, and presented as % uptake/μg protein.

3.3. Results

The uptake of ^{67}Ga-Dfo was monitored in the presence or absence of excess unlabelled Ga-Dfo in *S. aureus* from 0 to 6 h and at 24 h (Figure 3.2). Cells grown in media containing 50 μM Ga-Dfo competitive blocking control displayed excellent blocking, the uptake being close to cero from 0 to 6 h, followed by a low uptake level at 24 h. For the blocking control samples at short incubation times, the counts in the pellet samples were often lower than the background samples. This resulted in apparently negative extents of uptake, but in reality, the differences between pellet and background were very small, and the apparently negative uptake was simply an artifact of the counting method. These samples were regarded as showing effectively zero uptake.

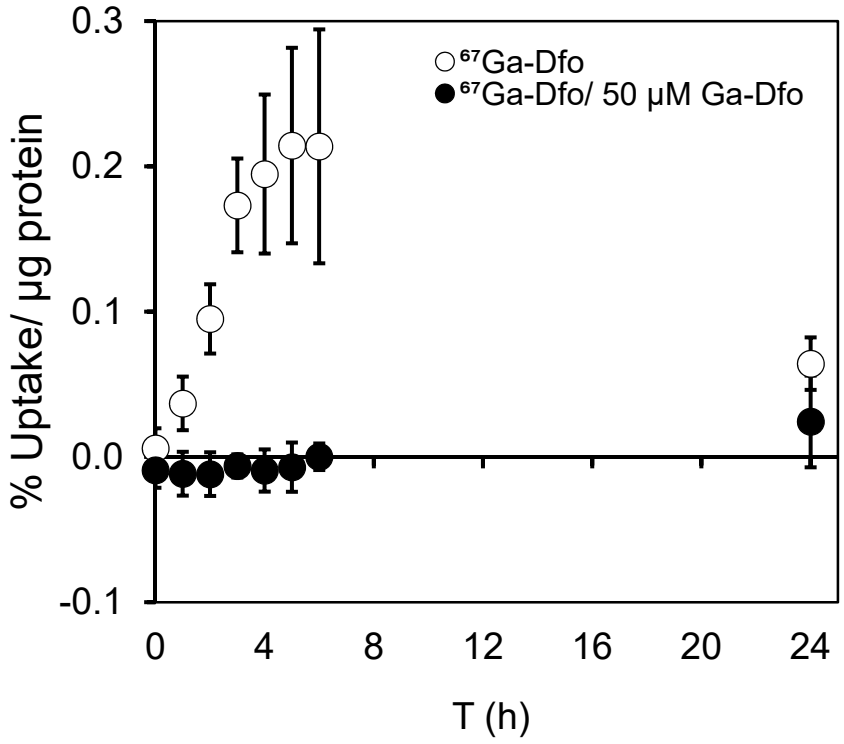

Figure 3.2 Standard ^{67}Ga-Dfo % uptake normalized to protein.
% Uptake from 7.4 Bq/ µL ^{67}Ga-Dfo was monitored in the absence or presence of 50 µM Ga-Dfo competitive blocking control.

Likewise, Dfo-derivatives ^{67}Ga-Dfo-*N*-hexyl (Figure 3.3), ^{67}Ga-Dfo-*N*-(2-methylquinoline) (Figure 3.4),^{67}Ga-Dfo-Eoc (Figure 3.5),^{67}Ga-Dfo-EG_3-NH_2 (Figure 3.6) and ^{67}Ga-Dfo-cipro (Figure 3.7) were tested. Competitive blocking controls for all derivatives showed results similar to ^{67}Ga-Dfo. ^{67}Ga-Dfo-cipro reached the highest levels of uptake from the group of derivatives tested, and was the closest to ^{67}Ga-Dfo. There was negligible ^{67}Ga-Dfo-*N*-hexyl uptake during the initial 6 h, which make it the worst derivative tested. As for the rest of tested probes, they shared very similar uptake levels reaching close to half of ^{67}Ga-Dfo-cipro maximum uptake level at 6 h.

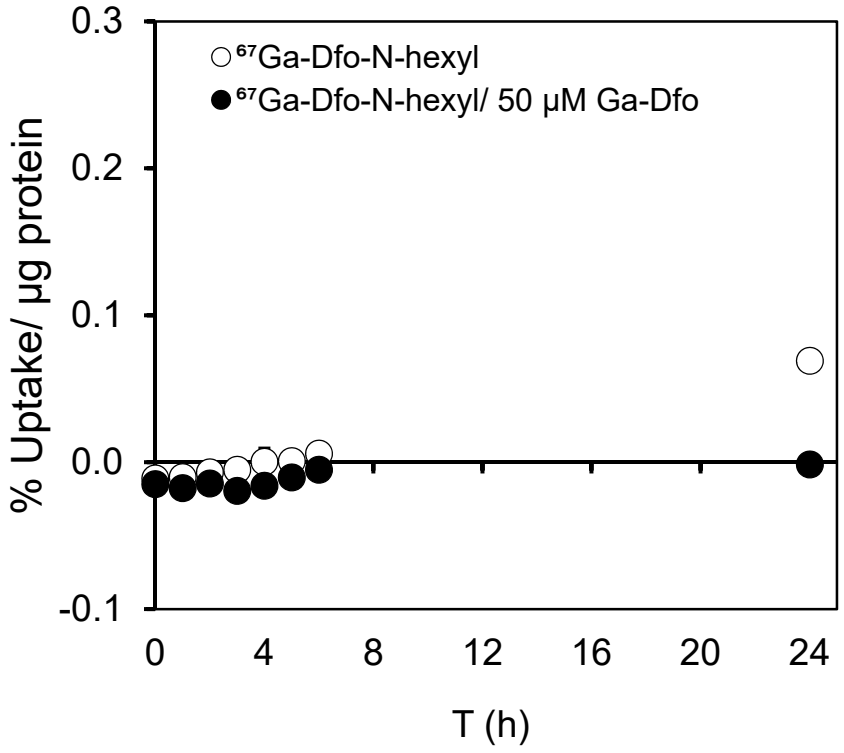

Figure 3.3 ^{67}Ga-Dfo-*N*-hexyl % uptake normalized to protein.
% Uptake from 7.4 Bq/ µL ^{67}Ga-Dfo-*N*-hexyl was monitored in the absence or presence of 50 µM Ga-Dfo competitive blocking control.

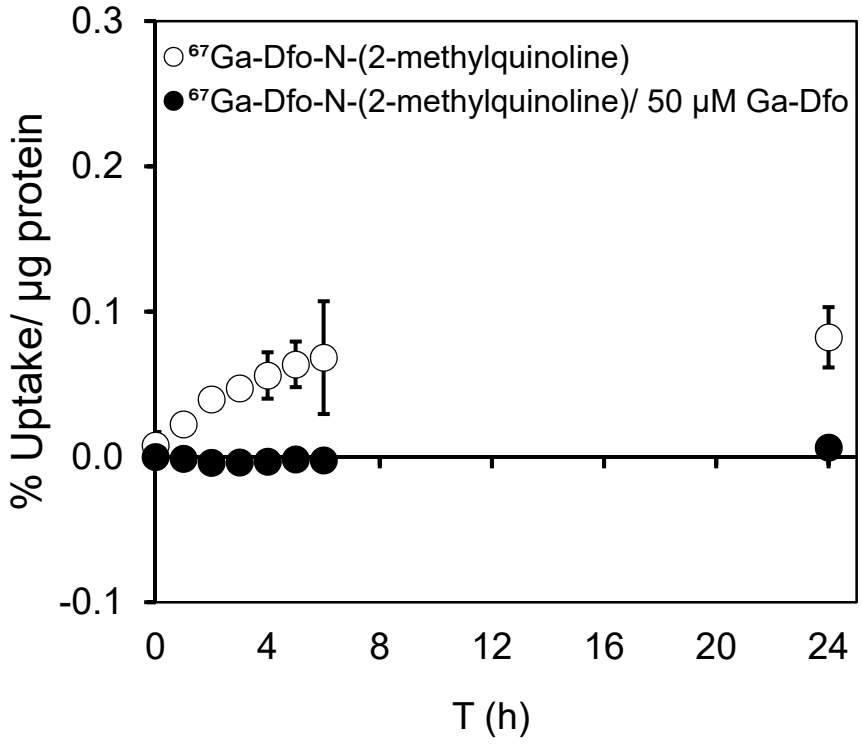

Figure 3.4 ^{67}Ga-Dfo-*N*-(2-methylquinoline) % uptake normalized to protein. % Uptake from 7.4 Bq/ µL ^{67}Ga-Dfo-*N*-(2-methylquinoline) was monitored in the absence or presence of 50 µM Ga-Dfo competitive blocking control.

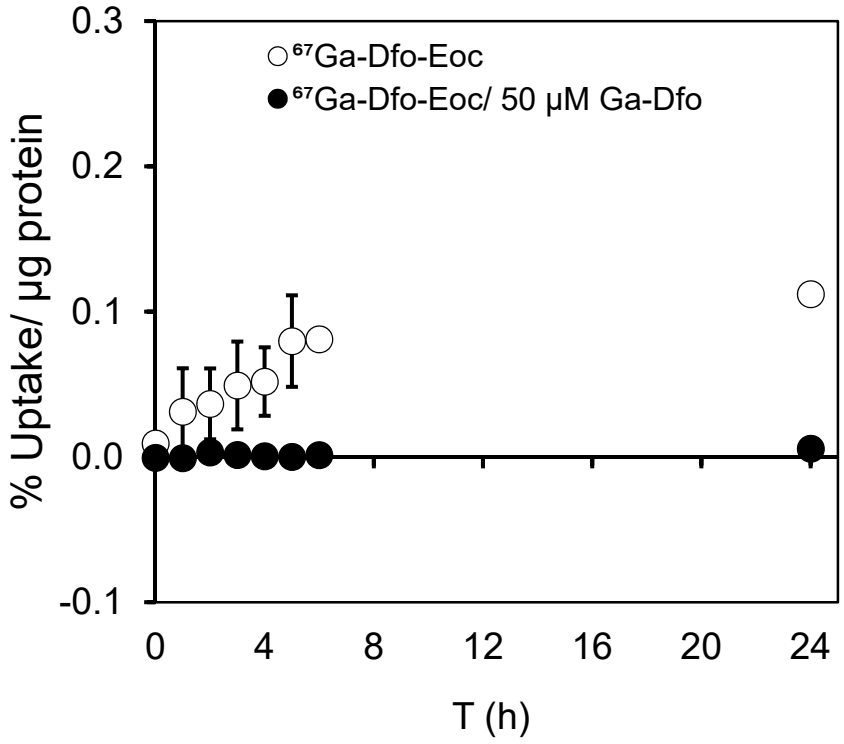

Figure 3.5 ^{67}Ga-Dfo-Eoc % uptake normalized to protein.
Uptake from 7.4 Bq/ µL ^{67}Ga-Dfo-Eoc was monitored in the absence or presence of 50 µM Ga-Dfo competitive blocking control.

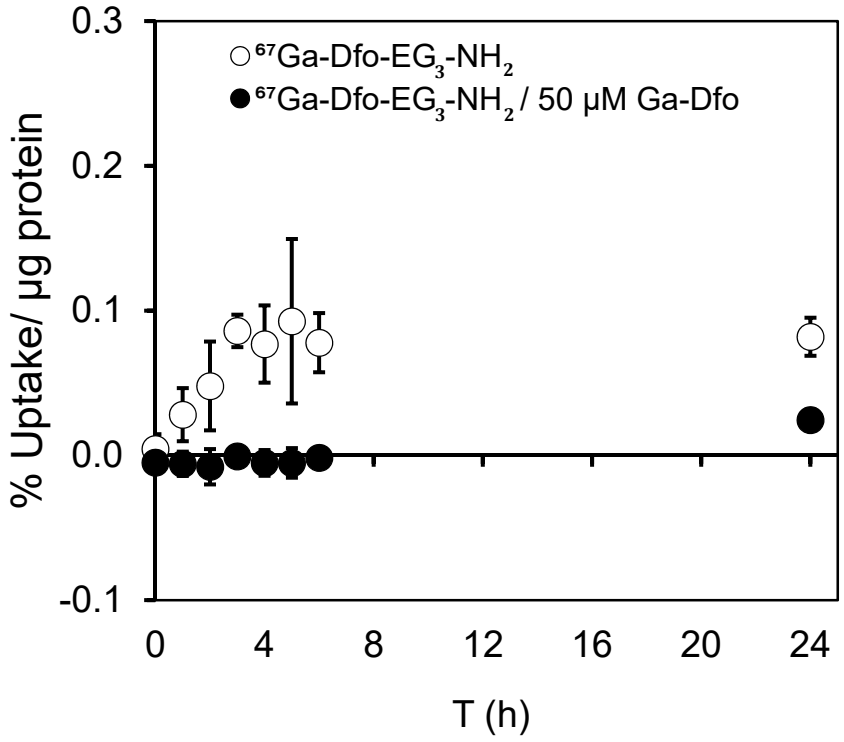

Figure 3.6 ^{67}Ga-Dfo-EG$_3$−NH$_2$ % uptake normalized to protein.
Uptake from 7.4 Bq/ µL ^{67}Ga-Dfo-EG$_3$-NH$_2$ was monitored in the absence or presence of 50 µM Ga-Dfo competitive blocking control.

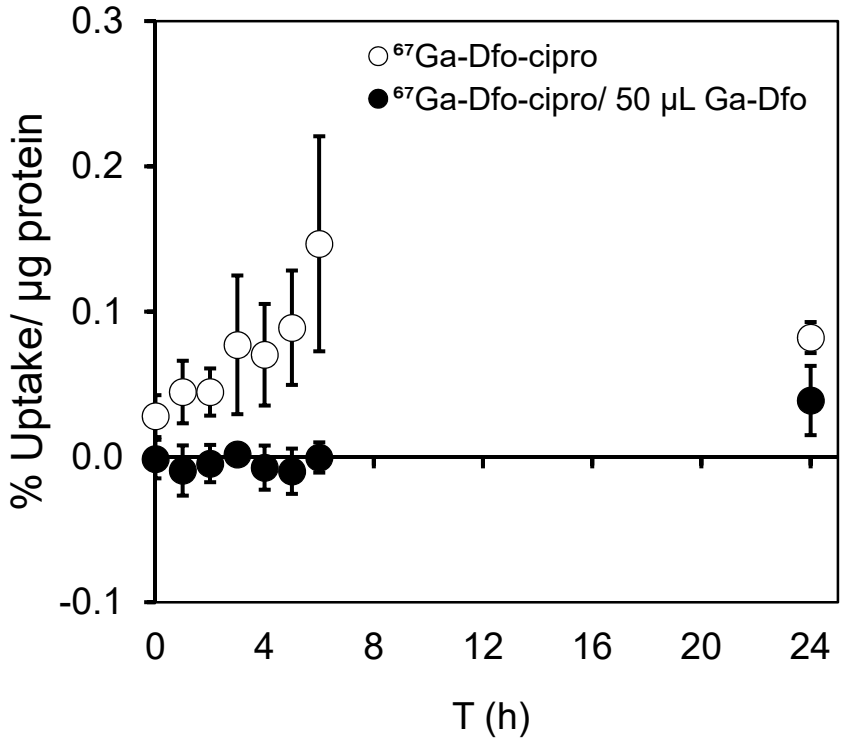

Figure 3.7 ^{67}Ga-Dfo-cipro % uptake normalized to protein.
Uptake from 7.4 Bq/ µL ^{67}Ga-Dfo-cipro was monitored in the absence or presence of 50 µM Ga-Dfo competitive blocking control.

In the first 6 h of *in vitro* uptake assays, roughly linear increases in % uptake/ µg of protein was observed. The slope of the curves was determined. Then, uptake rate of ^{67}Ga-Dfo and derivatives was defined as the slope of the linear portion of the uptake, and relative uptake rate was calculated as follow:

relative uptake rate = m / $m_{standard}$,

where m = slope of % uptake / µg of protein

$m_{standard}$ = slope of % uptake / µg of protein for ^{67}Ga-Dfo.

Relative uptake rate results were combined with previous results from other derivatives synthesized by Joseph Ioppolo and tested in cultures by Deanna Caldwell (Figure 3.8). ^{67}Ga-Dfo-*N*-hexyl had very slow uptake, whereas the cipro,

Eoc, EG_3-NH_2 and *N*-(2-methylquinoline) derivatives were among the best, with relative uptake rates of 0.36 to 0.45.

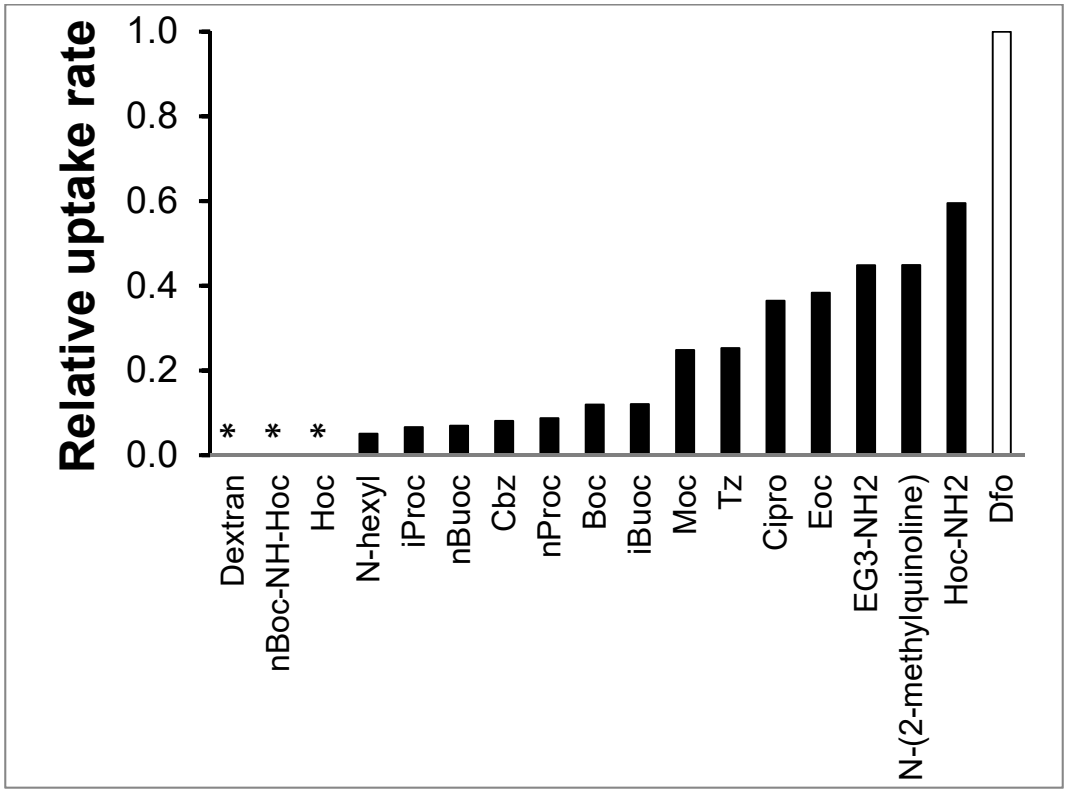

Figure 3.8 Relative uptake rate of ^{67}Ga-Dfo and derivative compounds during the initial 6 h.
(This graph includes the results of all derivatives previously tested by Deanna Caldwell) *Non-reported negative values belonging to unsuccessful compounds ^{67}Ga-Dfo-Dextran, ^{67}Ga-Dfo-nBoc-NH-Hoc and ^{67}Ga-Dfo-Hoc.

3.4. Discussion

Based on the relative uptake rates (Figure 3.8), the 6−aminohexyloxycarbonyl amine derivative of DFO (Dfo-Hoc-NH_2) remained the closest to ^{67}Ga-Dfo's uptake rate in *S. aureus* with a relative uptake rate of 0.60 ± 0.05. Dfo-*N*-(2-methylquinoline), Dfo-EG_3-NH_2, Dfo-Eoc and Dfo-cipro derivatives had relative uptake rates around 0.4. Therefore, most of recent tested compounds were closer to the best observed, namely ^{67}Ga-Dfo, compared with the

majority of previously tested derivatives, with the exception of the *N*-hexyl derivative.

Biodistribution studies in murine models of *S. aureus* infection performed by Megan Blacker using Hoc-NH_2, Eoc and cipro derivatives of labelled Dfo showed increased infected thigh to non-infected thigh uptake ratio for ^{67}Ga-Dfo-Eoc compared to ^{67}Ga-Dfo 1 h after systemic administration while the rest of compounds tested had equal or worst performance than standard Dfo. Fast blood clearance was observed for all compounds while urine was the main route of clearance. Unfortunately, ^{67}Ga-Dfo-Eoc showed 4 times less accumulation in kidneys than standard ^{67}Ga-Dfo. Eoc conjugates also showed high non-specific binding in the intestines and liver like the rest of compounds tested. Increased lipophilicity of compounds correlated with increased uptake in liver. (Megan Blacker, personal communication).

The fact that ^{67}Ga-Dfo-Eoc showed slower renal clearance and increased uptake at the site of infection, demonstrated the potential that can be achieved with the design of Dfo-based probes. Nevertheless, there is still the need of further work on the development of probes with enhanced specificity. On the other hand, the assessment of Dfo conjugated to ciprofloxacin additionally pointed out the potential of Dfo as an antibiotic adjuvant for the development of a new generation of antibiotics even though it did not look good *in vivo*.

In vitro bacterial uptake was generally favored in the presence of more hydrophilic complexes with log$D_{7.4}$ values closer to the unsubstituted Dfo (Table

3.2, Figure 3.8); however, the most successful compound targeting bacteria *in vitro* (^{67}Ga-Dfo-Hoc-NH_2) was also the most hydrophilic ($\log D_{7.4} = -1.96 \pm 0.02$) (Omid Beiraghi, personal communication). This compound failed to be the most favorable one during *in vivo* assays, probably due to higher kidney accumulation than Dfo, in addition to high levels of accumulation in liver and intestine.

^{67}Ga-Dfo was taken up by active transport, as shown by the lack of uptake in cultures at 4 °C (Deanna Caldwell, personal communication). The ability of unlabelled Ga-Dfo to block uptake of ^{67}Ga-Dfo and the ^{67}Ga-labelled derivatives showed that all were taken up by a Dfo-specific pathway (Figures 3.2 to 3.7).

The cause of decreased ^{67}Ga-Dfo uptake at 24 h is not known, but could be due to an increased efflux rate starting at some point after 6 h of incubation. Similar effects were noticeable for Dfo-cipro and Dfo-EG_3-NH_2 derivatives. Less hydrophilic compounds ^{67}Ga-Dfo-Eoc, ^{67}Ga-Dfo-*N*-(2-methylquinoline) and ^{67}Ga-Dfo-*N*-hexyl on the other hand, did not show decreased % uptake/ µg of protein at 24 h compared to 6 h values. Nevertheless, at 24 h the overall uptake level was very similar for all of them (≈ 0.08 % uptake/ µg protein).

Chapter 4 - **TARGETING BACTERIA WITH VANCOMYCIN DERIVATIVES**

4.1. Introduction

Vancomycin is a glycopeptide antibiotic used for the treatment of Gram-positive bacterial infections, the most prominent causative agent of soft tissue and biomaterial-associated infections.[21] It is the last-resort treatment for methicillin-resistant *S. aureus* (MRSA), the most common hospital-acquired pathogen. MRSA is also responsible for many FUO cases triggered by nosocomial infections.[53, 72]

Vancomycin-*trans*-cyclooctene (vanc-TCO), synthesized by modifying the primary amine group on the glycopeptide with trans-cyclooctene, was able to bind to Gram-positive bacteria similarly to unmodified vancomycin. Vanc-TCO, once anchored to the cell surface, was a platform for one of the fastest and most selective known bioorthogonal reactions with tetrazine (Tz)-modified nanoprobes. Chung *et al.* also showed that this two-step labelling procedure gave superior results compared with direct labelling with antibiotic-nanoparticle conjugates.[73]

In the light of these promising results, we decided to explore the potential of this bioorthogonal approach through the use of vanc-TCO conjugates for the pre-targeting of Gram-positive *S. aureus*, followed by labelling with tetrazine-modified Dfo, i.e., ^{67}Ga-Dfo-Tz. Unmodified vancomycin and Ga-Dfo were used as competitive blocking controls, whereas pre-targeting of Gram-negative *E. coli* was used as a negative control. *In vitro* assays for the direct targeting of bacteria using ^{67}Ga-Dfo-vanc were also carried out. Compared to Dfo, preliminary data for

direct and bioorthogonal targeting showed that vancomycin derivatives labelled bacteria with higher sensitivity and efficiency. While Dfo took about 6 h to reach its maximum uptake level, ^{67}Ga-Dfo-vanc reached a similar or higher uptake value within a few minutes. Differences in radioactivity binding between the one-step and two-step labelling methods using vancomycin conjugates are still not clear; further studies are required.

4.2. Materials and Methods

^{67}Ga-Dfo-vanc, ^{67}Ga-Dfo-Tz and vanc-TCO were synthesized by Omid Beiraghi from the Valliant Research Group (Figure 4.1).

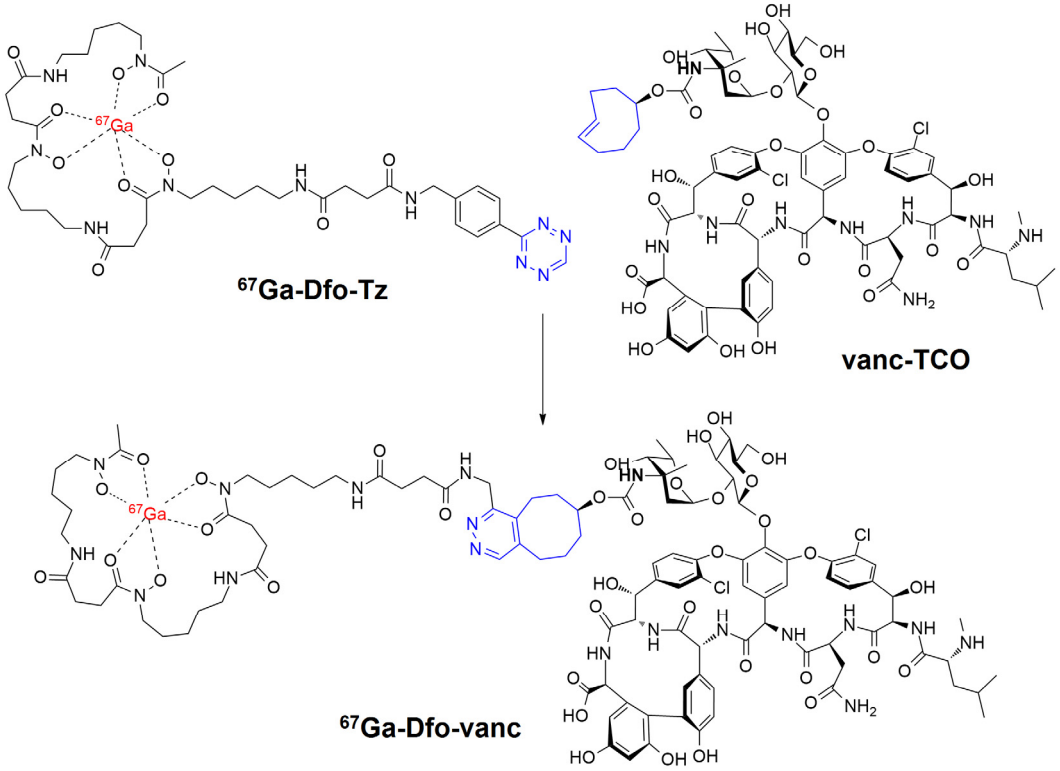

Figure 4.1 Structures of vanc-TCO, ^{67}Ga-Dfo-Tz and ^{67}Ga-Dfo-vanc.
vanc-TCO: *trans*-cyclooctene derivative of vancomycin; ^{67}Ga-DFO-Tz: tetrazine derivative of ^{67}Ga-labelled DFO; ^{67}Ga-DFO-vanc: click product of ^{67}Ga-DFO-Tz and vanc-TCO. (Figure courtesy of Omid Beiraghi).

4.2.1. In vitro targeting of S. aureus using ^{67}Ga-Dfo-Vanc

A 20% glycerol preservation culture of *S. aureus* (ATCC 25923) was scratched and grown in 45 mL of Tris Minimal Succinate medium,[69] which included 10 μM $FeCl_3$ (TMS_{10}) at 37 °C with 300 rpm shaking for 16 to 24 h. The OD_{600} of the culture was measured, and the aliquot size needed to make 4.5 mL cultures with OD_{600} = 2 was calculated. The aliquots were pelleted by centrifugation at 12 500 *g* for 1 min, washed in fresh TMS_{10}, then pelleted again and finally resuspended in 4.5 mL of medium.

The labelling medium consisted of 5 mL of TMS_{10} containing 7.4 Bq/ μL of ^{67}Ga-Dfo-vanc. Medium for blocking experiments also contained 200 μM of unlabelled vancomycin. Blocking assays were required to confirm that ^{67}Ga-Dfo-vanc is taken up through the same pathway as vancomycin.

Binding assays were initiated by resuspending the *S. aureus* cells in the ^{67}Ga-containing medium in the presence or absence of 200 μM vancomycin. Cultures were incubated at 37 °C with shaking at 300 rpm for up to 6 h. Aliquots (500 μL) were tested every 15 min within the first hour, then at 2 h and 6 h. The aliquots were centrifuged at 12 500 *g* for 1 min, then, to ensure that the pellets were not disturbed, 480 μL of supernatant was collected into a 12 × 55 mm Ria plastic test tube (PerkinElmer). Pellets were washed with 500 μL ice-cold phosphate buffered saline (PBS), pH 7.4, (Life Technologies) and centrifuged at

12 500 *g* for 1 min. Again, to ensure pellets were not disturbed, only 500 µL of each supernatant was removed and collected into the same Ria test tube for counting. Each remaining pellet was resuspended in 400 µL of 5 % sodium dodecyl sulfate (SDS, w/v) and left to lyse for 30 to 45 min at room temperature. A 300 µL aliquot of each lysed pellet was transferred to a separate Ria test tube for counting. The remaining lysed pellets were frozen at −20 °C for further protein assays. All Ria test tubes were counted for 1 min using Wizard 1470 Automatic Gamma Counter (PerkinElmer) at the end of the experiment. The resulting count per minute (cpm) values were used to calculate % binding of ^{67}Ga-Dfo-vanc. Binding and blocking assays for each ^{67}Ga-Dfo-vanc were completed in duplicate.

The frozen lysed pellets were thawed at room temperature and protein concentrations were determined following manufacturer's instructions using Pierce™ BCA Protein Assay Kit and bovine serum albumin as a standard. The total protein concentration of every pellet was determined in triplicate.

The binding to bacterial cells was expressed as the ratio of ^{67}Ga in the pellet as a fraction of the total radioactivity (% binding = cpm_{pellet} / (cpm_{pellet} + $cpm_{supernatant}$) × 100%). It was normalized to the total protein concentration, and reported as % binding/µg protein.

4.2.2. In vitro targeting of E. coli using ^{67}Ga-Dfo-vanc

The same protocol was followed as for *S. aureus* cells, using a scratch of a 20 % glycerol preservation culture of *E. coli* (ATCC 700926).

4.2.3. Bioorthogonal approach for in vitro targeting of S. aureus using vancomycin-trans-cyclooctene (vanc-TCO) and ^{67}Ga-Dfo-succinyl-tetrazine (^{67}Ga-Dfo-Tz)

A 20 % glycerol preservation culture of *S. aureus* (ATCC 25923) was scratched and grown in 45 mL of Tris Minimal Succinate medium,[69] which included 10 µM $FeCl_3$ (TMS_{10}) at 37 °C with 300 rpm shaking for 16 to 24 h. The OD_{600} of the culture was measured, and the aliquot size needed to make 4.5 mL cultures with OD_{600} = 2 was calculated. The aliquots were pelleted by centrifugation at 12 500 *g* for 1 min, washed in fresh TMS_{10}, then pelleted again and finally resuspended in 4.5 mL of medium. In the first incubation step, culture tubes (1) and (2) contained 4.5 mL TMS_{10} plus 20 µM vanc-TCO; culture tube (3) contained 4.5 mL TMS_{10} plus 20 µM vanc-TCO and 200 µM vancomycin. Re-suspended cells were left to incubate at 37 °C with shaking at 300 rpm, for 30 min (experiment #1) or 60 min (experiment #2). After the first incubation, cultured cells were centrifuged at 12 500 *g* for 1 min, washed in 4.5 mL of fresh TMS_{10}, centrifuged again at 12 500 *g* for 1 min and re-suspended. In the second incubation step, culture tube (1) contained 4.5 mL TMS_{10} with 7.4 Bq/ µL of ^{67}Ga-Dfo-Tz, and culture tube (2) contained 4.5 mL TMS_{10} with 7.4 Bq/ µL of

^{67}Ga-Dfo-Tz and 50 μM Ga-Dfo. In the first experiment (experiment #1), culture tube (3) contained 4.5 mL TMS_{10} with 7.4 Bq / μL of ^{67}Ga-Dfo-Tz and 50 μM Ga-Dfo. In experiment #2, culture tube (3) contained 4.5 mL TMS_{10} with 7.4 Bq/ μL of ^{67}Ga-Dfo-Tz, 50 μM Ga-Dfo, and 200 μM vancomycin. ^{67}Ga-Dfo-Tz was expected to react with vanc-TCO bound to cells during the first incubation period. The resulting ^{67}Ga-Dfo-vanc complex should remain attached to the cell surface. Culture tube (2) was designed to monitor ^{67}Ga-Dfo-Tz uptake through the siderophore uptake pathway. Culture tube (3) was a double control where both the Ga-Dfo uptake pathway and vancomycin binding were blocked with excess unlabelled Ga-Dfo and vancomycin, respectively.

Bioorthogonal labelling was conducted at 37 °C and shaking at 300 rpm for up to 6 h. Aliquots (500 μL) were taken every 15 min within the first hour, then at 2 h and 6 h using the same method as in Section 4.2.1, with all assays performed in triplicate.

4.3. Results

4.3.1. In vitro targeting of S. aureus using ^{67}Ga-Dfo-vanc

Using pre-formed ^{67}Ga-Dfo-vanc, 32 % bound to *S. aureus* as quickly as could be measured; that is, within 5 min of exposure. The percentage of binding appeared to decline to 23 % during the first 2 h (Figure 4.2); however, it is not clear that this decrease was statistically significant. In the competitive

blocking control, the addition of 200 µM vancomycin in the medium decreased binding below 8 % for all samples.

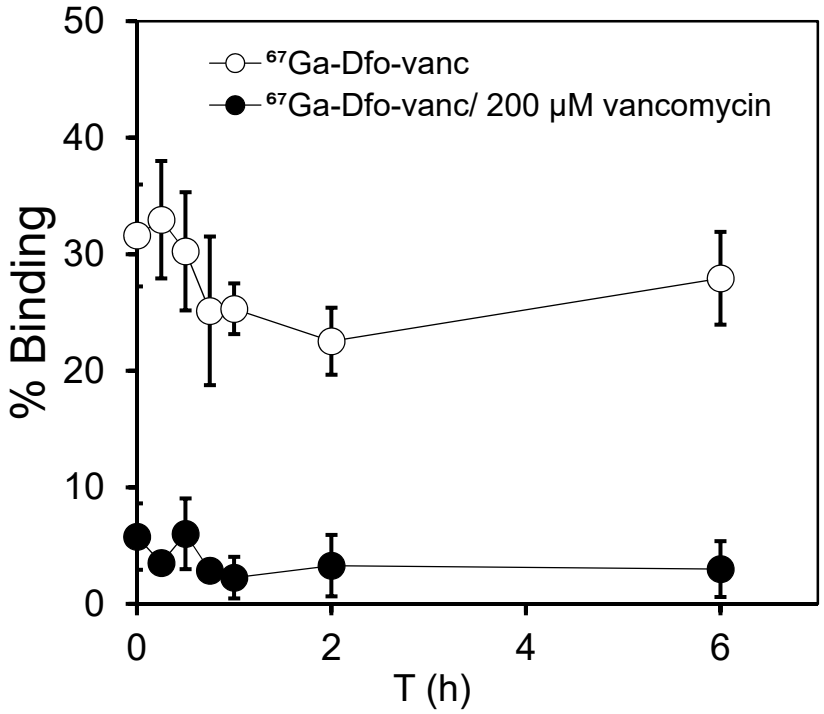

Figure 4.2 % Binding of ^{67}Ga-Dfo-vanc to *Staphylococcus aureus.*
Binding from 7.4 Bq/ µL ^{67}Ga-Dfo-vanc was determined in the presence or absence of 200 µM vancomycin as a competitive blocking control.

Since the overall percentage of binding would be affected by bacterial growth, protein assays were performed to monitor cell growth (Figure 4.3). *S. aureus* in TMS_{10} displayed a > 2-fold increase in protein concentration at t = 6 h, whereas cells grown in the presence of 200 µM vancomycin showed

negligible growth over 6 h.

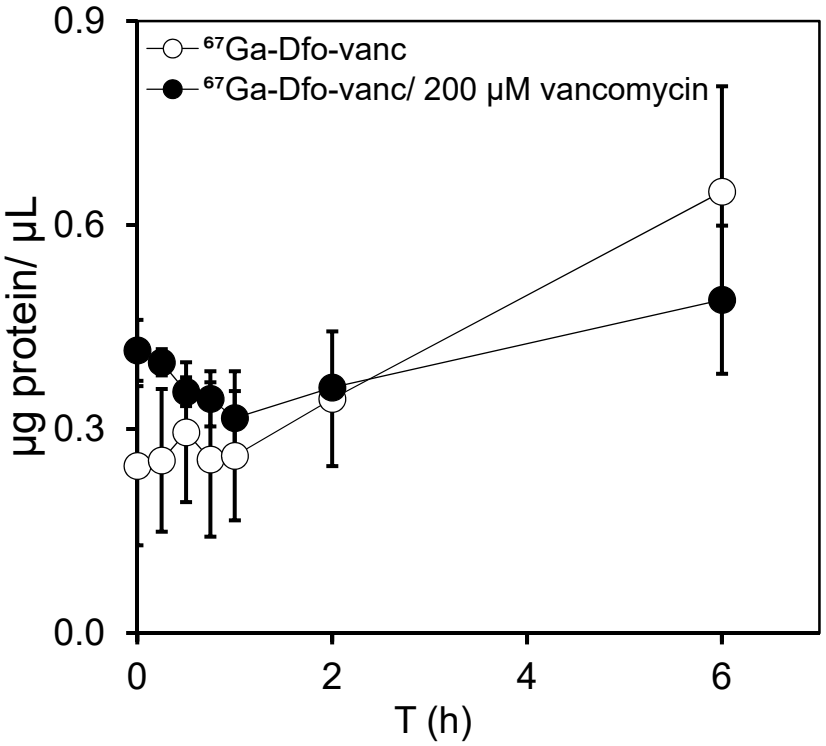

Figure 4.3 *S. aureus* growth monitored by changes in protein concentration over 6 h.

Protein concentration of non-blocked and blocked samples were determined with the BCA protein assay and expressed in µg of protein / µL of media. Non-blocked samples corresponded to cells grown in the presence of 7.4 Bq/ µL of ^{67}Ga-Dfo-vanc. Blocked samples had 200 µM vancomycin added as a competitive blocking control.

^{67}Ga-Dfo-vanc binding to bacterial cells was normalized for cell growth by dividing by the protein concentration (Figure 4.4). Maximum binding levels of 0.2 and 0.5 % / µg of protein were reached within the first 30 min of the experiment. After the first hour, an apparent decline in % binding/ µg of protein was observed to a minimum value of 0.09 ± 0.03 at 6 h. The decrease in binding is only apparent, as the total percentage of radioactivity bound was relatively constant during the experiment while the cells continued to grow. As a result,

dividing binding by protein concentration yielded an apparent decrease in binding. Blocked samples showed less than 0.05 % binding/ µg of protein overall.

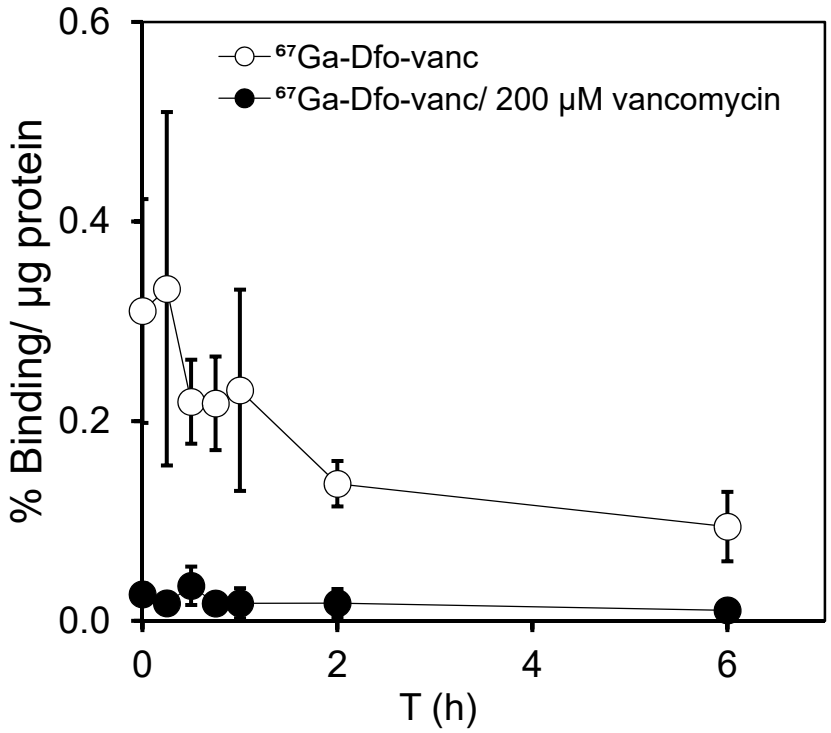

Figure 4.4 % Binding of ^{67}Ga-Dfo-Vancomycin to *S. aureus* normalized to protein. % binding of 7.4 Bq/ µL ^{67}Ga-Dfo-vanc with or without 200 µM vancomycin (competitive blocking control) normalized to µg of protein.

4.3.2. In vitro targeting of E. coli using ^{67}Ga-Dfo-Vanc

A plot of ^{67}Ga-Dfo-vanc binding to *E. coli* with or without 200 µM vancomycin showed little binding, as expected (Figure 4.5) Percent binding was

< 6 % at all times for both non-blocked and blocked samples.

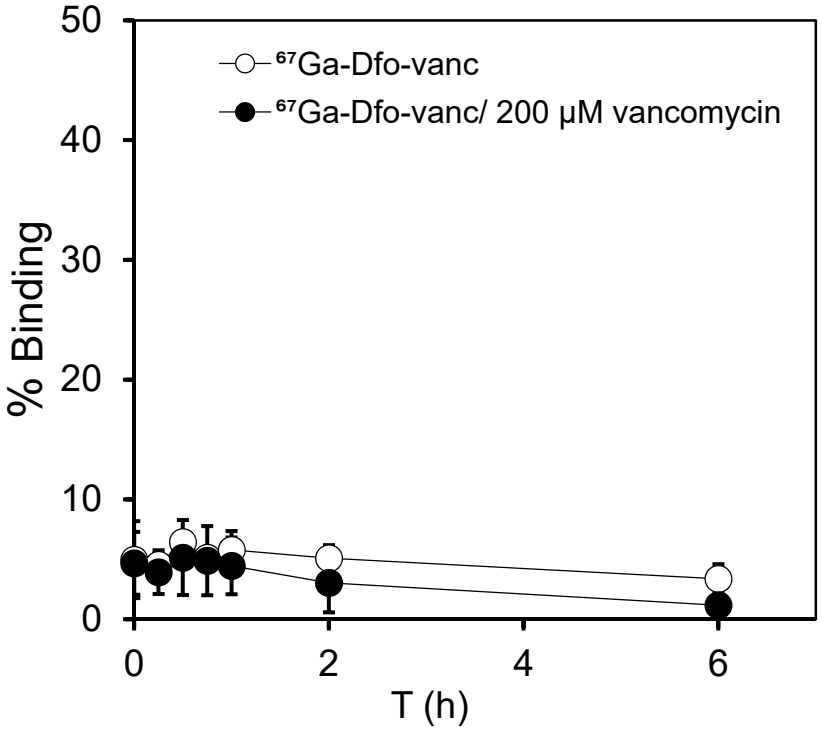

Figure 4.5 % Binding of ^{67}Ga-Dfo-vanc to *E. coli.*
% Binding from 7.4 Bq/ μL ^{67}Ga-Dfo-vanc was determined in the absence or presence of 200 μM vancomycin.

E. coli protein concentration monitored vs. time of non-blocked and blocked samples shared a similar pattern. (Figure 4.6)

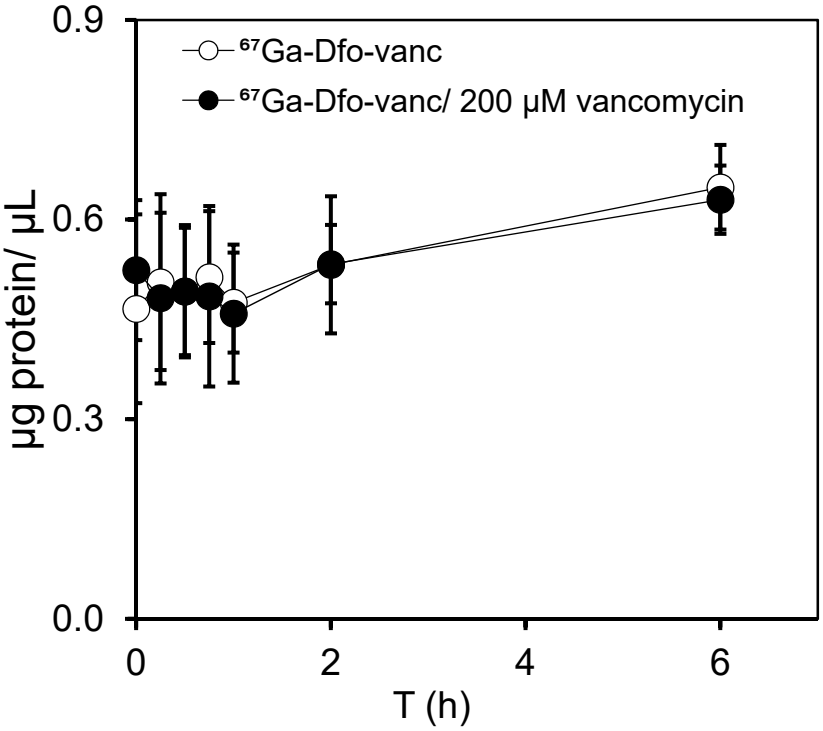

Figure 4.6 *E. coli* growth monitored by changes in protein concentration during 6 h. Protein concentration of both non-blocked and blocked samples were determined by BCA protein assay and expressed in µg of cell protein per µL of media. Non-blocked samples corresponded to cells grown in the presence of 7.4 Bq/ µL of ^{67}Ga-Dfo-vanc. Blocked samples also contained 200 µM vancomycin.

^{67}Ga-Dfo-vanc binding to *E. coli* was < 0.04 % / µg of protein along each entire experiment (Figure 4.7). Non-blocked and blocked samples had similar results at every time point.

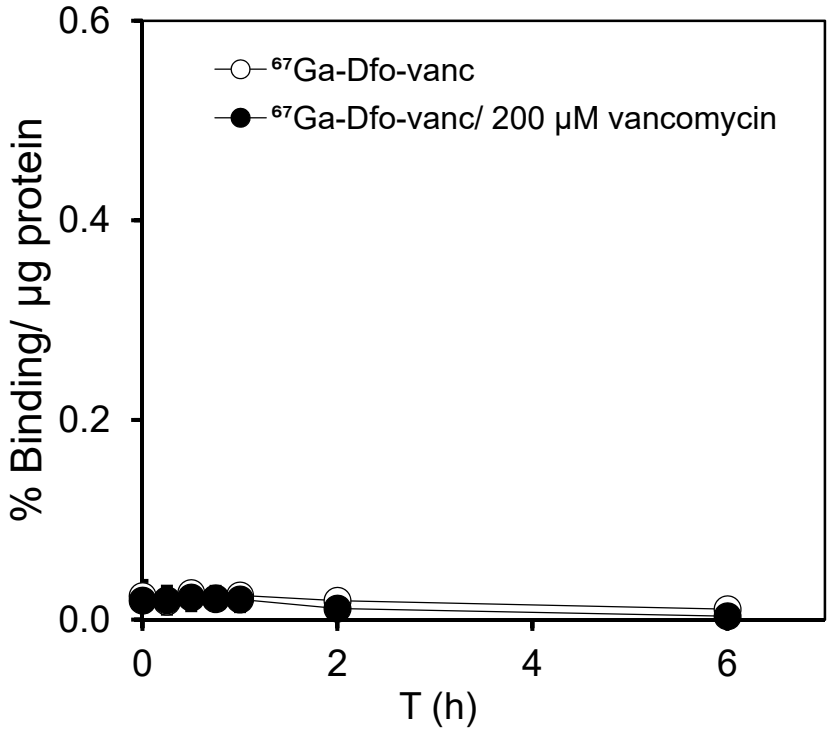

Figure 4.7 % Binding of ^{67}Ga-Dfo-Vancomycin to *Escherichia coli* normalized to protein.

% Binding of 7.4 Bq/ µL ^{67}Ga-Dfo-vanc with or without 200 µM vancomycin was normalized to µg protein.

4.3.3. Bioorthogonal labelling of S. aureus using vancomycin-trans-cyclooctene (vanc-TCO) and ^{67}Ga-Dfo-succinyl-tetrazine (^{67}Ga-Dfo-Tz).

The bioorthogonal labelling approach involved a first incubation of *S. aureus* with vanc-TCO, followed by a second incubation with ^{67}Ga-Dfo-Tz. Either compound could show non-specific binding or uptake, so Ga-Dfo and vancomycin were used as blocking compounds.

In the first bioorthogonal labelling assay, *S. aureus* cells bound 35 % of ^{67}Ga-Dfo-Tz in the unblocked sample, and 37 % when 50 µM Ga-Dfo was added in the second incubation step. There was 19 % radioactivity binding with 200 µM

vancomycin in the first incubation and 50 μM Ga-Dfo in the second step (Figure 4.8). At 6 h, binding increased to 45 % for samples without vancomycin, and 28 % with it.

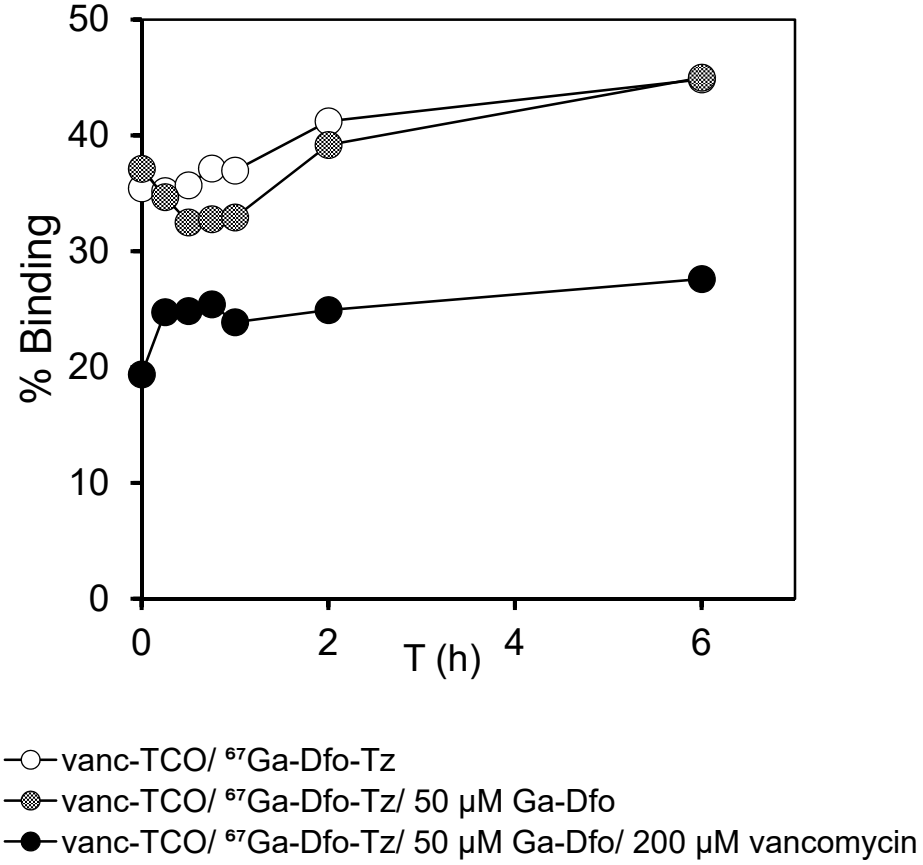

Figure 4.8 % Binding to *S. aureus* during bioorthogonal experiment #1.
% Binding following pre-targeting with vanc-TCO and labelling with ^{67}Ga-Dfo-Tz (7.4 Bq/ μL) with or without blocking with 50 μM Ga-Dfo or 50 μM Ga-Dfo and 200 μM vancomycin.

Bacterial growth was monitored with protein assays (Figure 4.9). Protein concentrations increased similarly for all samples during the course of the experiment.

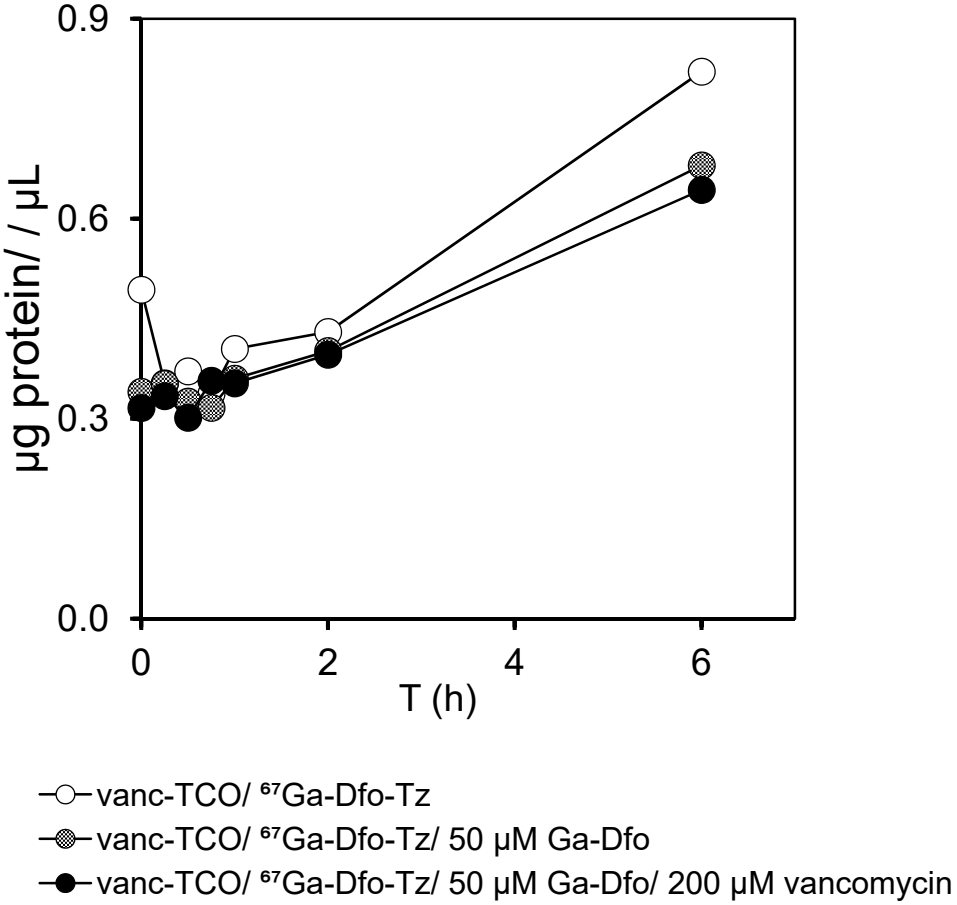

Figure 4.9 Protein concentration in *S. aureus* cultures during bioorthogonal labelling experiment #1.

Protein concentration of cells pre-targeted with vanc-TCO and later grown in labelling media containing ^{67}Ga-Dfo-Tz (7.4 Bq/ µL) with or without blocking with 50 µM Ga-Dfo or 50 µM Ga-Dfo and 200 µM vancomycin.

Percent binding was normalized to protein and plotted vs. time (Figure 4.10). During the first 2 h the % binding in non-blocked and Ga-Dfo-blocked samples was relatively stable around 0.2 % binding/ µg protein which decreased by half at 6 h. Samples containing 200 µM vancomycin in the first incubation with vanc-TCO showed about half of the labelling observed with non-blocked

samples, and decreased to very close to the non-blocked samples at t = 6 h.

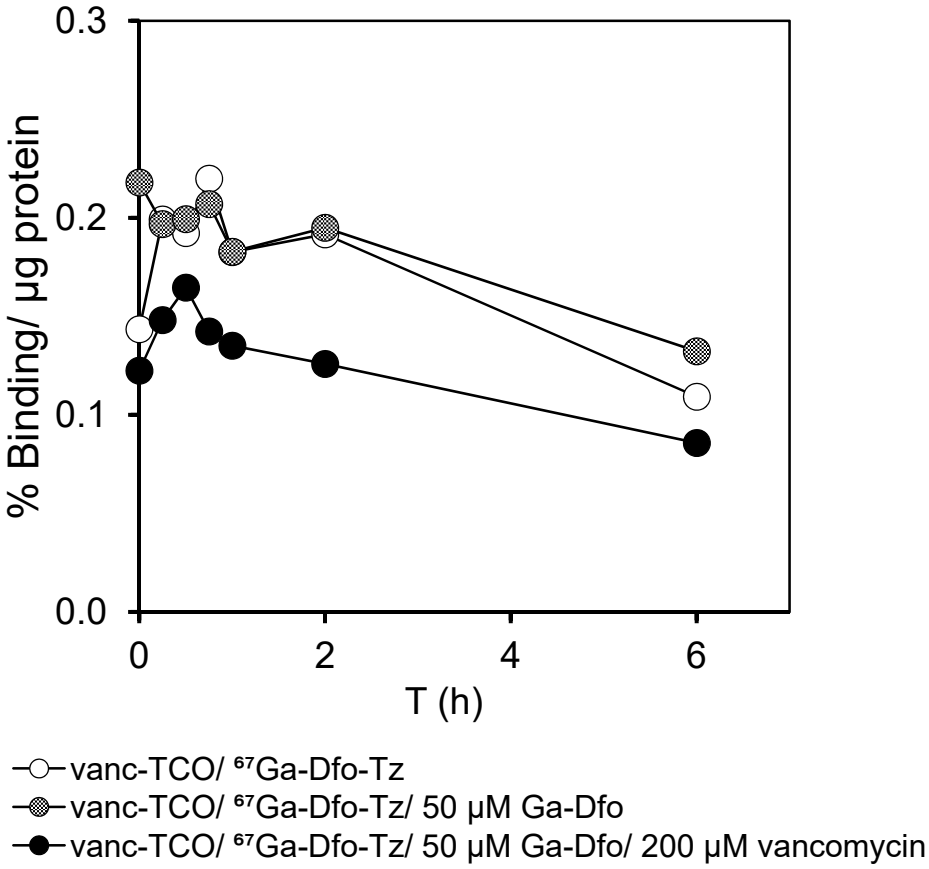

Figure 4.10 Normalized % binding to *S. aureus* for bioorthogonal experiment #1. Normalized % binding to *S. aureus* with vanc-TCO and ^{67}Ga-Dfo-Tz in the presence or absence of 50 µM Ga-Dfo or 50 µM Ga-Dfo plus 200 µM vancomycin, normalized to µg of bacterial protein.

In contrast to experiment #1, where the ^{67}Ga-Dfo-Tz was used the day it was made, the ^{67}Ga-Dfo-Tz solution in experiment #2 was 5 days old. The first incubation time of *S. aureus* with vanc-TCO was increased from 30 min to 1 h in experiment #2. In addition, in experiment #2, 200 µM vancomycin was present in both the first and second incubation steps in culture tube (3).

Percent binding in all samples started around 2 to 4%. At t = 6 h, non-blocked samples reached 7 % while samples blocked with Ga-Dfo reached 4 % and samples blocked with Ga-Dfo and vancomycin were about 1 % (Figure 4.11).

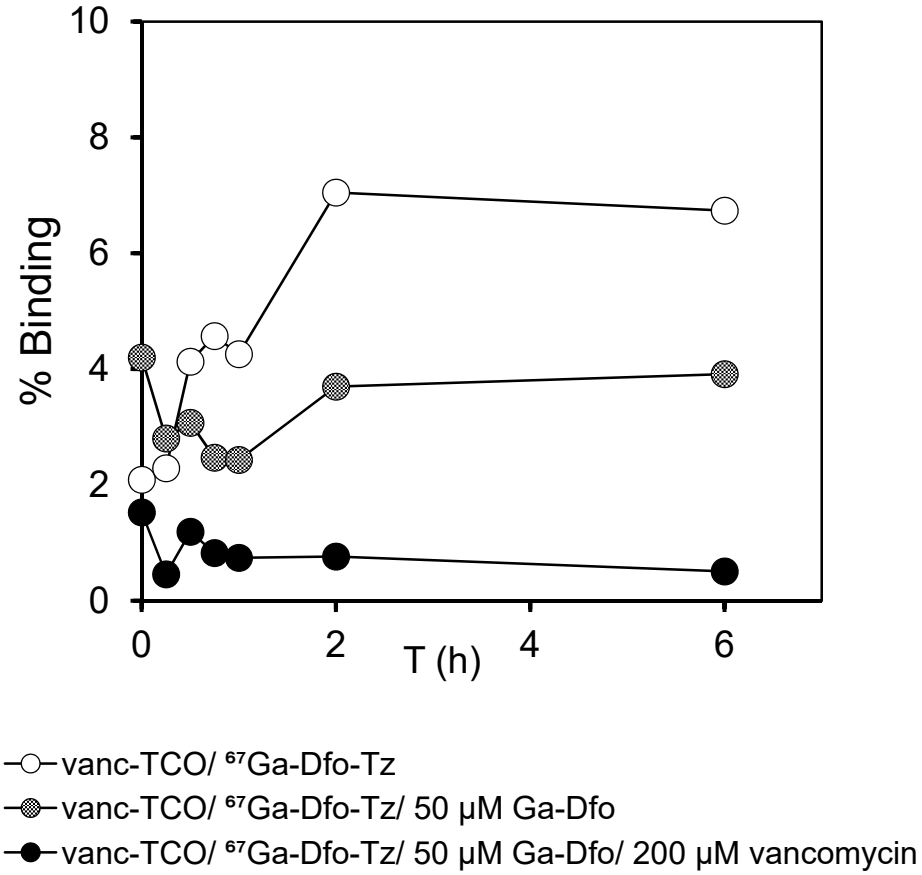

Figure 4.11 % Binding to *S. aureus* during bioorthogonal labelling experiment #2. % Binding following pre-targeting with vanc-TCO and labelling with ^{67}Ga-Dfo-Tz (7.4 Bq/ µL) with or without blocking with 50 µM Ga-Dfo or 50 µM Ga-Dfo and 200 µM vancomycin.

.

Bacterial growth was monitored by plotting µg protein per µL of media (Figure 4.12). Protein concentration increased similarly for all samples during the entire experiment.

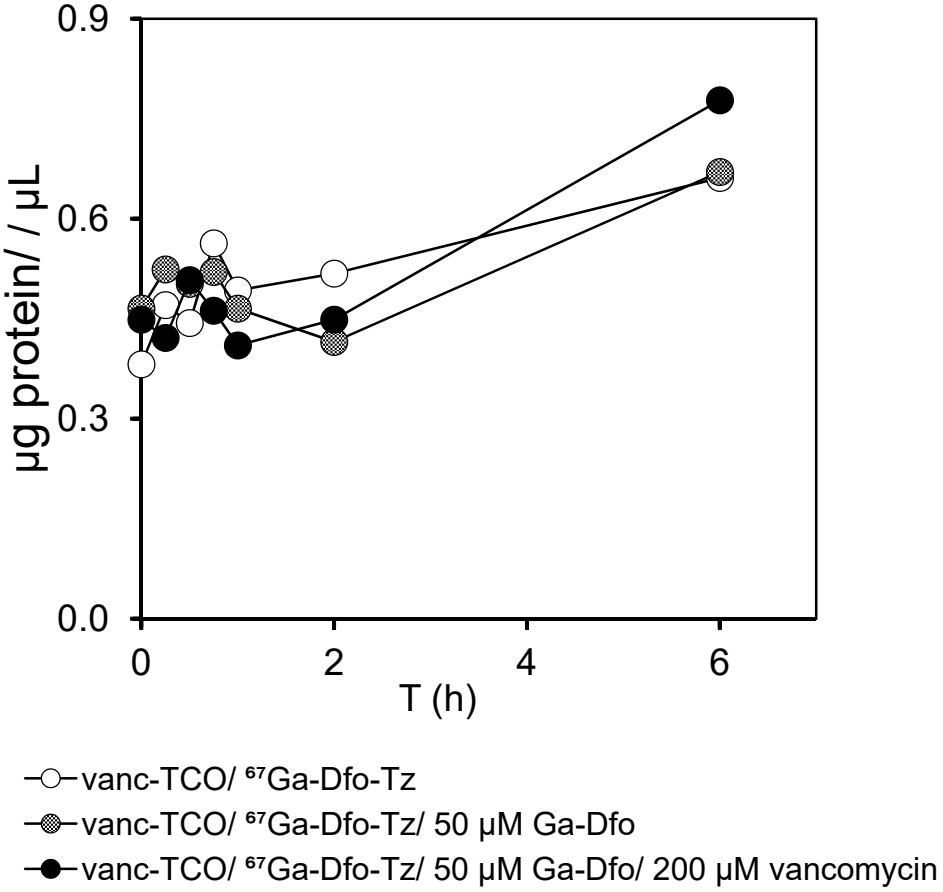

Figure 4.12 Protein concentration in *S. aureus* cultures during bioorthogonal labelling experiment #2.

Protein concentration of cells pre-targeted with vanc-TCO and later grown in labelling media containing ^{67}Ga-Dfo-Tz (7.4 Bq/ µL) with or without blocking with 50 µM Ga-Dfo or 50 µM Ga-Dfo and 200 µM vancomycin.

Percent binding was normalized to protein and plotted vs. time (Figure 4.13). This time, double-blocked samples remained below a value of 0.01 % / µg protein during the entire experiment. Non-blocked samples started at 0.01 % / µg protein, reached a peak value of 0.03 % / µg protein at 2 h and finally decreased to 0.02 % / µg protein at 6 h. Samples blocked with 50 µM Ga-Dfo showed an

average of 0.01 % / µg protein within the first hour, rising to 0.02 % / µg protein at 2 h followed by a decline to about 0.01 % / µg protein.

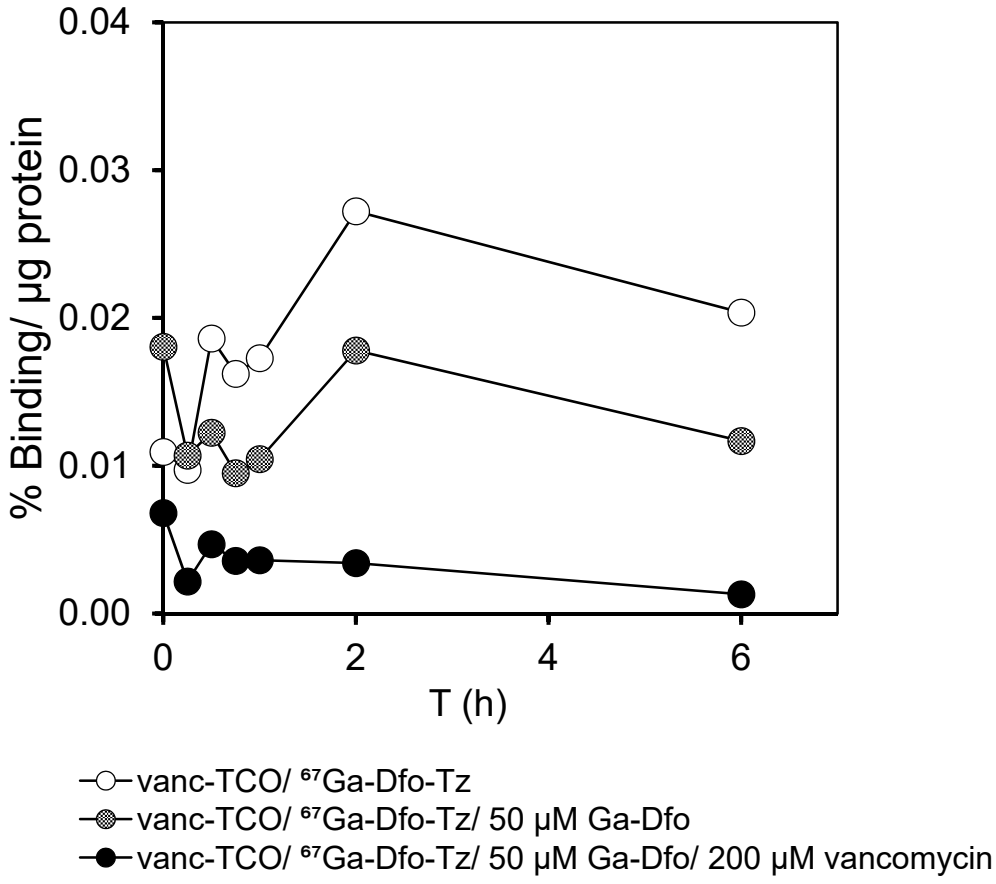

Figure 4.13 Normalized % binding to *S. aureus* for bioorthogonal experiment #2. Normalized % binding to *S. aureus* with vanc-TCO and ^{67}Ga-Dfo-Tz in the presence or absence of 50 µM Ga-Dfo or 50 µM Ga-Dfo plus 200 µM vancomycin, normalized to µg of bacterial protein.

4.4. Discussion

4.4.1. In vitro targeting of S. aureus using ^{67}Ga-Dfo-vanc.

^{67}Ga-Dfo-vanc showed fast binding in *S. aureus* culture that could lead to quick *in vivo* targeting of infections while the probe is still in circulation, a highly

desirable characteristic for a molecular imaging probe. Around 29 % of ^{67}Ga-Dfo-vanc bound to *S. aureus* within 5 minutes and remained attached during the first hour of exposure (Figure 4.2). This corresponded to a normalized binding capacity averaging 0.26 % / µg protein, slightly higher than the average normalized uptake for ^{67}Ga-Dfo at 6 h (Figure 4.4; Figure 3.2).

In contrast to the iron-siderophore-uptake pathway, vancomycin is not internalized via an active-transport mechanism. Instead, it can quickly form hydrogen bonds with the terminal D-alanyl-D-alanine (D-Ala-D-Ala) moieties of the cross-linking peptide of the peptidoglycan that forms the Gram-positive cell wall. This helps to explain the differences in speed between labelling mediated via vancomycin binding compared to labelling via siderophore uptake.

The binding of ^{67}Ga-Dfo-vanc normalized to protein levels decreased considerably after 6 h, whereas the total amount of bound label remained constant at ≈ 28 %. That is, a large fraction of ^{67}Ga-Dfo-vanc bound almost immediately, and no more binding occurred as the number of cells, as reflected in the increasing protein concentration, increased over time. There are several possible explanations for this. One is that all of the "active" form of ^{67}Ga-Dfo-vanc was bound quickly, and the remaining ^{67}Ga was either (i) in complex with degraded Dfo-vanc or other impurities, or (ii) was free ^{67}Ga(III) in solution. Alternatively, ^{67}Ga-Dfo-vanc may have bound to soluble peptidoglycan fragments in solution. Bacterial cells routinely shed and recycle peptidoglycan.[74] Finally, it is also

possible that free ^{67}Ga-Dfo-vanc was degraded, for example, by secreted bacterial enzymes.

^{67}Ga-Dfo-vanc binding was almost completely blocked by vancomycin (Figure 4.2, Figure 4.4). This showed that ^{67}Ga-Dfo-vanc binding to *S. aureus* cells was predominantly or completely through the vancomycin moiety, and that there was little or no non-specific binding. The chemical concentration of ^{67}Ga-Dfo-vanc (0.4 μM, or 0.6 μg/ mL) in the growth media was negligible compared with the minimum inhibitory concentration of vancomycin, 2 μg/ mL.[53] Thus, ^{67}Ga-Dfo-vanc had little or no effect on cell growth, while the 200 μM vancomycin used in blocking experiments was enough to block *S. aureus* growth.

E. coli growth was unaffected by the presence of 200 μM vancomycin, as expected for a Gram-negative bacterium (Figure 4.6). As expected, there was essentially no ^{67}Ga-Dfo-vanc binding to *E. coli* (Figure 4.5, Figure 4.7) for both non-blocked and blocked samples. Again, the small % binding observed might be explained by non-specific interactions of the labelled complex at the cell surface.

4.4.2. Bioorthogonal labelling of S. aureus.

In the first experiment, ^{67}Ga-Dfo-vanc binding in the sample blocked with 50 μM Ga-Dfo was indistinguishable from the unblocked sample (Figure 4.8). The sample blocked with 200 μM vancomycin in the first incubation and 50 μM Ga-Dfo in the second had lower, but still significant binding. It is not clear why this happened.

Similar to ^{67}Ga-Dfo-vanc binding, the % binding, when normalized to protein concentration decreased by half at 6 h (Figure 4.10), while the total amount of bound radioactivity was essentially constant (Figure 4.8). This apparent decline was most likely due to the fact that vanc-TCO was present only in the first incubation step. It was washed away in the centrifugation and washing step before adding fresh media for the second incubation step. Thus, the concentration of free vanc-TCO in the second incubation solution would have been negligible, so none would have been available to bind newly formed cells. To sum up, readily active ^{67}Ga-Dfo-Tz in the media quickly reacted with vanc-TCO pre-bound to bacteria, but new growing bacteria lacked bound vanc-TCO, resulting in no targeting of new cells. The small increase in % binding over time could be due to slower click-binding of ^{67}Ga-Dfo-Tz to less accessible vanc-TCO on the pre-targeted cells.

Using 200 μM vancomycin as a competitive blocking control for vanc-TCO during the 30 min of the first incubation showed some blocking effect with lower % binding values close to half of the non-blocked samples (Figure 4.8, Figure 4.10). Although there is some evidence of competitive blocking, the apparent level binding in blocked samples was higher than expected. The reasons for this are unknown, and it was not observed in experiment #2, so it was not pursued further.

In the second experiment, 200 μM vancomycin was included in both the first and second incubations, and the first incubation time was increased to

60 min. Surprisingly, the cells continued to grow in the medium containing 200 μM vancomycin (Figure 4.12). The reason for this is not known. Cell growth was similar in the non-blocked media in experiments #1 and #2 (Figure 4.9; Figure 4.12) as well as in direct binding of ^{67}Ga-Dfo-vanco (Figure 4.3).

In experiment #2, the % binding for all samples was less than in experiment #1 (Figure 4.11 vs. Figure 4.8). The normalized % binding values were roughly 10-fold lower than in experiment #1 (Figure 4.13 vs. Figure 4.10). The normalized % binding values in experiment #2 were within the same range as for the blocked samples during direct binding of ^{67}Ga-Dfo-vanc to both, *S. aureus* (Figure 4.4) and *E. coli* (Figure 4.7), though the relevance of this observation is not clear. A likely cause of the low binding in experiment #2 was the fact that the ^{67}Ga-Dfo-Tz solution used was 5 days old. The stability of ^{67}Ga-Dfo-Tz was not studied beyond 24 h, but it is expected to degrade over several days according to Omid Beiraghi (personal communication). Thus, the low overall binding in experiment #2 could be due to ^{67}Ga-Dfo-Tz degradation.

In spite of the low overall binding, the observed pattern was what would have been expected based on previous experiments. That is, there was significant and early ^{67}Ga binding in the non-blocked sample, which increased gradually over 6 h (Figure 4.11). There was similarly early binding in the 50 μM Ga-Dfo blocking control, but less increase over time. That would imply that at least some of the observed increase in binding over time in the non-blocked sample was due to ^{67}Ga-Dfo-Tz uptake through the siderophore uptake pathway. The medium,

TMS_{10}, contained 10 μM Fe(III). These are not strongly iron-limiting conditions, but apparently enough to activate the siderophore uptake pathways. There was little uptake at any time in the medium containing 200 μM vancomycin. This implies that most of the observed binding in the non-blocked sample was due to the desired mechanism, namely vanc-TCO binding to peptidoglycan and the click reaction with ^{67}Ga-Dfo-Tz.

In summary, the results from experiment #1 were difficult to explain. In experiment #2, there were some apparent problems, namely the low overall level of ^{67}Ga binding, and some inconsistencies, namely the continued growth of *S. aureus* in media containing 200 μM vancomycin. Nevertheless, the pattern of ^{67}Ga binding in the experimental sample and the blocking controls suggests that the bioorthogonal labelling approach did work, and that further experiments to resolve the inconsistencies and get more consistent results are in order.

Chapter 5 - **CONCLUSIONS AND FUTURE WORK**

5.1. Conclusions

In the process of developing a new solid-phase iron-chelator, namely Dfo-Sepharose resin, we explored different methods to improve the colorimetric Fe(III) with different CAS buffer cleaning procedures aimed to eliminate unknown contaminants that interfered with the assay's accuracy. We demonstrated that pre-cleaning CAS buffer using Chelex® 100 efficiently removed contaminants interfering with the absorption spectra. Although we were not able to eliminate negative apparent Fe(III) concentration values, Chelex® 100 treatment at least alleviated the problem, giving reduced negative Fe(III) concentration less often than before treatment.

The need for an alternative buffer system became clear when Fe(III) appeared to be lost from solution over time. Adding 0.5 mM 5-SSA, a weak Fe(III) chelator, helped to stabilize Fe(III) in solution for up to 48 h. Including 0.5 mM 5-SSA in TMS medium did not negatively interfere with cell growth. At the same time, it helped to alleviate negative apparent Fe(III) concentration values. What is more, the addition of 5-SSA enhanced the bioavailability of Fe(III) in the media and supported cell growth in TMS_{10} and TMS_0. However, it is not clear why the capacity of the resin seemed to decline after 2 h of treatment in the presence of 0.5 mM of 5-SSA despite the high affinity of Dfo-Sepharose for Fe(III). So far, we can only state that Dfo-Sepharose resin has an iron-binding

capacity of at least 1.4 ± 0.3 nmol/μL of wet resin and pre-treating TMS with this resin for 16 to 24 h reduces Fe(III) to undetectable levels using CAS assay.

In culture assays of the uptake of Dfo-derivatives targeting the Dfo uptake pathway demonstrated that they were all taken up, though at different rates. Some of the new Dfo-derivatives, including ^{67}Ga-Dfo-*N*-(2-methylquinoline), ^{67}Ga-Dfo-EG$_3$-NH$_2$, ^{67}Ga-Dfo-Eoc and ^{67}Ga-Dfo-cipro showed similar uptake rates and higher ultimate uptake levels than previous derivatives. Hydrophobic substituents of Dfo derivatives increased the serum half-life of compounds, but also increased non-specific binding to liver and intestines. More hydrophilic compounds, on the other hand, tended to experience the same quick clearance fate of Dfo. ^{67}Ga-Dfo-Eoc was one of the most promising Dfo-derivatives, as it had good uptake levels in assays in culture and good selectivity between the infected and non-infected thigh during *in vivo* assays compared to standard ^{67}Ga-Dfo. Nonetheless, its total low uptake in the infected thigh in conjunction with high levels of non-specific binding to the gastrointestinal tract will not favor this probe a suitable infection imaging agent. Finding Dfo derivatives able to detect infection with high affinity and selectivity while having longer serum half-life remains challenging.

Dfo conjugated with the antibiotic ciprofloxacin displayed the potential of Dfo derivatives as adjuvants for either standard or novel antibiotics.

Specifically targeting the bacterial surface has promise for the design of molecular imaging probes for bacterial infections. Preliminary results following

one- and two-step labelling of *S. aureus* with ^{67}Ga-Dfo-vanc reached higher labelling signal levels within minutes of exposure while Dfo-derivatives needed at least 6 h to reach their highest uptake levels. The fast binding procedure should most likely enhance the overall chances of targeting infection *in vivo.*

5.2. Future work

Further iron-binding resin capacity studies are still required for Dfo-Sepharose resin. ICP-MS analysis is a highly sensitive method to consider for the final validation of iron scavenging resins. The fact that bacteria are still able to grow in Dfo-Sepharose-treated TMS medium implies that not all the Fe(III) has been removed, in spite of the Fe(III) concentration being too low to detect by the CAS assay.

New Dfo-derivatives are still needed for the development of molecular imaging probes targeting the Dfo-uptake pathway with enhanced affinity, selectivity and pharmacokinetic properties. Alternatively, future studies of Ga-Dfo derivatives should also focus on the development of therapeutic agents as valuable adjuvants to antibiotics.

One thing that was left to be further explored during our studies of probes targeting the peptidoglycan of Gram-positive bacteria, was the added effect of Dfo binding protein interactions to the binding effect of vancomycin in iron depleted conditions. It would be interesting to try *in vitro* binding of ^{67}Ga-Dfo-vanc to *S. aureus* in TMS_0 using excess Ga-Dfo as a control. *In vitro* click-chemistry binding of vanc-TCO and ^{67}Ga-Dfo-Tz to *S. aureus* in TMS_0 should be

done in order to also study the potential added effect of iron-siderophore-binding protein to the bioorthogonal approach. Preliminary *in vitro* assays have shown that ^{67}Ga-Dfo-Tz can get internalized in the cells. We need to see how this might affect the overall efficiency of labelling through the two-step binding in iron scarcity conditions using excess Ga-Dfo as a competitive control as well. Prior to performing two-step labelling procedure in iron-depleted media, the original bioorthogonal experiment carried out in TMS_0 should be reproduced. Later on, we finally need to compare results from both, *in vitro* binding and *in vitro* click-chemistry binding to further conclude which of these methods is actually the most successful one.

References

(1) Martin, R. B. (1988) Bioinorganic chemistry of aluminum. *Met. Ions Biol. Syst.* (Sigel, H., Ed.), pp 1–57, Marcel Dekker, Inc., New York and Basel.

(2) Harris, W. R., and Pecoraro, V. L. (1983) Thermodynamic binding constants for gallium transferrin. *Biochemistry 22*, 292–299.

(3) Harris, W. R. (1986) Thermodynamics of gallium complexation by human lactoferrin. *Biochemistry 25*, 803–8.

(4) Aramini, J. M., McIntyre, D. D., and Vogel, H. J. (1994) Gallium(3+) Binding to Ovotransferrin and Its Half-Molecules: A Multinuclear NMR Study. *J. Am. Chem. Soc. 116*, 11506–11511.

(5) Merkx, M., and Averill, B. a. (1998) Ga^{3+} as a functional substitute for Fe^{3+}: Preparation and characterization of the $Ga^{3+}Fe^{2+}$ and $Ga^{3+}Zn^{2+}$ forms of bovine spleen purple acid phosphatase. *Biochemistry 37*, 8490–8497.

(6) Wencewicz, T. a, Long, T. E., Möllmann, U., and Miller, M. J. (2013) Trihydroxamate siderophore-fluoroquinolone conjugates are selective sideromycin antibiotics that target *Staphylococcus aureus*. *Bioconjug. Chem. 24*, 473–86.

(7) Mansueto, P., Di Lorenzo, G., Rizzo, M., Di Rosa, S., Vitale, G., Rini, G., Mansueto, S., and Affronti, M. (2008) Fever of unknown origin in a Mediterranean survey from a division of internal medicine: Report of 91 cases during a 12-year-period (1991-2002). *Intern. Emerg. Med. 3*, 219–225.

(8) Iikuni, Y., Okada, J., Kondo, H., and Kashiwazaki, S. (1994) Current fever of unknown origin 1982-1992. *Intern. Med. 33*, 67–73.

(9) Petersdorf, R. G., and Beeson, P. B. (1961) Fever of unexplained origin: report on 100 cases. *Medicine (Baltimore). 40*, 1–30.

(10) Kumar, R., Basu, S., Torigian, D., Anand, V., Zhuang, H., and Alavi, A. (2008) Role of modern imaging techniques for diagnosis of infection in the era of ^{18}F-fluorodeoxyglucose positron emission tomography. *Clin. Microbiol. Rev. 21*, 209–24.

(11) Cooney, M. J., and El-matary, W. (2013) Case Report Celiac Disease Presenting as Fever of Unknown Origin *2013*, 5–7.

(12) Gemmel, F., Dumarey, N., and Welling, M. (2009) Future Diagnostic Agents. *Semin. Nucl. Med. 39*, 11–26.

(13) Goldsmith, S. J., and Vallabhajosula, S. (2009) Clinically Proven Radiopharmaceuticals for Infection Imaging: Mechanisms and Applications. *Semin. Nucl. Med. 39*, 2–10.

(14) Alberto, Christopher, P., Manuel, B., Lee, F., John, M., Henry, R., Donald, S., James, S., and Signore. (2004) Society of Nuclear Medicine Procedure Guideline for ^{111}In-Leukocyte Scintigraphy for Suspected Infection / Inflammation. *Soc. Nucl. Med. Proced. Guidel.* 1–6.

(15) Signore, A. (2013) About inflammation and infection. *EJNMMI Res. 3*, 1.

(16) Eggleston, H., and Panizzi, P. (2014) Molecular Imaging of Bacterial Infections in vivo: The Discrimination between Infection and Inflammation. *Informatics 1*, 72–99.

(17) Buscombe, J. R., Miller, R. F., Lui, D., and Ell, P. J. (1991) Combined ^{67}Ga citrate and ^{99m}Tc-human immunoglobulin imaging in human immunodeficiency virus-positive patients with fever of undetermined origin. *Nucl. Med. Commun. 12*, 583–592.

(18) Signore, A., Mather, S. J., Piaggio, G., Malviya, G., and Dierckx, R. A. (2010) Molecular Imaging of Inflammation / Infection : Nuclear Medicine and Optical Imaging Agents and Methods. *Chem. Rev. 110*, 3112–3145.

(19) Zerda, A. De, Bodapati, S., Teed, R., Schipper, M. L., and Keren, S. (2011) A Comparison Between Time Domain and Spectral Imaging. *Mol imaging Biol 12*, 500–508.

(20) Chi, C., Du, Y., Ye, J., Kou, D., Qiu, J., Wang, J., Tian, J. (2014) Intraoperative Imaging-Guided Cancer Surgery: From Current Fluorescence Molecular Imaging Methods to Future Multi-Modality Imaging Technology. *Theranostics 4*, 1072–1084.

(21) van Oosten, M., Schäfer, T., Gazendam, J. A. C., Ohlsen, K., Tsompanidou, E., de Goffau, M. C., Harmsen, H. J. M., Crane, L. M. A, Lim, E., Francis, K. P., Cheung, L., Olive, M., Ntziachristos, V., van Dijl, J. M., and van Dam, G. M. (2013) Real-time in vivo imaging of invasive- and biomaterial-associated bacterial infections using fluorescently labelled vancomycin. *Nat. Commun. 4*, 2584.

(22) Andrews, S. C., Robinson, A. K., and Rodriguez-Quiñones, F. (2003) Bacterial iron homeostasis. *FEMS Microbiol. Rev. 27*, 215–237.

(23) Posey, J. E. (2000) Lack of a Role for Iron in the Lyme Disease

Pathogen. *Science 288*, 1651–1653.

(24) Hider, R. (1984) Siderophore mediated absorption of iron, in *Structure and Bonding 58* (Clarke, M. J. et al., Ed.), pp 26–87. Springer-Verlag, Berlin, Heidelberg, New York, Tokyo.

(25) O'Brien, I. G., Gibson, F. (1970) The structure of enterochelin and related 2,3-dihydroxy-N-benzoylserine conjugates from *Escherichia coli*. *Acta 21*, 393–402.

(26) Emery, T. (1982) Iron metabolism in humans and plants. *Am. Sci. 70*, 626–632.

(27) Neilands, J. B. (1982) Microbial envelope proteins related to iron. *Annu. Rev. Microbiol. 36*, 285–309.

(28) Köster, W. (2001) ABC transporter-mediated uptake of iron, siderophores, heme and vitamin B12. *Res. Microbiol. 152*, 291–301.

(29) Fukushima, T., Allred, B. E., Sia, A. K., Nichiporuk, R., Andersen, U. N., and Raymond, K. N. (2013) Gram-positive siderophore-shuttle with iron-exchange from Fe-siderophore to apo-siderophore by *Bacillus cereus* YxeB. *Proc. Natl. Acad. Sci. 110*, 13821–13826.

(30) Fukushima, T., Allred, B. E., and Raymond, K. N. (2014) Direct evidence of iron uptake without iron reduction in the Gram-positive siderophore-shuttle mechanism of *Bacillus cereus* YxeB. *ACS Chem. Biol. 9*, 2092–2100.

(31) Stintzi, a, Barnes, C., Xu, J., and Raymond, K. N. (2000) Microbial iron transport via a siderophore shuttle: a membrane ion transport paradigm. *Proc. Natl. Acad. Sci. U. S. A. 97*, 10691–10696.

(32) Szurmant, H., Fukushima, T., and Hoch, J. A. (2007) The essential YycFG two-component system of *Bacillus subtilis*. *Methods Enzymol. 422*, 396–417.

(33) Winkelmann, G. (1990) Structural and stereochemical aspects of iron transport in fungi. *Biotechnol. Adv. 8*, 207–231.

(34) Winkelmann, G. (2002) Microbial siderophore-mediated transport. *Biochem. Soc. Trans. 30*, 691–696.

(35) Petrik, M., Haas, H., Laverman, P., Schrettl, M., Franssen, G. M., Blatzer, M., and Decristoforo, C. (2014) ^{68}Ga-triacetylfusarinine C and ^{68}Ga-ferrioxamine E for aspergillus infection imaging: Uptake specificity in various microorganisms. *Mol. Imaging Biol. 16*, 102–108.

(36) R. Sephton Smith, M.A., M.B., B. C. (1962) Iron excretion in Thalassaemia major after administration of chelating agents. *Br. Med. J.* 1577–1580.

(37) Braun, V. (2001) Iron uptake mechanisms and their regulation in pathogenic bacteria. *Int. J. Med. Microbiol. 291*, 67–79.

(38) Tufano T. P., Raymond K. N. (1981) Coordination chemistry of microbial iron transport compounds. 21. Kinetics and mechanism of iron exchange in hydroxamate siderophore complexes. *J. Am. Chem. Soc. 103(22)*, 6617–6624.

(39) Rodgers S.J., Raymond, K. N. (1983) Ferric ion sequestering agents. 11. Synthesis and kinetics of iron removal from transferrin of catechoyl derivatives of desferrioxamine B. *26(3)*, 439–42.

(40) Kim, C.-M., Park, Y.-J., and Shin, S.-H. (2007) A widespread deferoxamine-mediated iron-uptake system in *Vibrio vulnificus*. *J. Infect. Dis. 196*, 1537–45.

(41) Hallaway, P. E., Eaton, J. W., Panter, S. S., and Hedlund, B. E. (1989) Modulation of deferoxamine toxicity and clearance by covalent attachment to biocompatible polymers. *Proc. Natl. Acad. Sci. U. S. A. 86*, 10108–10112.

(42) Shepherd, G. (2005) Deferoxamine, in *Encyclopedia of Toxicology* (Wexler, P., Anderson, B., Peyster, A., Gad, S. C., Hakkinen, P. J. B., Kamrin, M., Locey, B., Mehendale, H. M., Pope, C., Ed, L. S.) Second Edition, pp 731–733. Academic Press, Oxford.

(43) Pitkin, D. H., Mico, B. A., Sitrin, R. D., and Nisbet, L. J. (1986) Charge and lipophilicity govern the pharmacokinetics of glycopeptide antibiotics. *Antimicrob. Agents Chemother. 29*, 440–4.

(44) Pattan, S. R., Dighe, N. S., Hariprasad, C. K ., Pattan, J. S., Daithankar, A. V., Gaware, V. M., Hole, M. B. (2009) Synthesis and evaluation of some new 6-Fluro-quinolin-4 (1H)-one derivatives for their anti-microbial activities. *J. Pharm. Sci. Res. 1*, 55–60.

(45) Siddappa, K., Reddy, P. C., Kote, M., Metre, M., Tambe, M., Reddy, T. (2010) Synthesis, Characterization and Antimicrobial Studies of 3-[(2-Hydroxy-quinolin-3-ymethylene)-amino]-2-methyl-3H-quinazolin-4-one and its metal(II) Complexes. *Proc Indian Natn Sci Acad 76*, 163–170.

(46) Neuman, M. (1988) Clinical pharmacokinetics of the newer antibacterial 4-quinolones. *Clin. Pharmacokinet. 14*, 96–121.

(47) Forrest, A., Nix, D. E., Ballow, C. H., Goss, T. F., Birmingham, M. C., and Schentag, J. J. (1993) Pharmacodynamics of Intravenous Ciprofloxacin in Seriously Ill Patients *Antimicrob Agents Chemother. 37,* 1073–1081.

(48) Archibald, A. R., Hancock, I. C., and Harwood, C. R. (1993) *Bacillus subtilis* and Other Gram-Positive Bacteria (Sonenshein, A. L., Losick, R., and Hoch, J. A., Eds.), pp 381-410, American Society of Microbiology.

(49) Höltje, J. V. (1998) Growth of the stress-bearing and shape-maintaining murein sacculus of *Escherichia coli. Microbiol. Mol. Biol. Rev. 62*, 181–203.

(50) Gilbert, Y., Deghorain, M., Wang, L., Xu, B., Pollheimer, P. D., Gruber, H. J., Errington, J., Hallet, B., Haulot, X., Verbelen, C., Hols, P., and Dufrêne, Y. F. (2007) Single-molecule force spectroscopy and imaging of the vancomycin/D-Ala-D-Ala interaction. *Nano Lett. 7*, 796–801.

(51) Zheng, T., Bullock, J. L., and Nolan, E. M. (2012) Siderophore-mediated cargo delivery to the cytoplasm of *Escherichia coli* and *Pseudomonas aeruginosa*: syntheses of monofunctionalized enterobactin scaffolds and evaluation of enterobactin-cargo conjugate uptake. *J. Am. Chem. Soc. 134*, 18388–400.

(52) Moet, G. J., Jones, R. N., Biedenbach, D. J., Stilwell, M. G., and Fritsche, T. R. (2007) Contemporary causes of skin and soft tissue infections in North America, Latin America, and Europe: Report from the SENTRY Antimicrobial Surveillance Program (1998-2004). *Diagn. Microbiol. Infect. Dis. 57*, 7–13.

(53) Dhand, A., and Sakoulas, G. (2012) Reduced vancomycin susceptibility among clinical *Staphylococcus aureus* isolates ("the MIC Creep"): implications for therapy. *F1000 Med. Rep. 4*, 4.

(54) Rice, L. B. (2008) Federal Funding for the Study of Antimicrobial Resistance in Nosocomial Pathogens: No ESKAPE. *J. Infect. Dis. 197*, 1079–1081.

(55) Pendleton, J. N., Gorman, S. P., and Gilmore, B. F. (2013) Clinical relevance of the ESKAPE pathogens. *Expert Rev. Anti. Infect. Ther. 11*, 297–308.

(56) Boucher, H. W., Talbot, G. H., Bradley, J. S., Edwards, J. E., Gilbert, D., Rice, L. B., Scheld, M., Spellberg, B., and Bartlett, J. (2009) Bad bugs, no drugs: no ESKAPE! An update from the Infectious Diseases Society of America. *Clin. Infect. Dis. 48*, 1–12.

(57) Johnson, N. B., Hayes, L. D., Brown, K., Hoo, E. C., and Ethier, K. A. (2014) CDC National Health Report: leading causes of morbidity and mortality and associated behavioral risk and protective factors-United States, 2005-2013. *MMWR. Surveill. Summ. 63 Suppl 4*, 3–27.

(58) Pallin, D. J., Egan, D. J., Pelletier, A. J., Espinola, J. A., Hooper, D. C., and Camargo, C. A. (2008) Increased US Emergency Department Visits for Skin and Soft Tissue Infections, and Changes in Antibiotic Choices, During the Emergence of Community-Associated Methicillin-Resistant *Staphylococcus aureus. Ann. Emerg. Med. 51*, 291–298.

(59) Ray, G. T., Suaya, J. A., and Baxter, R. (2013) Incidence, microbiology, and patient characteristics of skin and soft-tissue infections in a U.S. Population: a retrospective population-based study. *BMC Infect. Dis. 13*, 252.

(60) Boucher, H. W., and Corey, G. R. (2008) Epidemiology of methicillin-resistant *Staphylococcus aureus*. *Clin. Infect. Dis. 46 Suppl 5*, S344–S349.

(61) Eugene Sanders, W. E., and Sanders, C. C. (1997) *Enterobacter spp.*: Pathogens poised to flourish at the turn of the century. *Clin. Microbiol. Rev. 10*, 220–241.

(62) WHO. (2014) Antimicrobial resistance: global report on surveillance. *World Health Organization, 10-11*.

(63) Alexander, D. B., and Zuberer, D. a. (1991) Use of chrome azurol S reagents to evaluate siderophore production by rhizosphere bacteria. *Biol. Fertil. Soils 12*, 39–45.

(64) Barton, L., and Hemming, B. C. (1993) Iron chelation in plants and soil microorganisms, pp 400- 401, Academic Press, San Diego.

(65) Schwyn, B., and Neilands, J. B. (1987) Universal chemical assay for the detection and determination of siderophores. *Anal. Biochem. 160*, 47–56.

(66) Perrin, D. D.; Dempsey, B. (1974) Buffers for pH and metal ion control. pp 35, Chapman and Hall.

(67) R. J. Beynon; J. S. Easterby. (1996) Buffer Solutions: The Basics. pp 70-79, IRL PRESS at Oxford University Press.

(68) Bio-Rad Laboratories. (2000) Chelex 100 and Chelex 20 Chelating Ion Exchange Resin Instruction Manual, 1-13.

(69) Sebulsky, M. T., Speziali, C. D., Shilton, B. H., Edgell, D. R., and Heinrichs, D. E. (2004) FhuD1, a ferric hydroxamate-binding lipoprotein in *Staphylococcus aureus*: a case of gene duplication and lateral transfer. *J. Biol. Chem. 279*, 53152–9.

(70) Magini, M. (1988) X-ray diffraction of ions in aqueous solutions: hydration and complex formation (Magini, M., Ed.) illustrated, pp 102-109, CRC Press, the University of Michigan.

(71) Hughes, D. (2003) medicine and infection detection: the relative effectiveness of imaging with ^{111}In-oxine-, ^{99m}Tc-HMPAO-, and ^{99m}Tc-stannous fluoride colloid-labeled leukocytes and with ^{67}Ga-Citrate*. *J. Nucl. Med. Technol. 31*, 196–201.

(72) Al-Tonbary, Y. A., Soliman, O. E., Sarhan, M. M., Hegazi, M. A., El-Ashry, R. A., El-Sharkawy, A. A., Salama, O. S., and Yahya, R. (2011) Nosocomial infections and fever of unknown origin in pediatric hematology/oncology unit: A retrospective annual study. *World J. Pediatr. 7*, 60–64.

(73) Chung, H. J., Reiner, T., Budin, G., Min, C., Liong, M., Issadore, D., Lee, H., and Weissleder, R. (2011) Ubiquitous Detection of Gram-Positive Bacteria with Bioorthogonal Magneto fluorescent Nanoparticles 8834–8841.

(74) Johnson, J., Fisher, J., and Mobashery, S. (2013) Bacterial cell wall recycling. *Ann. new york Acad. 1277*, 54–75.